Initial-value problem for small perturbations in an idealized detonation in a circular pipe

by
Ivan V. Shalaev

A Dissertation Submitted to the Faculty of the

Department of Aerospace and Mechanical Engineering

In Partial Fulfillment of the Requirements
For the Degree of

Doctor of Philosophy
With a Major in Aerospace Engineering

In the Graduate College

The University of Arizona

2 0 0 8

THE UNIVERSITY OF ARIZONA
GRADUATE COLLEGE

As members of the Dissertation Committee, we certify that we have read the dissertation prepared by Ivan V. Shalaev entitled Initial-value Problem for Small Perturbations in an Idealized Detonation in a Circular Pipe and recommend that it be accepted as fulfilling the dissertation requirement for the Degree of Doctor of Philosophy

_____ Date: 11/06/08
Anatoli Tumin

_____ Date: 11/06/08
Thomas F. Balsa

_____ Date: 11/06/08
Moysey Brio

_____ Date: 11/06/08
Hermann F. Fasel

Final approval and acceptance of this dissertation is contingent upon the candidate's submission of the final copies of the dissertation to the Graduate College.

I hereby certify that I have read this dissertation prepared under my direction and recommend that it be accepted as fulfilling the dissertation requirement.

_____ Date: 11/06/08
Dissertation Director: Anatoli Tumin

STATEMENT BY AUTHOR

This dissertation has been submitted in partial fulfillment of requirements for an advanced degree at The University of Arizona and is deposited in the University Library to be made available to borrowers under rules of the Library.

SIGNED: Ivan V. Shalaev

ACKNOWLEDGMENTS

I would like to sincerely thank my advisor, Anatoli Tumin, for all of his time and energy. His brilliant expertise, enthusiasm and patient guidance made this dissertation possible.

I also would like to thank my committee members, Thomas Balsa, Moysey Brio and Hermann Fasel for their valuable comments and suggestions. I am grateful to Dr. Fasel for the possibility to use the computing power of the UofA CFD laboratory and to Dr. Frank Husmeier for the help with calculations' setup. I would like to thank my office mate, Carlos Chiquete, for his useful remarks while the text was being forged.

I am most grateful to AME staff members Barbara Heefner and Dianne Smith for their hard work and joyful help.

Many thanks to all my friends from Russia and Germany and USA and Kazakhstan and France and Spain and Mexico and Ukraine and India and Madagascar for providing inspiring conversations and a great company throughout the years.

And a very special thanks to my parents, Vladimir and Raisa, and sister Tatiana for their constant love and solid support.

DEDICATION

To my parents

Table of Contents

Table of Contents—*Continued*

Table of Contents—*Continued*

List of Figures

List of Figures—*Continued*

List of Figures—*Continued*

List of Figures—*Continued*

List of Figures—*Continued*

List of Figures—*Continued*

List of Tables

List of Frequently Used Symbols

a pipe radius

$\mathbf{A}_r, \mathbf{A}_\phi, \mathbf{A}_z$ matrices in the general system of equations, Eq. (2.11), page 47

$\mathbf{C}$ matrix in the general system of equations, Eq. (2.11), page 47

$\mathbf{C}_m$ matrix in the transformed system of equations, Eq. (3.13), page 54

D dimensional velocity of detonation wave, Eq. (1.1), page 24

D_q detonation velocity scaled with the speed of sound in the quiescent gas, page 40

D_s detonation velocity scaled with the speed of sound behind the shock, page 46

D_{CJ} Chapman-Jouguet detonation velocity, Eq. (2.7), page 40

$\mathbf{D}_0$ initial-data column in the transformed system of equations, Eq. (3.13), page 54

e specific internal energy, page 37

$\tilde{E}$ dimensional activation energy, page 25

f overdrive factor, page 40

$\mathbf{F}_1, \mathbf{F}_2$ columns in the solution of the transformed system of equations, Eq. (3.18), page 56

$\mathbf{g}_r, \mathbf{g}_\phi, \mathbf{g}_t$ columns in the general system of equations, Eq. (2.11), page 47

$\mathbf{h}_r, \mathbf{h}_\phi, \mathbf{h}_t$ columns in the Rankine-Hugoniot conditions on shock, Eq. (2.12), page 48

J_n Bessel function of the first kind

$\mathbf{J}_l$ matrix of the eigenfunction expansion, Eq. (3.11), page 52

k_{nm} radial parameter, Eq. (3.9), page 52

M_s Mach number of the flow behind the shock in the frame moving with the shock wave, Eq. (2.4), page 40

n azimuthal wave number, Eq. (3.3), page 50

p pressure

Q heat release scaled with the quiescent gas temperature, page 40

$\mathbf{q}$ vector of dependent variables, page 47

$\mathbf{Q}_j$ fundamental solutions of direct problem, Eq. (3.16), page 55

$\mathbf{q}_{nm}$ solution of the transformed system of equations, Eq. (3.18), page 56

$\mathbf{q}_{DM,s}$ discrete mode corresponding to the eigenvalue τ_s, Eq. (I.2), page 123

$\tilde{Q}$ dimensional heat release of a reaction, page 25

r radial coordinate

R_{ms} receptivity coefficient corresponding to the eigenvalue τ_s, Eq. (3.25), page 60

R_g a gas constant

T temperature

t time

u velocity

V denominator in the solution, Eq. (3.23), page 58

$\mathbf{Y}$ matrix in the Rankine-Hugoniot conditions on shock, Eq. (2.12), page 48

$\mathbf{y}_j$ fundamental solutions of adjoint problem, Eq. (3.19), page 57

z axial coordinate

β heat release scaled with the temperature behind the shock, page 40

γ specific heat ratio

λ reaction progress, page 29

μ_j characteristic numbers of direct problem, Eq. (3.17), page 56

ν specific volume

ω reaction rate, page 38

ϕ azimuthal coordinate

ψ perturbation of the shock surface, page 46

ρ density

τ Laplace transform parameter, Eq. (3.4), page 50

τ_s eigenvalue, discrete spectrum, page 58

θ activation energy scaled with the temperature behind the shock, page 40

ϑ normal mode, Eq. (4.1), page 62

Superscripts

* dimensionless base flow quantity, Eq. (2.3), page 39

l laboratory system of coordinates, Eq. (2.9), page 46

T transposed vector

Subscripts

\+ after the shock wave, page 38

\- before the shock wave, page 38

0 initial disturbance, Eq. (3.1), page 49

∞ quantity at the end of the reaction zone, $z \to \infty$, page 56

ϕ azimuthal direction

b burnt gas, Eq. (1.1), page 24

n the n-th term of Fourier series, order of Bessel function, page 50

q quiescent gas, Eq. (1.1), page 24

r radial direction

s steady flow behind the shock wave, page 39

t time

z axial direction

Other Symbols

$'$ perturbation, page 47

$\bar{}$ complex conjugation

$\hat{}$ Laplace transform, Eq. (3.4), page 50

Abstract

The thesis is devoted to the investigation of the initial-value problem for linearized Euler equations utilizing an idealized one-reaction detonation model in the case of three-dimensional perturbations in a circular pipe.

The problem is solved using the Laplace transform in time, Fourier series in the azimuthal angle, and expansion into Bessel's functions of the radial variable.

For each radial and azimuthal mode, the inverse Laplace transform can be presented as an expansion of the solution into the normal modes of discrete and continuous spectra. The dispersion relation for the discrete spectrum requires solving the homogeneous ordinary differential equations for the adjoint system and evaluation of an integral through the reaction zone.

The solution of the initial-value problem gives a convenient tool for analysis of the flow receptivity to various types of perturbations in the reaction zone and in the quiescent gas.

1. Introduction

The word "detonation" comes from the Latin word *detonare* - to expend thunder. This type of combustion has been known for quite a long time. In 1747 James [2] stated that "Detonation may be look'd upon as a Kind of Calcination, perform'd in the Fire, by Means of Nitre, and other sulphureous Substances". As to experimental investigations, in 1799 it was published that "Professor Wurzer, of Bohn, ... obtained a detonation which rendered him deaf for several days" [3].

In the present consideration the combustion will be analyzed for gaseous media only. In general, there are two types of combustion waves in gases: detonation and deflagration. The latter is the most common combustion phenomenon - a deflagration wave propagates with subsonic velocity (with respect to the reactants ahead of the wave) by means of diffusion of heat and mass. The burning medium heats the adjacent region of reactants to the ignition temperature and the combustion wave moves on. The characteristics of detonation are different.

A detonation process propagates with a supersonic velocity. The general scheme is the following: reactants are adiabatically compressed by the leading shock wave, then the species undergo preparative chemical changes inside an induction zone, that comes right after the shock. The induction zone is followed by the region where the reaction processes occur, converting the prepared reactants into products - this region is called the reaction zone. The density and pressure decrease through the reaction

zone, providing the shock wave with energy to propagate further into the reactants.

Unlike the detonation in solids, the first systematic studies of detonation in gases were reported only in the end of the XIX$^{\text{th}}$ century. Two groups of French scientists examined the behavior of gaseous explosives to find the reasons of firedamp accidents in mines. In 1881 Berthelot and Vieille [4] and independently Mallard and Le Châtelier [5] published, with a two-week difference, their first experimental results. The measured reaction propagation speed was strikingly high - 2.5 kilometers per second. The subsequent work of the French scientists and the thorough experiments by Dixon [6] led to a number of theoretical models and explanations of the detonation phenomenon.

The first qualitative theory to predict detonation speed was formulated independently by Chapman [7] (in 1899) and Jouguet [8, 9] (in 1905). It is worth noting that V. A. Mikhelson was the very first person to develop a similar theory of detonation in gases. His paper was published in Russia in 1893 [10], but the publication was unknown to the non-Russian scientific world, and the theory was named after Chapman and Jouguet only.

The flow model, called the CJ model, depicts one-dimensional combustion waves propagating through a reactant that is assumed to be a perfect gas. The scheme of the flow is shown on Fig. 1.1.

Let the wave propagate with velocity D into quiescent medium of density ρ_q and pressure p_q - the initial state of gas. Then, let the reaction products have velocity

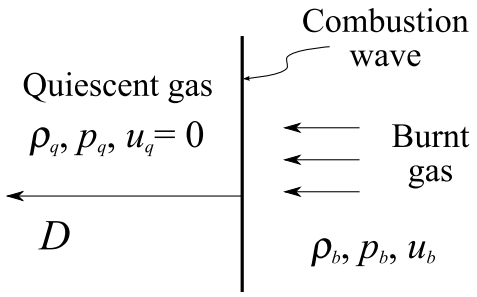

Figure 1.1: Chapman-Jouguet detonation flow scheme in a fixed laboratory system of coordinates.

u_b, density ρ_b and pressure p_b at the point where the variations of state parameters are negligible - the point of the final state of gas. Then the conservation of mass and momentum, written in the system of coordinates attached to the wave, gives

$$\begin{aligned} \rho_b \left(D - u_b\right) &= \rho_q D \\ p_b - p_q &= \rho_q u_b D \end{aligned} \tag{1.1}$$

By elimination of u_b, these two equations can be written as one:

$$\Re = \rho_q^2 D^2 - \frac{p_b - p_q}{\nu_q - \nu_b} = 0 \tag{1.2}$$

where $\nu = \rho^{-1}$ is the specific volume. In $p - \nu$ plane Eq. (1.2) describes a straight line called the "Rayleigh line" [11] which has a constant slope equal to $-\rho_q^2 D^2$, the squared mass flux per unit area.

The energy conservation condition for the wave can be written in the following

form

$$e_b + p_b\nu_b + \frac{1}{2}(D - u_b)^2 = e_q + p_q\nu_q + \frac{1}{2}D^2 \tag{1.3}$$

where $e_b = e(p_b,\ \nu_b)$, $e_q = e(p_q,\ \nu_q)$ are specific internal energies. The elimination of u_b and D from Eq. (1.3) by means of Eqs. (1.1) gives the equation of so called "Hugoniot curve" [12]:

$$\mathcal{H} = e_b - e_q - \frac{1}{2}(p_b + p_q)(\nu_q - \nu_b) = 0 \tag{1.4}$$

Therefore, the Hugoniot curve (1.4) is a rectangular hyperbola in $p - \nu$ plane.

Once the initial state parameters are given, the Hugoniot curve determines the locus of all possible final states for any detonation velocity D. For an ideal gas the equation of state and the internal energy definition can be written as

$$\begin{aligned} p\nu &= R_g T, \\ e_q &= C_{v,q} T_q = \frac{p_q \nu_q}{\gamma_q - 1}, \\ e_b &= C_{v,b} T_b - \tilde{Q} = \frac{p_b \nu_b}{\gamma_b - 1} - \tilde{Q}, \end{aligned} \tag{1.5}$$

where $\tilde{Q}$ is the reaction heat release, R_g is a gas constant, C_v is specific heat of the gas at constant volume, and $\gamma = C_p/C_v$ is specific heat ratio. From now on it is assumed, that $\gamma_q \approx \gamma_b \approx \gamma$ is known, as the chemical details of the combustion mechanisms are

rather complicated, and are beyond the scope of the present research.

The amount of heat released in a specific reaction is assumed to be constant. The value of $\tilde{Q}$ can be found with the help of standard codes, such as CEA [13] and STANJAN [14], so it is considered to be known as well.

So far, there are five unknowns, ν_b, p_b, u_b, D and e_b, for four equations, Eqs. (1.1), Eq. (1.4) and Eq. (1.5). One more constraint is needed to close the system. Further analysis of $p - \nu$ plane may provide ideas for the possible closure.

The conservation relations (1.2) and (1.4) must be satisfied all at once, so only the points of the lines' intersection on $p - \nu$ plane give the steady detonation solutions. Three possible scenarios are shown on Fig. 1.2.

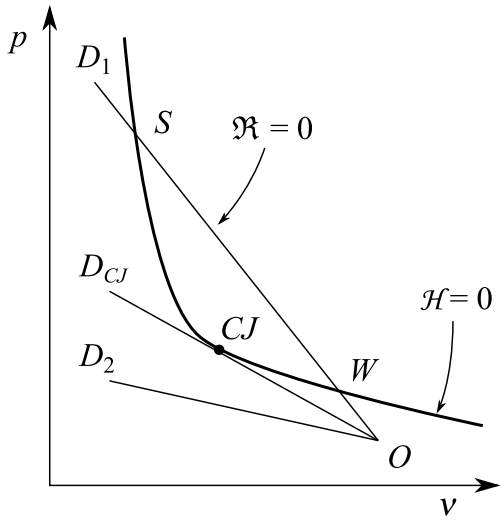

Figure 1.2: Diagram of Rayleigh lines and Hugoniot curve for Chapman-Jouguet detonation model.

For $D = D_1$ the slope of the Rayleigh line is large enough to cross the Hugoniot curve two times. So there are two solutions: a weak detonation at point W, and a

strong, or overdriven, detonation at point S. It can be shown that the final state speed for the strong solution is subsonic, $D - u < c = \sqrt{\gamma p \nu}$, while for the weak solution it is supersonic, $D - u > c$. If the Rayleigh and Hugoniot lines are tangent, $D = D_{CJ}$, then there is a unique solution called the CJ point, and for this point the final state flow is sonic, $D - u = c$. For $D = D_2$ there are no intersections, thus no detonation solution is possible for $D < D_{CJ}$.

The strong solution cannot be sustained for detonations that propagate freely: the flow at the final state is subsonic and the shock wave can be attenuated by perturbations propagating upstream to the shock [15]. Therefore, the strong solution can be neglected in the further analysis of unsupported detonations. The weak and CJ solutions are discussed below.

Chapman [7] postulated that the tangent solution, or solution with minimum velocity is the only possible detonation regime, as this velocity value agrees remarkably well with the experimental results. Jouguet [8] proposed the solution with sonic velocity of reaction products to be the correct one. Also he noted that this solution corresponds to the minimum change of entropy during the reaction. It can be shown that the arguments of Chapman and Jouguet are equivalent.

The CJ criterion of minimum velocity provides the closure for the system of Eqs. (1.1), (1.4) and (1.5). Also it allows to predict values of detonation velocity within the accuracy of several percent. Nevertheless, the postulate neither explains the exclusion of weak detonations, nor can it be justified from the physical fundamentals of the flow.

Almost forty years after the Chapman and Jouguet hypothesis, in the beginning of 1940s, Zel'dovich [16], von Neumann [17] and Döring [18] independently introduced a detonation theory that extends the CJ results by the investigation of the reaction zone.

In the ZND theory it is assumed that the shock wave is much thinner than the zone of chemical reaction. This assumption is physically reasonable, as the number of intermolecular collisions that can bring a molecule to a mechanical equilibrium is much lower than the number of collisions that can initiate a chemical reaction. The scheme of ZND detonation structure is shown on Fig. 1.3.

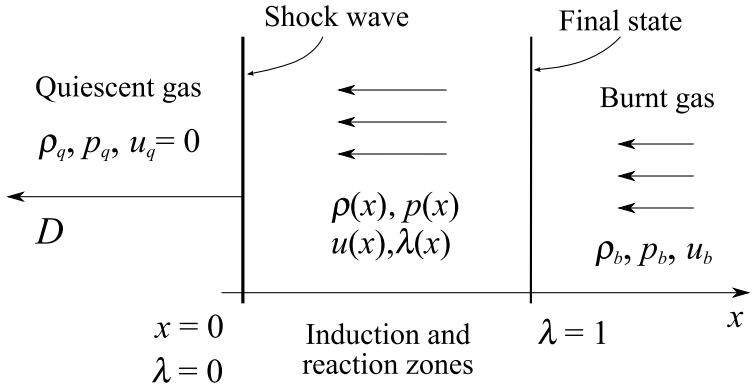

Figure 1.3: ZND detonation flow scheme in a fixed laboratory system of coordinates.

The reaction progress, λ, in the quiescent gas ahead of the wave is zero, $\lambda = 0$. The shock that leads the wave is a jump discontinuity that adiabatically compresses the gas. The shock is followed by the induction zone where the dissociation processes develop and the matter is converted to the reacting state with a slight variation of thermodynamic parameters, i.e. density and pressure. The induction zone is followed

by the reaction zone that ends at the final state plane, the same as in CJ model. The flow in the reaction zone is steady in the coordinate system connected to the shock. The shock and the reaction zone propagate together at the detonation velocity D.

As the solution is steady between the shock and the final state, the conservation of mass and momentum are the same as for CJ model. The equations (1.1) hold between any points in the assumed constant state. The energy definition now depends on the reaction progress variable λ that varies from 0 for the fresh mixture, to 1 for completely burnt medium:

$$e\left(p,\ \nu,\ \lambda\right) = \frac{p\nu}{\gamma - 1} - \lambda\tilde{Q}, \tag{1.6}$$

and the Eq. (1.4) is transformed to the form

$$\mathcal{H} = e\left(p,\ \nu,\ \lambda\right) - e\left(p_q,\ \nu_q,\ 0\right) - \frac{1}{2}\left(p + p_q\right)\left(\nu_q - \nu\right) = 0 \tag{1.7}$$

The $p - \nu$ diagram for the generalized energy equation is shown on Fig. 1.4.

The detonation is steady through the reaction zone, so there is only one value for the velocity of shock wave. Thus the single variable λ defines the state completely as the state point moves down the Rayleigh line. On Fig. 1.4 it is shown that immediately behind the shock the state point is N, that lies on the Hugoniot curve $\lambda = 0$ (the gas is compressed adiabatically). As the reaction proceeds the state point

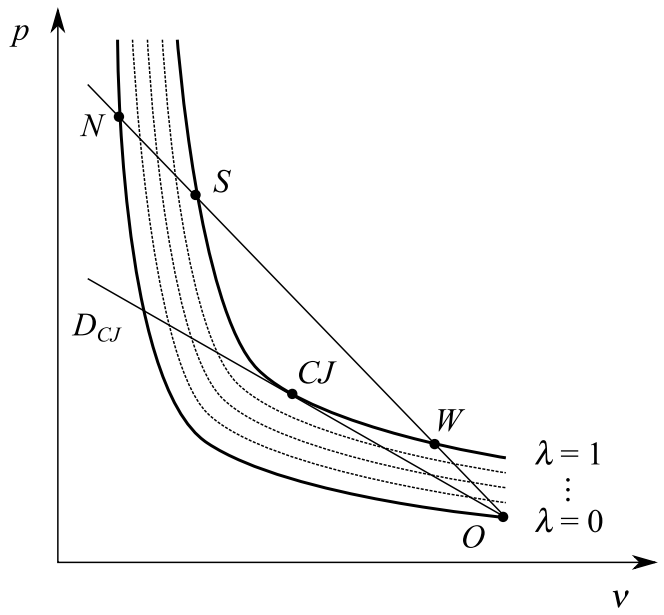

Figure 1.4: Diagram of Rayleigh lines and Hugoniot curves for ZND detonation model.

moves down the Rayleigh line until the end of reaction zone at point S. At each point on the Rayleigh line between N and S there is a unique value of λ determined from the Hugoniot relation. The corresponding values of p and ν can be found from conservation conditions (1.2) and (1.7).

Thus the state is completely specified at every point between the initial point N and the point of the strong detonation regime S. The strong solution is excluded for an unsupported detonation, so the only possible option for the detonation to exist is the tangency point, or CJ regime. For the case of the overdriven detonation, both CJ and strong solutions are possible. However, the weak solution W is still obtainable, but only in the case when the partially reacted Hugoniot curves ($0 < \lambda < 1$) intersect each other [17]. Such cases are called pathological detonations [15] and are beyond

the scope of present analysis.

The ZND theory adopts an inviscid flow model. To show that the omission of viscous effects is reasonable, the estimate of Reynolds number should be performed. It can be done from the intermolecular collision point of view [19] as follows.

Using the Boltzmann distribution law, the probability for one molecule to achieve an energy E in one collision is estimated as $\exp\left(-\tilde{E}/RT\right)$, where R is universal gas constant. Therefore, the required number of collisions can be estimated as $n_{col} \approx \exp\left(\tilde{E}/RT\right)$. The velocity of the medium behind the shock can be written as $D - u_s \approx c_s$, where c_s is the sound speed behind the shock. The length of the reaction zone can be estimated as $\Delta \approx l_{fp} n_{col}$, where l_{fp} is a mean free path of a particle in the reaction zone. Let ν_s be the kinematic viscosity of the gas behind the shock wave, and the viscosity can be estimated as $\nu_s \approx c_s l_{fp}$. The Reynolds number estimate is then

$$Re_s = \frac{(D - u_s)\,\Delta}{\nu_s} \approx \frac{c_s \Delta}{c_s l_{fp}} \approx n_{col} \tag{1.8}$$

and, for the typical values of activation energy, $\tilde{E} = 50$ kcal/mole, and temperature $T = 2000$ K, the number of collisions is estimated as $n_{col} \approx 3 \cdot 10^5 >> 1$, therefore, the inviscid flow model is valid for the investigations of detonation phenomenon.

The one-dimensional ZND theory is the base of theoretical detonation research even today. However, the experiments show that the nature of detonation is essentially three-dimensional. The so-called spinning detonation is an example of the phenomenon's complexity. In 1926, Campbell and Woodhead [20] observed that det-

onation in circular pipes exhibits a highly luminous region which traces a helical path along the walls of the pipe at a nearly constant angular frequency.

Later it was shown that for normally detonating mixtures the spin detonation regime is the only possible detonation regime near the limits of propagation of the shock [19]. Lee [15] called the spinning detonation "... nature's last resort for maintaining the detonation mode of combustion for most mixtures". The structure of the phenomenon was studied carefully and comprehensively by Voitsekhovskiy, Mitrofanov and Topchiyan [21] and Schott [22].

The detonation waves are considered to be intrinsically unstable. Williams [23] states that "few, if any, real combustible gas mixtures admit stable planar Chapman-Jouguet waves": the loss of stability leads to three-dimensional structures in the flow. The investigation of detonation instability mechanisms, even with the implementation of one-dimensional ZND theoretical model, can provide the physical explanation of the variety of experimental results.

The analysis of detonation stability was initiated by Shchelkin in 1959 [24]. He considered the simplified model of the phenomenon called square-wave detonation: the shock is followed by an induction zone with constant thermodynamic parameters, and the reaction is completed instantaneously at the end of the induction zone. The similar flow behavior can be achieved at the limit of large activation energies, $E \to \infty$.

The qualitative results of Shchelkin were followed by work of Zaidel who performed the conventional stability analysis of the square-wave model in 1961 [25]. The review

of the square-wave model analysis was presented by Erpenbeck in 1963 [26], where it was shown that the model leads to an enumerable infinite set of discrete modes that may have an arbitrary large growth rate in time. However, even with the existence of the growing modes, the square-wave model is attractive due to its simplicity.

In 1980s Buckmaster with coworkers performed the asymptotic analysis of the square-wave detonation, for $E \to \infty$ (see [27], [28]). The calculated spectrum of the problem still possessed the modes with unbounded growth rate. Nevertheless, the numerical studies of detonations with high activation energies performed by Short in 1997 [29] depicted the reasonable agreement, in a certain range of parameters, between the asymptotical analysis of the square-wave model and the stability calculations based on ZND flow model.

The stability analysis of the steady ZND detonation was established by J.J. Erpenbeck in series of papers in 1960s. The first paper [30] treated the initial-value problem for the linearized reactive Euler equations for a one-reaction unbounded flow. The base steady state was considered as one-dimensional overdriven ZND flow and the perturbations were assumed to be three-dimensional and time-dependent. The system of partial differential equations was converted to an inhomogeneous ODE system by means of Fourier transform in spatial transverse coordinates and Laplace transform in time. It was shown that the solution may have poles at the right-hand side of the Laplace variable plane and thus the flow may be unstable. The dispersion relation for the poles was formulated in explicit form but was not solved numerically. Instead,

Erpenbeck [31] used the principle of argument in order to establish the existence of the poles in the case of idealized one-reaction detonations.

In his works Erpenbeck studied the stability of step shocks [32], the case of two-reaction detonation [33], the stability problem with zero activation energy [34], and with the transverse spatial wavelength limit $2\pi/\varepsilon \rightarrow 0$ (where ε is the transverse wave number) [35]. Also he treated the nonlinear stability problem for one- and two-dimensional detonations [36, 37]. The summary of the detonation stability research over the decade can be found in the Erpenbeck's paper published in 1969 [38].

Another method to deal with the stability problem is the normal-mode approach. In this method the perturbations are assumed to depend exponentially on time, $\exp(\tau t)$ where τ has to be determined. The system of partial differential (Euler) equations is converted to an inhomogeneous system of ordinary differential equations in the shock-attached coordinates. The boundary conditions are set both on the shock and at the end of the reaction zone. In 1963 Pukhnachev [39, 40] applied this technique to the problem of idealized CJ detonation in round pipes. Abouseif and Toong [41] gave an approximate linear one-dimensional analysis for the normal mode instabilities.

In 1990 Lee and Stewart [42] investigated the one-dimensional detonation expansion into normal modes, providing the thorough analysis of the neutral stability boundaries and the behavior of the unstable spectra in the space of the heat release Q, activation energy E and overdrive factor f. They integrated the ODE system start-

ing with the post-shock values ($x = 0_+$) for the velocity, pressure, specific volume, and reaction progress perturbations. At the end of the reaction zone ($x \to +\infty$), the solution's boundedness constraint was formulated as an algebraic relation for the perturbations. This constraint served as the dispersion relation, solved with the help of a shooting algorithm in order to find the eigenvalue τ. The initial guess for the shooting procedure was provided by means of a "carpet search" technique. The analysis was extended to the two-dimensional perturbations by Sharpe [43] and Short and Stewart [1]. The normal mode analysis of detonation stability in a confined cylindrical geometry was performed by Kasimov and Stewart [44].

The thorough overview of detonation research and stability investigations can be found in the book by Wildon Fickett and William C. Davis [45]. The recently published work of John H. S. Lee [15] considers the detonation phenomenon from its physical fundamentals and gives the present state-of-art in the detonation research.

The normal-mode approach had been used in hydrodynamic stability theory for a long time before Morkovin [46] and Reshotko [47] showed that the receptivity problem also plays important role in understanding of the flow response mechanics. The possible strategy is to solve the initial value problem corresponding to a system of partial differential equations describing the flow. This method involves the Laplace transform in time to obtain the formal solution. The inverse Laplace transform leads to an expansion of the solution into normal modes of continuous and discrete spectra. The mode weights correspond to receptivity of the flow to the given initial perturbation.

The example of the application of this technique is given in the paper of Forgoston and Tumin [48], where the method is applied to solve the initial value problem in hypersonic boundary layers. Tumin [49] revisited the Erpenbeck's approach by solving the initial-value problem for one-dimensional idealized detonation and showing that the acquired discrete spectrum is equivalent to the spectrum of the conventional normal mode analysis.

The initial-value problem for detonation in a circular pipe has not been considered yet. Erpenbeck [38] stated that this problem "involves some unsolved complications".

The objectives of the present work are the following: to solve the initial-value problem for three-dimensional perturbations in a circular pipe in idealized planar one-reaction detonation wave and to solve the receptivity problem for different types of initial disturbances.

Chapter 2 of this dissertation is devoted to the formulation of the problem, consideration of steady-state solutions and derivation of the governing equations for perturbations. In Chapter 3 the initial-value problem is formulated and the transformation of the system of governing partial differential equations to the ODE system is shown. In Chapter 4 the discrete spectrum of the problem is considered. Chapter 5 is devoted to the spectrum calculations. Chapter 6 represents the numerical results of receptivity analysis for different types of initial perturbations. The explicit form of equations, supplemental derivations and numerical results can be found in Appendices.

2. Problem Formulation

2.1 Governing Equations

The inviscid flow described by the Euler equations for a reactive gas is considered in this section. An ideal gas participates in a first-order, irreversible reaction without mole and specific heat change. It means that the number of moles of the reactant is negligible with respect to the total number of moles present in the pipe.

Thus, the gas constant, R_g, and the specific heat ratio, γ, are the same for the quiescent gas and in the reaction zone. We consider three-dimensional perturbations in a one-dimensional base flow. One can state the continuity, momentum, energy and the reaction progress equations in the laboratory frame as follows:

$$\begin{aligned} &\frac{D\rho}{Dt^l} + \rho\nabla^l \cdot \mathbf{u}^l = 0 \\ &\frac{D\mathbf{u}^l}{Dt^l} + \frac{1}{\rho}\nabla^l p = 0 \\ &\frac{Dh}{Dt^l} - \frac{1}{\rho}\frac{\partial p}{\partial t^l} = 0 \\ &\frac{D\lambda}{Dt^l} = \omega \end{aligned} \tag{2.1}$$

where ρ, p, and $\mathbf{u}^l$ are the density, pressure and velocity respectively; $D/Dt^l = \partial/\partial t^l + \mathbf{u}^l \cdot \nabla^l$ is the substantial derivative and superscript 'l' indicates the laboratory frame quantities. The total enthalpy is $h = e + p/\rho + {\mathbf{u}^l}^2/2$, where $e = p/(\gamma\rho - \rho) - \lambda\tilde{Q}$

is the specific energy for an ideal polytropic gas, λ is the reaction progress variable (λ is equal to zero in the quiescent gas, and grows to unity for the completely burnt mixture), and $\tilde{Q}$ is the dimensional heat release.

The first-order reaction rate is assumed in the form $\omega = \tilde{k}(1-\lambda)\exp(-\tilde{E}/R_g T)$, where $\tilde{E}$ is the dimensional activation energy, T is the temperature, and $\tilde{k}$ is a normalization constant. The system of equations is supplemented by the equation of state for an ideal gas, $p = \rho R_g T$. The energy equation can be rewritten in terms of pressure as

$$\frac{Dp}{Dt^l} + \gamma p \nabla^l \cdot \mathbf{u}^l - (\gamma - 1)\,\tilde{Q}\rho\omega = 0$$

The shock wave is considered as a discontinuity with Rankine-Hugoniot jump conditions:

$$\rho\left(\mathbf{u}^l - \mathbf{D}^l\right)\cdot\mathbf{n}\big|_+ = \rho\left(\mathbf{u}^l - \mathbf{D}^l\right)\cdot\mathbf{n}\big|_- = m$$

$$p_+ - p_- = m^2\left(\frac{1}{\rho_-} - \frac{1}{\rho_+}\right)$$

$$\mathbf{u}^l\cdot\mathbf{t}_1\big|_+ = 0, \quad \mathbf{u}^l\cdot\mathbf{t}_2\big|_+ = 0 \tag{2.2}$$

$$\frac{p_+}{(\gamma-1)\,\rho_+} - \frac{p_-}{(\gamma-1)\,\rho_-} = \frac{1}{2}\left(p_+ + p_-\right)\left(\frac{1}{\rho_-} - \frac{1}{\rho_+}\right)$$

$$\lambda_+ = \lambda_-$$

where subscript '+' stands for the parameters in the media after the shock wave, and subscript '−' corresponds to the parameters of quiescent media before the shock wave. The vector $\mathbf{n}$ is the unit normal, and vectors $\mathbf{t}_1$, $\mathbf{t}_2$ are independent unit tangents to the shock surface. The vector $\mathbf{D}^l = \mathbf{n}D$ is the shock velocity.

We use the parameters of the steady one-dimensional flow for scaling of the governing equations and the conditions on the shock. Density of the steady flow, ρ_s, its pressure, p_s, and the speed of sound behind the shock, c_s are the dimensional scales of the problem. The half-reaction zone length, l_c, is the characteristic length scale: it is the distance from the shock to the point where the reaction progress variable reaches the value of one half. The time scale is represented by ratio, $t_c = l_c/c_s$.

2.2 Steady State

We use cylindrical coordinate system, where the laboratory frame variables are r^l, ϕ^l, z^l, t^l - radial, angular, axial coordinates and time respectively, and the wave propagates along the axial coordinate z^l heading to $z^l = -\infty$. The steady-state parameters can be found from the system of conservation laws stated in a frame moving with the shock [50, 30]. The dimensionless distributions of pressure, p^*, velocity, u_z^*, and density, ρ^*, are written as

$$p^* = b_1 + (1 - b_1)\sqrt{1 - b_2\beta\lambda^*}, \quad u_z^* = \frac{1 - p^*}{\gamma M_s} + M_s, \quad \rho^* = \frac{M_s}{u_z^*} \tag{2.3}$$

where superscript '$*$' indicates the steady-state values, M_s is the Mach number of the flow behind the shock in the frame moving with the shock wave, and b_1, b_2 are

constants:

$$M_s = \frac{(\gamma-1)\,D_q^2+2}{2\gamma D_q^2-\gamma+1}, \quad b_1 = \frac{1+\gamma D_q^2}{2\gamma D_q^2-(\gamma-1)}, \quad b_2 = \frac{2\gamma M_s^2\,(\gamma-1)}{(1-b_1)^2\,(\gamma+1)} \tag{2.4}$$

The steady dimensionless detonation velocity, D_q, is scaled with the speed of sound in the quiescent gas. The dimensionless heat release, $\beta = \tilde{Q}/R_g T_s$, is based on the temperature behind the shock, T_s. The dimensionless reaction rate, ω^*, is defined as

$$\omega^* = k\,(1-\lambda^*)\exp\left(-\theta/T^*\right) \tag{2.5}$$

where $\theta = \tilde{E}/R_g T_s$ is the dimensionless activation energy, and k is the constant determined from the scaling:

$$k = \int_0^{1/2} \frac{u_z^*}{1-\lambda^*}\exp\left(\theta/T^*\right) d\lambda^*. \tag{2.6}$$

The steady-state flow is characterized by the overdrive factor $f = \left(D_q/D_{CJ}\right)^2$, where

$$D_{CJ} = \sqrt{1+\frac{(\gamma^2-1)\,Q}{2\gamma}} + \sqrt{\frac{(\gamma^2-1)\,Q}{2\gamma}} \tag{2.7}$$

is the Chapman-Jouguet detonation velocity scaled with the speed of sound in the quiescent gas (the shock Mach number), and $Q = \tilde{Q}/R_g T_q$ is the dimensionless heat

release scaled with the quiescent gas temperature, T_q. Another important steady-state parameter is the dimensionless activation energy scaled with T_q, $E = \tilde{E}/R_g T_q$. Also, it is convenient to express the reaction progress variable, λ^*, as a function of distance from the shock wave, z. The integration of the last equation in (2.1) gives the necessary relationship:

$$z = \int_0^{\lambda^*} \frac{u_z^*(\lambda)}{\omega^*(\lambda)} d\lambda = \frac{1}{k} \int_0^{\lambda^*} \frac{u_z^*(\lambda)}{1-\lambda} \exp\left(\rho^* \theta / p^*\right) d\lambda \tag{2.8}$$

Equations (2.3)-(2.8) completely describe the steady base flow according to the ZND detonation model. The examples of the steady flow parameters' behavior are given below.

Figures 2.1-2.4 illustrate the reaction progress variable λ^* as a function of z, and the flow parameters as functions of λ^*.

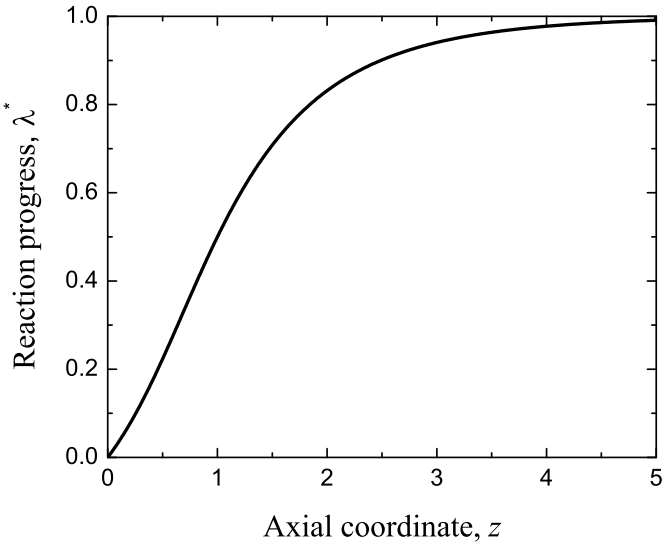

(a) Reaction progress, λ^*

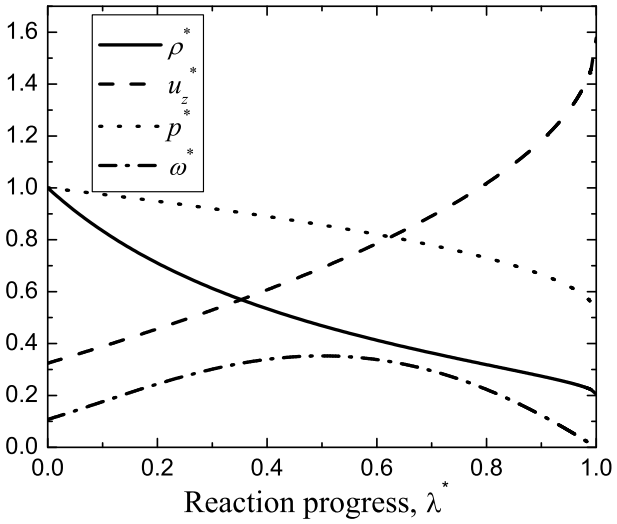

(b) Density, ρ^*, velocity, u_z^*, pressure, p^*, reaction rate, ω^*

Figure 2.1: Steady state profiles, $\gamma = 1.2$, $f = 1$, $Q = 50$, $E = 20$.

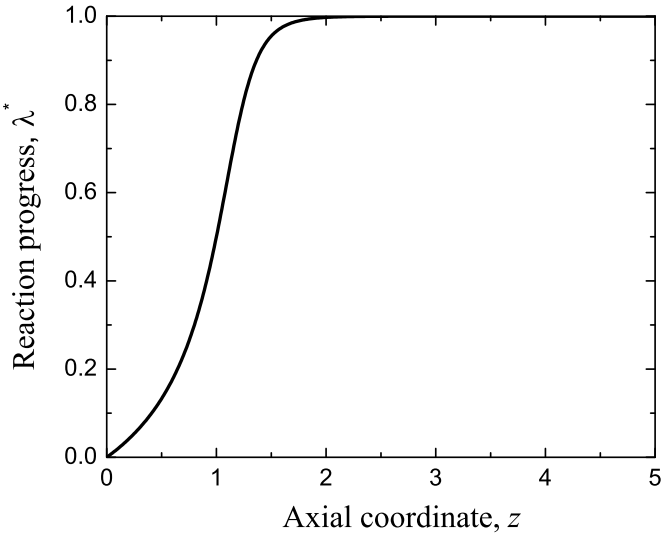

(a) Reaction progress, λ^*

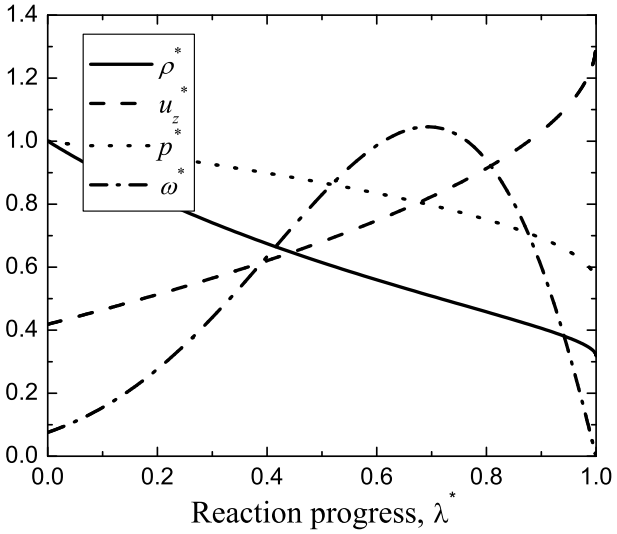

(b) Density, ρ^*, velocity, u_z^*, pressure, p^*, reaction rate, ω^*

Figure 2.2: Steady state profiles, $\gamma = 1.2$, $f = 1$, $Q = 10$, $E = 20$.

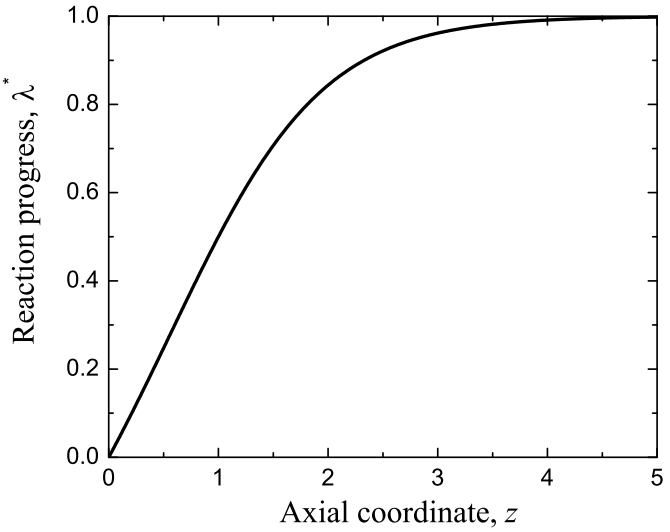

(a) Reaction progress, λ^*

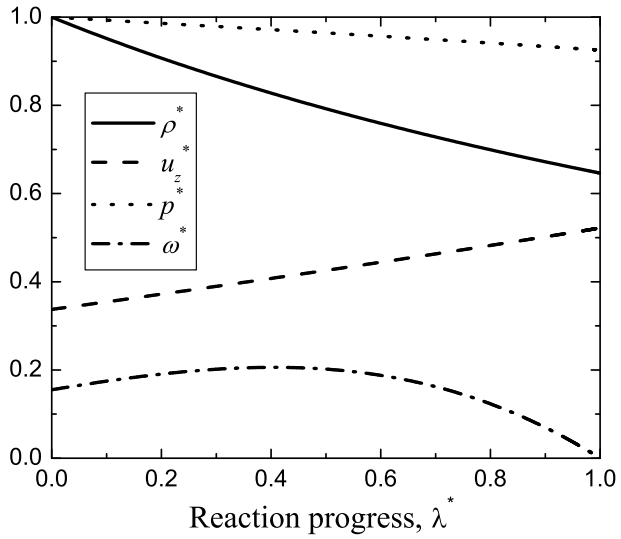

(b) Density, ρ^*, velocity, u_z^*, pressure, p^*, reaction rate, ω^*

Figure 2.3: Steady state profiles, $\gamma = 1.2$, $f = 3$, $Q = 10$, $E = 20$.

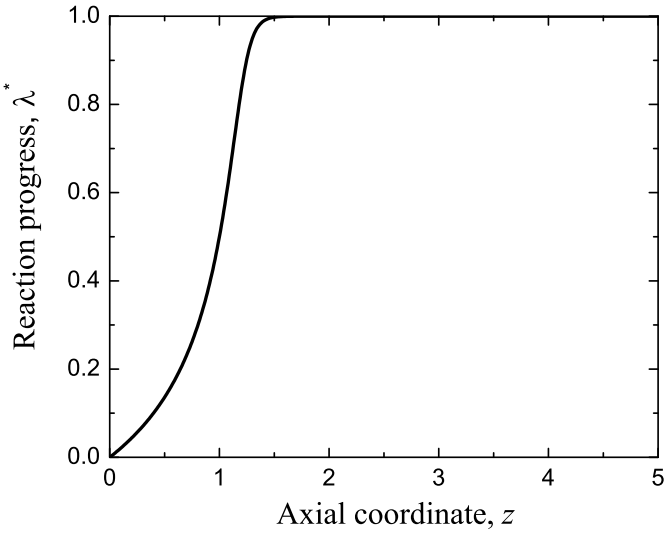

(a) Reaction progress, λ^*

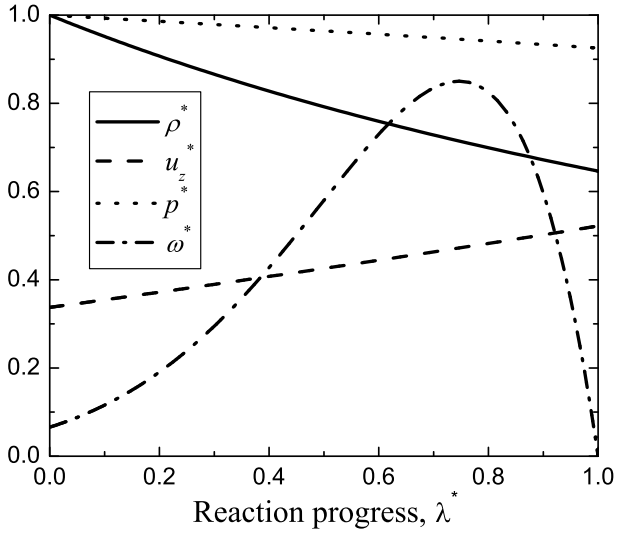

(b) Density, ρ^*, velocity, u_z^*, pressure, p^*, reaction rate, ω^*

Figure 2.4: Steady state profiles, $\gamma = 1.2$, $f = 3$, $Q = 10$, $E = 60$.

2.3 Governing Equations for Perturbations

The governing system of equations (2.1) is linearized over the steady-state mean flow. First, the coordinate system is shifted from the laboratory frame to the one attached to the perturbed shock. The transformation to the shock-attached frame is done as follows:

$$t = t^l, \quad r = r^l, \quad \phi = \phi^l, \quad z = z^l - D_s t - \psi\left(r,\ \phi,\ t\right) \tag{2.9}$$

where $D_s < 0$ is the detonation velocity scaled with the speed of sound behind the shock, and $\psi\left(r,\ \phi,\ t\right)$ is the perturbation of the shock surface. The perturbation ψ is included into the coordinate transformation because the derivatives of the base flow in axial direction, d/dz, are not equal to zero. Therefore, a shift of the shock is accompanied by perturbations of local parameters stemming from the non-uniformity of flow in z direction. The particle velocity is measured with respect to the unperturbed shock wave frame:

$$u_z = u_z^l - D_s. \tag{2.10}$$

In principle, one can measure velocity with respect to the perturbed shock as it was introduced in [44]. However, this choice is not crucial because it leads just to redefinition of the streamwise velocity perturbation.

The six dependent variables - density, three velocity components, pressure and reaction progress can be written in vector notation as $\mathbf{q} = \left(\rho,\ u_r,\ u_\phi,\ u_z,\ p,\ \lambda\right)^T$

(superscript T stands for transposed). The perturbation is introduced as

$$\mathbf{q} = \mathbf{q}^* + \mathbf{q}'$$

where $\mathbf{q}^* = (\rho^*,\ 0,\ 0,\ u_z^*,\ p^*,\ \lambda^*)^T$ is the base flow vector determined in the previous section, and $\mathbf{q}' = \left(\rho',\ u_r',\ u_\phi',\ u_z',\ p',\ \lambda'\right)^T$ is the perturbation vector. Before the linearization with respect to disturbances, $\mathbf{q}'$ and ψ, the progress rate ω is expanded in Taylor series about the steady-state solution,

$$\omega = \omega^* + \frac{\partial \omega^*}{\partial \rho^*}\rho' + \frac{\partial \omega^*}{\partial p^*}p' + \frac{\partial \omega^*}{\partial \lambda^*}\lambda' + ...$$

After the linearization procedure, the governing equations (2.1) are recast in the shock-attached system of coordinates as follows

$$\frac{\partial \mathbf{q}'}{\partial t} + \mathbf{A}_r\frac{\partial \mathbf{q}'}{\partial r} + \mathbf{A}_\phi\frac{1}{r}\frac{\partial \mathbf{q}'}{\partial \phi} + \mathbf{A}_z\frac{\partial \mathbf{q}'}{\partial z} + \mathbf{C}\mathbf{q}' - \mathbf{g}_t\frac{\partial \psi}{\partial t} - \mathbf{g}_r\frac{\partial \psi}{\partial r} - \mathbf{g}_\phi\frac{1}{r}\frac{\partial \psi}{\partial \phi} = 0 \qquad (2.11)$$

where $\mathbf{A}_r$, $\mathbf{A}_\phi$, $\mathbf{A}_z$, and $\mathbf{C}$ are 6×6 matrices. The column vectors $\mathbf{g}_t$, $\mathbf{g}_r$, and $\mathbf{g}_\phi$ depend on the axial gradients of the base flow. If ρ^*, u_z^*, p^* and λ^* are constant, then the column vectors disappear and the shock perturbation ψ does not appear in the governing equations. In this case, one can also exclude ψ from the coordinate transformation (2.9). The matrices and vectors of the system (2.11) are presented in

Appendix A.

The linearized Rankine-Hugoniot conditions on the shock can be written in the form

$$\begin{aligned}\mathbf{q}'\left(r,\phi,z=0_+,t\right) =&\mathbf{Y}\mathbf{q}'\left(r,\phi,z=0_-,t\right)+\\ &+\mathbf{h}_t\frac{\partial\psi\left(r,\phi,t\right)}{\partial t}+\mathbf{h}_r\frac{\partial\psi\left(r,\phi,t\right)}{\partial r}+\mathbf{h}_\phi\frac{1}{r}\frac{\partial\psi\left(r,\phi,t\right)}{\partial\phi}\end{aligned} \tag{2.12}$$

Matrix $\mathbf{Y}$ and vectors $\mathbf{h}_t$, $\mathbf{h}_r$ and $\mathbf{h}_\phi$ are presented in Appendix B. One can recognize from Eq. (2.12) that the perturbation introduced in the quiescent gas, $\mathbf{q}'\left(r,\phi,z=0_-,t\right)$, enters the problem as the boundary condition depending on time. The vector $\mathbf{q}'\left(r,\phi,z=0_-,t\right)$ is treated as known, because the perturbations in the fresh mixture can be determined rather easily.

3. Initial-value Problem

We consider the solution of Eq. (2.11) that satisfies the following initial condition:

$$t = 0: \quad \mathbf{q}'(r,\, \phi,\, z,\, 0) = \mathbf{q}_0(r,\, \phi,\, z), \quad \psi(r,\, \phi,\, 0) = \psi_0(r,\, \phi) \tag{3.1}$$

where $\mathbf{q}_0 = (\rho_0,\, u_{r,0},\, u_{\phi,0},\, u_{z,0},\, p_0,\, \lambda_0)^T$ is the initial disturbance that satisfies the Rankine-Hugoniot condition on the shock. The term ψ_0 represents the initial perturbation of the shock surface. Also we impose the non-penetration boundary condition on the wall of the pipe:

$$r = a: \quad u_r'(a,\, \phi,\, z,\, t) = 0 \tag{3.2}$$

where a stands for the radius of the pipe.

3.1 Fourier and Laplace Transforms of the Perturbation Equations

We begin with the expansion of the perturbations in Fourier series with respect to the azimuthal variable ϕ:

$$\begin{aligned}
\mathbf{q}'(r,\ \phi,\ z,\ t) &= \frac{1}{2\pi}\sum_n \mathbf{q}_n(r,\ z,\ t)\exp(in\phi),\\
\mathbf{q}_0(r,\ \phi,\ z) &= \frac{1}{2\pi}\sum_n \mathbf{q}_{0,n}(r,\ z)\exp(in\phi);\\
\psi(r,\ \phi,\ t) &= \frac{1}{2\pi}\sum_n \psi_n(r,\ t)\exp(in\phi),\\
\psi_0(r,\ \phi) &= \frac{1}{2\pi}\sum_n \psi_{0,n}(r)\exp(in\phi)
\end{aligned} \tag{3.3}$$

where n is an azimuthal wave number. Then, applying the Laplace transform with respect to time:

$$\begin{aligned}
\hat{\mathbf{q}}_n(r,\ z,\ \tau) &= \int_0^\infty \mathbf{q}_n(r,\ z,\ t)\, e^{-\tau t}dt\\
\hat{\psi}_n(r,\ \tau) &= \int_0^\infty \psi_n(r,\ t)\, e^{-\tau t}dt
\end{aligned} \tag{3.4}$$

we arrive to the following system:

$$\begin{aligned}
\tau\hat{\mathbf{q}}_n + \mathbf{A}_r\frac{\partial\hat{\mathbf{q}}_n}{\partial r} + \mathbf{A}_\phi\frac{in}{r}\hat{\mathbf{q}}_n + \mathbf{A}_z\frac{\partial\hat{\mathbf{q}}_n}{\partial z} + \mathbf{C}\hat{\mathbf{q}}_n - \tau\mathbf{g}_t\hat{\psi}_n - \mathbf{g}_r\frac{\partial\hat{\psi}_n}{\partial r} - \mathbf{g}_\phi\frac{in}{r}\hat{\psi}_n =\\
= \mathbf{q}_{0,n} - \mathbf{g}_t\psi_{0,n}
\end{aligned} \tag{3.5}$$

The shock conditions, Eq. (2.12), are recast as follows:

$$\begin{aligned}\hat{\mathbf{q}}_n\left(r,\ z=0_+,\ \tau\right) =& \mathbf{Y}\hat{\mathbf{q}}_n\left(r,\ z=0_-,\ \tau\right)+ \\ &+\mathbf{h}_t\left(\tau\hat{\psi}_n\left(r,\ \tau\right)-\psi_{0,n}\left(r\right)\right)+\mathbf{h}_r\frac{\partial\hat{\psi}_n\left(r,\ \tau\right)}{\partial r}+\mathbf{h}_\phi\frac{in}{r}\hat{\psi}_n\left(r,\ \tau\right)\end{aligned} \tag{3.6}$$

3.2 Eigenfunction Expansion

The inhomogeneous system of equations (3.5) is solved with the help of the eigenfunction expansion method [51]. Consideration of the homogeneous system (3.5) leads to the separation of variables in the following form:

$$\hat{\mathbf{q}}_n\left(r,\ z,\ \tau\right)=\begin{pmatrix}\rho_n\left(z,\ \tau\right)R\left(r\right)\\ u_{r,n}\left(z,\ \tau\right)U_r\left(r\right)\\ u_{\phi,n}\left(z,\ \tau\right)U_\phi\left(r\right)\\ u_{z,n}\left(z,\ \tau\right)U_z\left(r\right)\\ p_n\left(z,\ \tau\right)P\left(r\right)\\ \lambda_n\left(z,\ \tau\right)\Lambda\left(r\right)\end{pmatrix},\ \hat{\psi}_n\left(r,\ \tau\right)=\psi_n\left(\tau\right)\Psi\left(r\right) \tag{3.7}$$

We substitute this form of variables into the homogeneous system of equations and arrive to the Bessel equations for the functions R, U_r, U_ϕ, U_z, P, Λ and Ψ that depend on radius r and the separation constant k. The explicit form of separation is the following [44, 52]:

$$\begin{aligned}R\left(r\right)=U_z\left(r\right)=P\left(r\right)=\Lambda\left(r\right)=\Psi\left(r\right)=J_n\left(kr\right),\\ U_r\left(r\right)=\frac{dJ_n\left(kr\right)}{dr},\quad U_\phi\left(r\right)=\frac{J_n\left(kr\right)}{r},\end{aligned} \tag{3.8}$$

where $J_n(kr)$ is a Bessel function of the first kind. The azimuthal index n is the order of the Bessel functions. The boundary condition (3.2) leads to the discrete spectrum of k_{nl} that is found from the equation

$$\left.\frac{dJ_n(k_{nl}r)}{dr}\right|_{r=a} = 0 \tag{3.9}$$

where subscript l stands for the number of the root of this equation.

Therefore, we are looking for a solution of inhomogeneous system (3.5) in the form of the eigenfunction expansion:

$$\hat{\mathbf{q}}_n(r,\ z,\ \tau) = \sum_{l=1}^{\infty} \begin{pmatrix} \rho_{nl}(z,\ \tau)\, J_n(k_{nl}r) \\ u_{r,nl}(z,\ \tau)\, k_{nl} J_n'(k_{nl}r) \\ u_{\phi,nl}(z,\ \tau)\, J_n(k_{nl}r)/r \\ u_{z,nl}(z,\ \tau)\, J_n(k_{nl}r) \\ p_{nl}(z,\ \tau)\, J_n(k_{nl}r) \\ \lambda_{nl}(z,\ \tau)\, J_n(k_{nl}r) \end{pmatrix},\ \hat{\psi}_n(r,\ \tau) = \sum_{l=1}^{\infty} \psi_{nl}(\tau)\, J_n(k_{nl}r) \tag{3.10}$$

or in matrix-vector form

$$\hat{\mathbf{q}}_n(r,\ z,\ \tau) = \sum_{l=1}^{\infty} \mathbf{J}_l(r)\, \mathbf{q}_{nl}(z,\ \tau) \tag{3.11}$$

where $\mathbf{J}_l$ is the 6×6 expansion matrix shown in Appendix C.

The values of roots $k_{nl}a$ are shown in Table 3.1.

	$n=0$	1	2	3	4	5	6	7
$l=1$	3.8317	1.8412	3.0542	4.2012	5.3176	6.4156	7.5013	8.5778
2	7.0156	5.3314	6.7061	8.0152	9.2824	10.5199	11.7349	12.9324
3	10.1735	8.5363	9.9695	11.3459	12.6819	13.9872	15.2682	16.5294
4	13.3237	11.706	13.1704	14.5859	15.9641	17.3128	18.6374	19.9419

Table 3.1: Roots $k_{nl}a$ of Eq. (3.9), where l represents number of the root, n is the order of Bessel function.

3.3 Equations for the Amplitude Functions

The eigenfunctions for the case of the ordinary circular pipe are the Bessel functions of the first kind. The functions have the following orthogonality property [53]:

$$\begin{gathered}\int_0^a J_n\left(k_{nl}r\right) J_n\left(k_{nm}r\right) r dr = \delta_{lm} d_m \\ d_m = \frac{k_{nm}^2 a^2 - n^2}{2k_{nm}^2} J_n^2\left(k_{nm}a\right)\end{gathered} \tag{3.12}$$

where δ_{lm} is the Kronecker delta, and k_{nm} is the m-th root of Eq. (3.9). With the help of the condition (3.12) the equations for the amplitude functions of the expansion (3.10) can be derived as

$$\mathbf{A}_z \frac{d\mathbf{q}_{nm}}{dz} + \left(\tau\mathbf{I} + \mathbf{C}_m\right)\mathbf{q}_{nm} - \left(\tau\mathbf{g}_t + \mathbf{g}_r + in\mathbf{g}_\phi\right)\psi_{nm} = \mathbf{D}_0\left(z\right) \tag{3.13}$$

This is an inhomogeneous system of ordinary differential equations with the axial coordinate z as an independent variable. The 6×6 coefficient matrix $\mathbf{C}_m$ and the initial-data vector $\mathbf{D}_0$ are given in Appendix D.

The main difficulty in derivation of the system (3.13) is the appearance of terms with an infinite sum in the continuity and the energy equations. The treatment of the term and the derivation of Eq. (3.13) are given in Appendix E.

The fully transformed shock condition is written as

$$\begin{aligned}\mathbf{q}_{nm}\left(z=0_{+},\,\tau\right)=&\mathbf{Y}\mathbf{q}_{nm}\left(z=0_{-},\,\tau\right)+\\&+\mathbf{h}_{t}\left(\tau\psi_{nm}\left(\tau\right)-\psi_{0,nm}\right)+\left(\mathbf{h}_{r}+in\mathbf{h}_{\phi}\right)\psi_{nm}\left(\tau\right),\end{aligned}\tag{3.14}$$

where $\psi_{0,nm}$ is the coefficient of the initial shock perturbation.

3.4 Solution of the Amplitude Function System

We are searching for the bounded solution of the initial-value problem (3.13)-(3.14). In order to write down the solution of Eq. (3.13) that satisfies the shock boundary condition (3.14) and is bounded at $z\rightarrow\infty$, we can implement the method of variation of parameters. That is we need to analyze the fundamental solutions of the homogeneous system (3.13) at $z\rightarrow\infty$. From now on, we consider overdriven detonation ($f>1$) to avoid singularities in the inverse of matrix $\mathbf{A}_{z}$. The homogeneous system is written as

$$\frac{d\mathbf{q}_{nm}}{dz}+\mathbf{A}_{z}^{-1}\left(\tau\mathbf{I}+\mathbf{C}_{m}\right)\mathbf{q}_{nm}=0\tag{3.15}$$

The system has six fundamental solutions: $\mathbf{Q}_{j}$, $j=1,...,6$. We consider the analytical behavior of the solutions at $z\rightarrow\infty$ in the following form [30]

$$\mathbf{Q}_{j}\left(z\right)=\mathbf{Q}_{j\infty}\exp\left(\mu_{j}z\right)\tag{3.16}$$

where the characteristic numbers μ_j can be written as

$$\begin{aligned}
\mu_1 &= \frac{u_\infty^* \tau + c_\infty \sqrt{\tau^2 + k_{nm}^2 c_\infty^2 \left(1 - M_\infty^2\right)}}{c_\infty^2 \left(1 - M_\infty^2\right)}, \\
\mu_2 &= \frac{u_\infty^* \tau - c_\infty \sqrt{\tau^2 + k_{nm}^2 c_\infty^2 \left(1 - M_\infty^2\right)}}{c_\infty^2 \left(1 - M_\infty^2\right)}, \\
\mu_3 &= \mu_4 = \mu_5 = -\frac{\tau}{u_\infty^*},\ \mu_6 = -\frac{\tau + C_\infty^{(66)}}{u_\infty^*},
\end{aligned} \tag{3.17}$$

where $C_\infty^{(66)}$ is the element of matrix $\mathbf{C}_m$ at $z \to \infty$; the mean velocity, u_∞^*, the speed of sound, c_∞, and the Mach number, M_∞, correspond to the flow parameters in the burnt gas.

For the overdriven case, $M_\infty < 1$, one can see that the first fundamental solution, $\mathbf{Q}_1(z)$, is unbounded at $z \to \infty$ as $\mathrm{Re}(\mu_1) > 0$ for $\mathrm{Re}(\tau) > 0$. The other fundamental solutions decay exponentially downstream from the shock wave. The amplitude vectors $\mathbf{Q}_{j\infty}$, $j = 1, ..., 6$ are presented in Appendix F.

Using these properties of the fundamental solutions, one can write down the bounded solution of Eq. (3.13) in the following form:

$$\begin{aligned}
&\mathbf{q}_{nm}(z,\ \tau) = \sum_{j=2}^{6} \left(a_j + \int_0^z (\mathbf{y}_j,\ \mathbf{F})\, dz' \right) \mathbf{Q}_j + \mathbf{Q}_1 \int_\infty^z (\mathbf{y}_1,\ \mathbf{F})\, dz', \\
&\mathbf{F} = \mathbf{F}_1 + \mathbf{F}_2 \psi_{nm},\ \mathbf{F}_1 = \mathbf{A}_z^{-1} \mathbf{D}_0,\ \mathbf{F}_2 = \mathbf{A}_z^{-1} \left(\tau \mathbf{g}_t + \mathbf{g}_r + in \mathbf{g}_\phi \right),
\end{aligned} \tag{3.18}$$

where $\mathbf{y}_j$ are fundamental solutions of the adjoint system of equations:

$$\frac{d\mathbf{y}}{dz} - \left[\mathbf{A}_z^{-1}\left(\bar{\tau}\mathbf{I} + \bar{\mathbf{C}}_m\right)\right]^T \mathbf{y} = 0 \tag{3.19}$$

where the bar stands for complex conjugation. The dot product is defined as $(\mathbf{y}, \mathbf{F}) = \sum_{i=1}^{6} \bar{y}_i F_i$, with $\bar{y}_i$ and F_i being the i-th components of vectors $\mathbf{y}$ and $\mathbf{F}$ respectively.

The fundamental solution, $\mathbf{y}_j$, of Eq. (3.19) can be obtained as a vector that is composed of cofactors of the j-th column of the matrix of the fundamental solutions $\mathbf{Q} = [\mathbf{Q}_1,\ \mathbf{Q}_2, ...,\ \mathbf{Q}_6]$ and is divided by $\det(\mathbf{Q})$ [54] with complex conjugation. Therefore, the fundamental solutions have the following property:

$$(\mathbf{y}_j, \mathbf{Q}_k) = \delta_{jk}, \quad j, k = 1, ..., 6 \tag{3.20}$$

where δ_{jk} is Kronecker delta. At $z \to \infty$, the adjoint fundamental solutions can be written in exponential form: $\mathbf{y}_j(z) = \mathbf{y}_{j\infty} \exp(-\bar{\mu}_j z)$, $j = 1, ..., 6$. The amplitude vectors, $\mathbf{y}_{j\infty}$, are given in Appendix G.

The coefficients $a_2, ..., a_6$ and the shock displacement ψ_{nm} can be found from the boundary conditions on shock, Eq. (3.14). Particularly, the shock displacement can

be represented as a ratio:

$$\psi_{nm} = -\frac{U}{V} = -\frac{\left(\mathbf{y}_1\left(0\right),\ \mathbf{Y}\mathbf{q}_{nm}\left(0_-\right) - \mathbf{h}_t\psi_{0,nm}\right) + \int_0^\infty \left(\mathbf{y}_1,\ \mathbf{F}_1\right) dz}{\left(\mathbf{y}_1\left(0\right), \tau\mathbf{h}_t + \mathbf{h}_r + in\mathbf{h}_\phi\right) + \int_0^\infty \left(\mathbf{y}_1, \mathbf{F}_2\right) dz} \tag{3.21}$$

where the denominator V depends on τ and k_{nm}.

As the coefficients and the shock displacement are known (see Appendix H), the solution (3.18) is known as well, and therefore, applying the expansion (3.10), we can write the formal solution of the initial-value problem as the inverse Laplace transform

$$\mathbf{q}_n\left(r, z, t\right) = \frac{1}{2\pi i}\int_{\sigma-i\infty}^{\sigma+i\infty} \hat{\mathbf{q}}_n\left(r, z, \tau\right) e^{\tau t} d\tau, \tag{3.22}$$

where the path of integration lies on the right-hand side of singularities of $\hat{\mathbf{q}}_n$.

The solution $\hat{\mathbf{q}}_n$ may have singularities on the complex plane τ, where the denominator in Eq. (3.21) is equal to zero:

$$V\left(\tau, k_{nm}\right) = \left(\mathbf{y}_1\left(0\right), \tau\mathbf{h}_t + \mathbf{h}_r + in\mathbf{h}_\phi\right) + \int_0^\infty \left(\mathbf{y}_1, \mathbf{F}_2\right) dz = 0 \tag{3.23}$$

Roots of Eq. (3.23), τ_s, were of the main interest for Erpenbeck [30, 31]. The limited power of computers at that time should explain why he did not try to solve Eq. (3.23) directly. Although zeros of V in the complex plane τ were associated with unstable modes, Erpenbeck did not discuss closing of the path of integration in Eq.

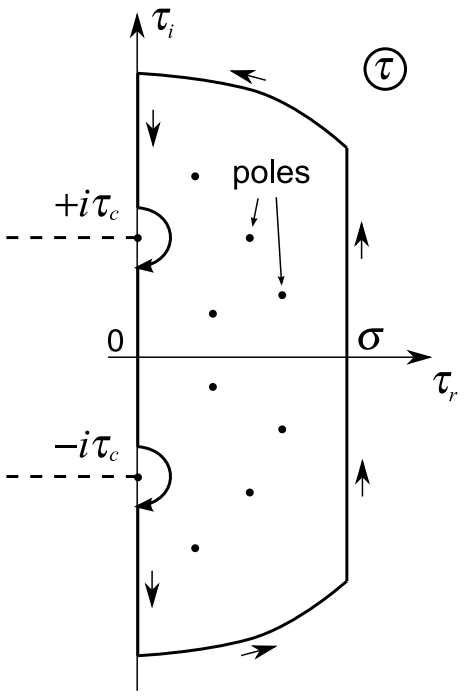

Figure 3.1: The integration path in an evaluation of the inverse Laplace transform with respect to τ.

(3.22) to explain how the residue values at the poles will originate in the solution. In addition to the poles, there are two branch points, as μ_1 and μ_2 of the solution (3.18) contain the square root of a complex number, $\sqrt{\tau^2 + k_{nm}^2 c_\infty^2 (1 - M_\infty^2)}$. Therefore, the branch points are located at $\tau = \pm i\tau_c = \pm i k_{nm} c_\infty \sqrt{1 - M_\infty^2}$. These points represent acoustic cut-off frequencies of the problem: the acoustic perturbations with $-\tau_c < \mathrm{Im}\,(\tau) < \tau_c$ die out exponentially [55].

In order to evaluate the inverse Laplace transform (3.22), one may consider a closure of the integration path. One of the options is shown on Fig. 3.1, where the path is kept at $\mathrm{Re}\,(\tau) \geq 0$. This choice provides the bounded solution at $z \to \infty$, and the result of the integration can be represented as a sum of the residue values

associated with roots of Eq.(3.23) and an integral along the imaginary axis, $\mathrm{Im}\,(\tau)$,

$$\mathbf{q}_n\,(r,z,t)=\sum_{m,s}\mathbf{J}_m R_{ms}\mathbf{q}_{DM,s}\,(z,k_{nm},\tau_s)\,e^{\tau_s t}+\frac{1}{2\pi i}\int_{-i\infty}^{i\infty}\sum_m \mathbf{J}_m\mathbf{q}_{nm}\,(z,k_{nm},\tau)\,e^{\tau t}d\tau \tag{3.24}$$

If a pole occurs on the imaginary axis, the path has to be deformed around the pole keeping $\mathrm{Re}\,(\tau)>0$. Tumin [49] showed that the choice of the path around the poles on the imaginary axis is crucial for constructing a solution consistent with the causality principle.

The result, Eq. (3.24), can be interpreted as an expansion of the solution of the initial-value problem into the modes of discrete and continuous spectra. The vectors $\mathbf{q}_{DM,s}$ in Eq. (3.24) are the discrete modes, and their weights, R_{ms}, are the receptivity coefficients:

$$R_{ms}=-\frac{\left[\left(\mathbf{y}_1\,(0)\,,\ \mathbf{Y}\mathbf{q}_{nm}\,(0_-)-\mathbf{h}_t\psi_{0,nm}\right)+\int_0^\infty\left(\mathbf{y}_1,\ \mathbf{F}_1\right)dz\right]_{\tau=\tau_s}}{\left(\partial V/\partial\tau\right)_{\tau=\tau_s}} \tag{3.25}$$

The derivation of R_{ms} and $\mathbf{q}_{DM,s}$ is given in Appendix I.

The modes of continuous spectrum come from fundamental solutions $\mathbf{Q}_1,...,\mathbf{Q}_6$ evaluated at $\tau=il$, where l is a real parameter (angular frequency). Their physical interpretation can be given based on the asymptotic behavior at $z\to\infty$. For example, the fundamental solution $\mathbf{Q}_1$ represents the upstream acoustic mode. One can see that the solution, Eq. (3.18), does not have the upstream acoustic mode at $z\to\infty$,

whereas the mode does exist upstream of the introduced initial perturbation. The fundamental solution $\mathbf{Q}_2$ represents the downstream acoustic wave, whereas $\mathbf{Q}_3$, $\mathbf{Q}_4$ and $\mathbf{Q}_5$ represent two vorticity modes and the entropy mode.

At some fixed value of coordinate z, one also may consider a closure in the left-hand side of the complex plane τ, as shown on Fig. 3.2. In this case, the input from the continuous spectrum will be reduced to evaluation of integrals along the branch cuts. Although the solution can also have poles at $\mathrm{Re}\,(\tau) < 0$, their input will be exponentially small for $t \to \infty$.

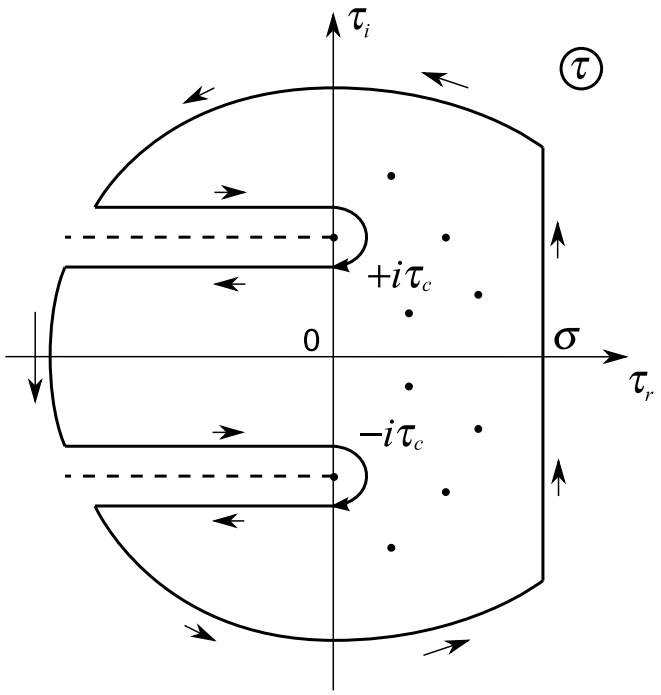

Figure 3.2: An alternative integration path in an evaluation of the inverse Laplace transform with respect to τ for a fixed value of z.

4. Discrete Spectrum

We begin the consideration of the discrete modes with the analysis of the normal-mode approach to the problem.

The conventional normal mode analysis of stability of detonations in a circular pipe [44] could be formulated in the shock-attached coordinate system as the following inhomogeneous system of ordinary differential equations (with $\psi_{nm} = 1$):

$$\mathbf{A}_z \frac{d\vartheta}{dz} + (\tau \mathbf{I} + \mathbf{C}_m)\,\vartheta = \tau \mathbf{g}_t + \mathbf{g}_r + in\mathbf{g}_\phi \tag{4.1}$$

with the initial condition at the shock

$$\vartheta\,(0_+) = \tau \mathbf{h}_t + \mathbf{h}_r + in\mathbf{h}_\phi \tag{4.2}$$

In the normal mode analysis, it is assumed that there is the following relation between the azimuthal and radial velocity components:

$$u_{\phi,nm}\,(z) = inu_{r,nm}\,(z) \tag{4.3}$$

and the system of equations (4.1) is reduced to a system of five equations. One can recognize that Eq. (4.3) means zero axial vorticity of the normal modes.

It can be shown that after exclusion of $u_{\phi,nm}(z)$ and the third equation in (4.1), the system of equations will be the same as the system of Eqs. (27) in the paper by Kasimov and Stewart [44] (up to the difference in the definition of the streamwise velocity perturbation: $u_{z,nm}$ in the present work is equal to $u'_z + \tau$ in [44]).

Solution of Eqs. (4.1) has to be bounded at $z \to \infty$. Kasimov [52] derived a radiation condition in a differential form taking into account that in the leading order the perturbation of the reaction progress variable, λ_{nm}, is negligible in the burnt gas. Thus, Eqs. (4.1), initial conditions (4.2) together with the radiation condition at $z \to \infty$, that will be discussed later, represent an eigenvalue problem for discrete spectrum $\tau = \tau_s$.

Following Tumin [49], one can show that the discrete spectrum in the normal mode analysis is equivalent to the discrete spectrum stemming from the initial-value problem formulation, i.e., to the roots of Eq. (3.23). The analysis is given in Appendix H.

The vectors $\mathbf{q}_{DM,s}$, that are the parts of the initial-value problem solution (3.24), are also the solution of the system (4.1)-(4.2) and are bounded at $z \to \infty$. Therefore, $\mathbf{q}_{DM,s}$ are equivalent to eigenfunctions stemming from the normal mode analysis. The discussion of $\mathbf{q}_{DM,s}$ is given in Appendix I.

Because the solution (3.24) does not include $\mathbf{Q}_1$ at $z \to \infty$, and the adjoint solution $\mathbf{y}_1$ is orthogonal to the other fundamental solutions, $\mathbf{Q}_2, ..., \mathbf{Q}_6$, the rear boundary

condition (the radiation condition) can be written straightforwardly as

$$\lim_{z\to\infty} (\mathbf{y}_1,\ \mathbf{q}_{nm}) = 0 \tag{4.4}$$

Using the first adjoint fundamental solution (G.1), one can write the radiation condition as the following algebraic relation at $z \to \infty$:

$$u_{r,nm}k_{nm}^2 u_\infty^* + \tau u_{z,nm} - p_{nm}\frac{1}{\gamma\rho_\infty^* c_\infty}\sqrt{\tau^2 + c_\infty^2\left(1-M_\infty^2\right)k_{nm}^2} + \\ + \frac{\lambda_{nm}C_\infty^{(56)}u_\infty^*\left[\tau^2 - u_\infty^{*2}k_{nm}^2\right]}{\gamma\rho_\infty^*\left[u_\infty^{*2}c_\infty^2 k_{nm}^2 - \tau c_\infty^2 C_\infty^{(66)} - \tau^2 c_\infty^2 + C_\infty^{(66)}u_\infty^* c_\infty\sqrt{\tau^2 + c_\infty^2\left(1-M_\infty^2\right)k_{nm}^2}\right]} = 0 \tag{4.5}$$

The perturbation of the reaction progress variable, λ_{nm}, is exponentially small in the burnt gas. Thus, the leading order of the radiation condition will be:

$$u_{r,nm}k_{nm}^2 u_\infty^* + \tau u_{z,nm} - p_{nm}\frac{1}{\gamma\rho_\infty^* c_\infty}\sqrt{\tau^2 + c_\infty^2\left(1-M_\infty^2\right)k_{nm}^2} = 0 \tag{4.6}$$

The main difference between the perturbations in a circular pipe and the perturbations in an unbounded domain, studied in [30, 31, 29, 1, 56] is that the perturbations confined in a pipe have discrete spectrum of the radial modes associated with zeros in Eq. (3.9). For a given pipe radius, the radial eigenfunctions are determined by the discrete values of k_{nm}, $m = 1, 2, ...$ However, the eigenvalue problem in z direction,

Eqs. (4.1), (4.2), and (4.6), is independent of the pipe radius itself. It means that "z eigenvalue problem" for τ_j, that determines growth rate of the perturbation in time, should be the same for the pipe detonations and for detonations in an unbounded domain. The transformations,

$$k_{nm}^2 u_{r,nm} = -iku_2', \; k_{mn} = k \tag{4.7}$$

where u_2' is the velocity component that is perpendicular to the mean flow direction (in notation used in [29, 1, 56]) and k is the corresponding wave number, establish the equivalence of the eigenvalue problems in a circular pipe [44, 52] and in an unbounded domain [29, 1, 56].

In the case of an unbounded domain, parameter k is a real parameter representing the Fourier transform in direction perpendicular to the mean flow. Having applied the transformation (4.7) to the radiation condition (4.6) and skipping indexes, one can find

$$-iku_2'u_\infty^* + \tau u_z - p\frac{1}{\gamma\rho_\infty^* c_\infty}\sqrt{\tau^2 + c_\infty^2\left(1 - M_\infty^2\right)k^2} = 0 \tag{4.8}$$

The constraint (4.8) was derived in [27] and was used in [29, 1] for the analysis of three-dimensional perturbations.

5. Spectrum Calculations

For the numerical implementation, we solve the reduced systems of differential equations of the direct, Eq. (4.1), and adjoint, Eq. (3.19), problems. Both systems contain five differential equations obtained by exclusion of the third component of the direct solution $\mathbf{q}_{nm}$, and by deletion of the third component of the adjoint solution $\mathbf{y}$, respectively.

The direct problem was solved numerically starting from the shock conditions (4.2) and finishing at some point $z = z_{max}$ situated far from any changes of flow characteristics. After obtaining the solution, the radiation condition, Eq. (4.6), was used to find the eigenvalue.

The adjoint problem was solved in a different way: we started with the asymptotic solution, Eq. (G.1), as an initial data at $z = z_{max}$, and integrated the equations toward the shock, $z = 0_+$. Then we used the dispersion relation (3.23) to find an eigenvalue. Both approaches, direct and adjoint, led to the same set of eigenvalues.

The direct and adjoint eigenvalue problems were solved by means of an iterative algorithm based on Newton's method. The initial guess for the Newton's method was supplied by code based on multi-domain spectral collocation method (SCM). Further details of the implemented numerical methods are discussed in Appendix K.

In the case of one-dimensional perturbations, the SCM technique was utilized with the rear-boundary condition included into the algorithm [57]. The inclusion was

possible because the boundary condition was a linear function of the eigenvalue τ. Fig. 5.1 illustrates the eigenvalue map for one-dimensional perturbations obtained with the help of three-domain SCM at $f = \gamma = 1.2$, $E = Q = 50$. Number of polynomials for each domain in this example is $N = 100$.

In the case of three-dimensional perturbations, the rear-boundary condition (4.6) cannot be expressed in a form of polynomial with powers of τ. Therefore, the conventional methods ([58, 59]), that are developed for problems where eigenvalues appear in a nonlinear form, cannot be applied and we had to enforce homogeneous boundary conditions on the perturbation at some large distance z_{max}. Such boundary condition brings the discretized continuous spectrum (along the imaginary axis) into the map together with spurious modes.

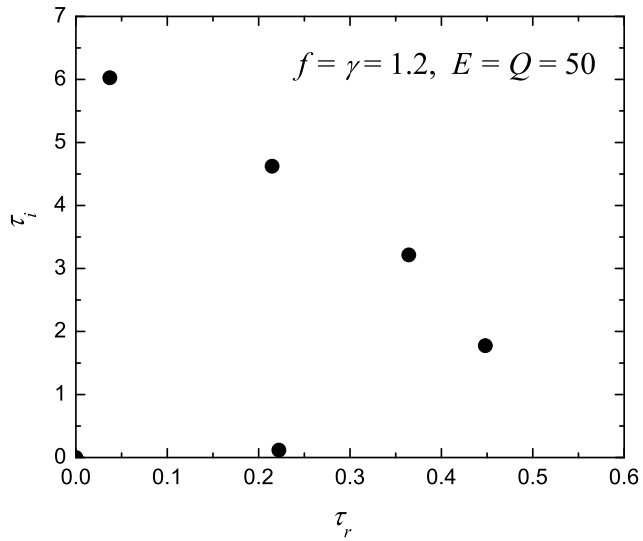

Figure 5.1: Eigenvalue map for one-dimensional perturbations obtained with the help of three-domain spectral collocation method.

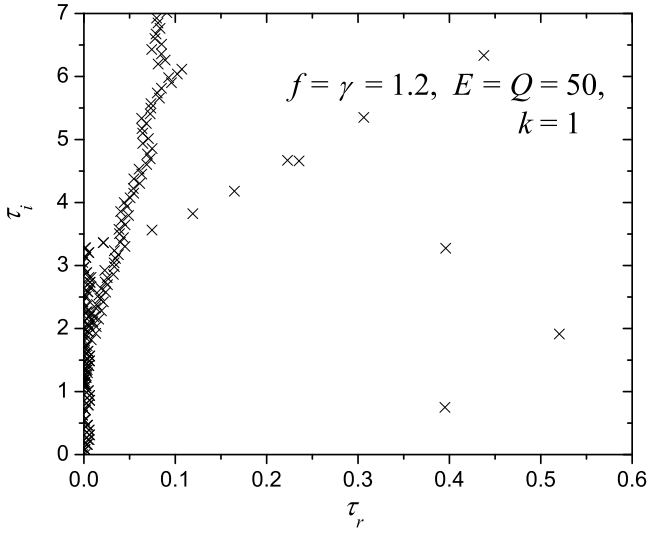

Figure 5.2: Eigenvalue map for three-dimensional perturbations obtained with the help of three-domain spectral collocation method.

The spectrum for three-dimensional perturbations is displayed on Fig. 5.2 for the following set of parameters: $f = 1.2$, $\gamma = 1.2$, $E = Q = 50$ and $k = 1$ (because k_{nm} in this analysis is a parameter, we omit the subscripts of the azimuthal mode and the radial modes numbers): there are four distinct discrete unstable modes and discretized continuous spectrum. One more discrete mode is hidden among the atomized debris.

Figure 5.3 shows the behavior of function based on the radiation condition equation (4.6):

$$RC\left(z\right) = k^2 u_{\infty}^{*} u_{r,nm}\left(z\right) + \tau u_{z,nm}\left(z\right) - p_{nm}\left(z\right) \frac{1}{\gamma \rho_{\infty}^{*} c_{\infty}} \sqrt{\tau^2 + c_{\infty}^2 \left(1 - M_{\infty}^2\right) k^2}, \quad (5.1)$$

where parameter $k = 1$, and the considered eigenvalue is $\tau = \tau_r + i\tau_i = 0.39516 +$

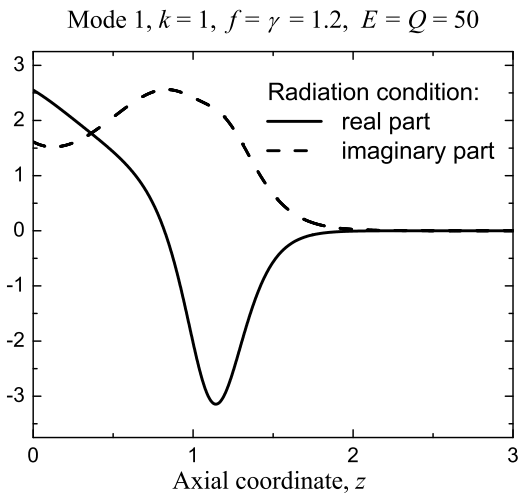

Figure 5.3: Real and imaginary parts of the function $RC\,(z)$, Eq. (5.1).

$i0.74902 = \tau_{M1}$ - the mode with the lowest frequency τ_i on Fig. 5.2. The function $RC\,(z)$ can be used as an indicator: if RC vanishes for large z values, then the eigenvalue really belongs to the discrete spectrum.

Figure 5.4 demonstrates the real and imaginary parts of the eigenfunction $\mathbf{q}_{nm} = (\rho_{nm},\ u_{r,nm}\,,\ u_{z,nm},\ p_{nm},\ \lambda_{nm})^T$ that corresponds to the eigenvalue τ_{M1}. Numbers in the legends indicate the components of the eigenfunction vector $\mathbf{q}_{nm}$.

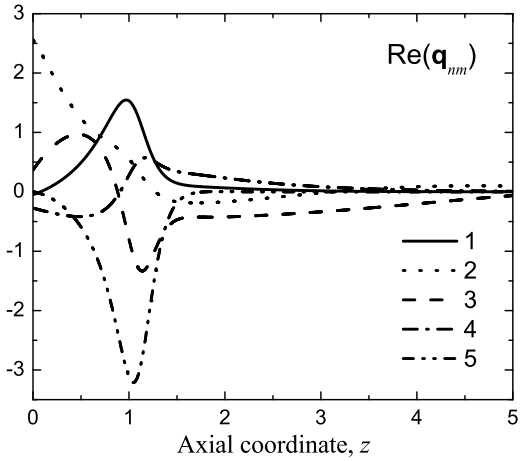

(a)

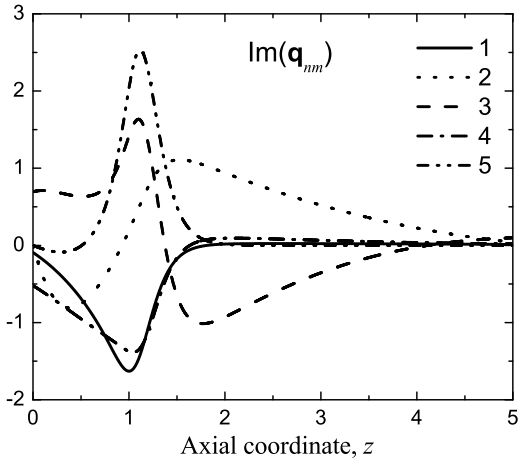

(b)

Figure 5.4: Real (a) and imaginary (b) parts of the eigenfunctions at $\tau = 0.39516 + i0.74902$, $f = 1.2$, $\gamma = 1.2$, $E = Q = 50$ and $k = 1$. Numbers 1 through 5 indicate components of the vector $\mathbf{q}_{nm}$.

Figure 5.5 shows the real and imaginary parts of the adjoint solution, $\mathbf{y}$, at the same parameters as in Fig. 5.4.

Figure 5.6 illustrates dependence of the eigenvalues on the parameter k for nine modes. One may compare these plots with Figures 7a and 7b in paper of [1], respectively. The comparison simply illustrates the statement that the spectra of the z eigenvalue problem for a circular pipe and an unbounded domain are equivalent. The lines represent results obtained from the analysis of both direct and adjoint problems, whereas the symbols represent the results of [1].

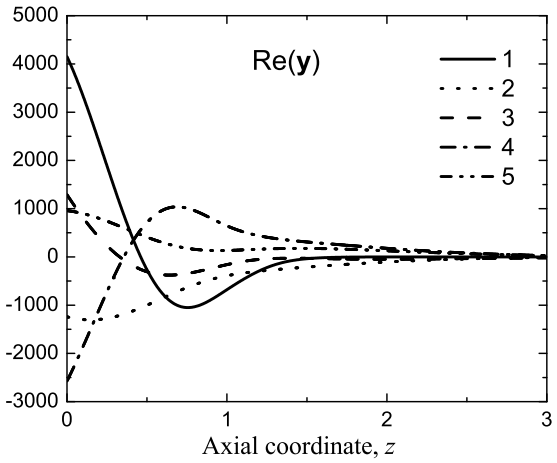

(a)

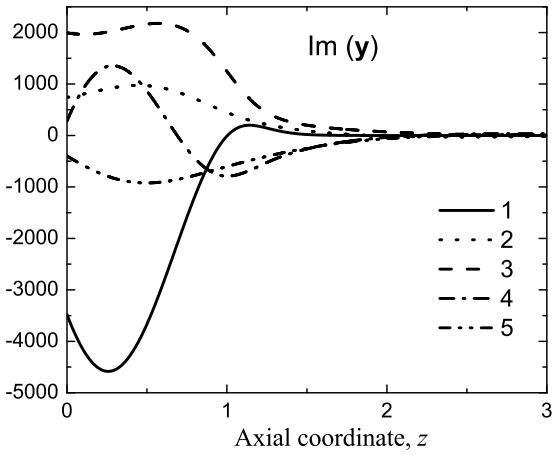

(b)

Figure 5.5: Real (a) and imaginary (b) parts of the eigenfunctions of adjoint problem at $\tau = 0.39516 + i0.74902$, $f = 1.2$, $\gamma = 1.2$, $E = Q = 50$ and $k = 1$. Numbers 1 through 5 indicate components of the vector $\mathbf{y}$.

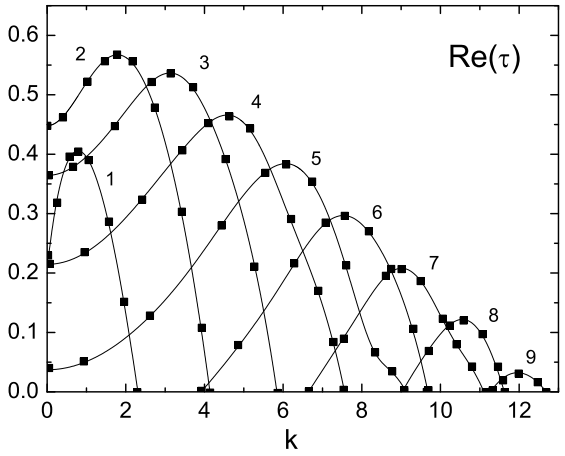

(a)

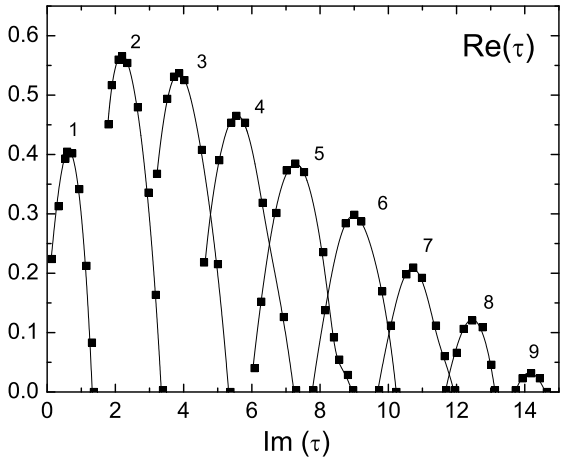

(b)

Figure 5.6: Stability spectrum showing (a) $\mathrm{Re}\,(\tau)$ vs k and (b) $\mathrm{Im}\,(\tau)$ vs $\mathrm{Re}\,(\tau)$ for the nine unstable modes at $f = \gamma = 1.2$, $E = Q = 50$. Lines - results from analysis of the direct and adjoint problems; the symbols - the results of [1].

6. Receptivity Analysis

6.1 Initial Perturbations Placed in Quiescent Gas

6.1.1 Axial Vorticity Perturbation

The first case to be investigated is an azimuthal velocity perturbation, u'_ϕ, localized in the pipe at $z \in [-z_2, -z_1]$, where $z = 0$ is the shock location. The medium inside the interval rotates with constant speed w. The perturbation at the shock location can be written as a function of time as

$$u'_\phi (r, \phi, z = 0_-, t) = (H(t - t_1) - H(t - t_2))\, wr, \tag{6.1}$$

where H is a Heaviside function, t_1 is the time that takes the shock wave to arrive to the point $-z_1$, $t_1 = z_1/D_s$, t_2 is the time when the shock arrives to the end-point of perturbation, $-z_2$, and $t_2 = z_2/D_s$.

In other words, the rigid-body rotation of a localized portion of quiescent gas which is approached by the shock wave of speed D_s is considered in this section.

The transformed perturbation, after Fourier expansion and Laplace transformation, has the following form:

$$\hat{u}_{\phi,0} (r, z = 0_-, \tau) = \frac{wr}{\tau} \left(e^{-\tau t_1} - e^{-\tau t_2} \right). \tag{6.2}$$

There is no dependence on ϕ, therefore the only nonzero coefficient of Fourier expansion (3.3) is the coefficient with azimuthal index $n = 0$.

The Bessel expansion of the azimuthal component of velocity is shown in Appendix E, and the transformed initial perturbation is

$$\begin{aligned} u_{\phi,0m}\left(z = 0_{-}\right) =& a_{0m}\frac{w}{\tau}\left(\exp\left(-\tau t_1\right) - \exp\left(-\tau t_2\right)\right), \\ a_{0m} =& \frac{1}{d_{0m}}\int_0^a J_0\left(k_{0m}r\right) r^3 dr, \end{aligned} \tag{6.3}$$

note that $r = \sum_m a_{0m} J_0\left(k_{0m}r\right)/r$, and k_{0m} are the roots of Eq. (3.9).

For the considered perturbation the azimuthal index $n = 0$, therefore, the axial vorticity term (E.27) is equal to zero. The receptivity coefficient (3.25) is found to be zero as well with the help of the properties of the matrix $\mathbf{Y}$ and the fundamental vector $\mathbf{y}_1$. Thus, the solution of the initial-value problem does not include discrete modes.

The azimuthal velocity component can be derived as

$$u_{\phi,0m}\left(z,\tau\right) = u_{\phi,0m}\left(z = 0_{-}\right)\exp\left(\int_0^z -\frac{\tau}{u_z^*}dz'\right), \tag{6.4}$$

and all other components of the amplitude solution (3.18) are equal to zero. The

general solution of the initial-value problem, Eq. (3.24), can be written as

$$u'_\phi(r,z,t) = wr\left[H\left(t - t_1 - \int_0^z \frac{dz'}{u_z^*}\right) - H\left(t - t_2 - \int_0^z \frac{dz'}{u_z^*}\right)\right]. \qquad (6.5)$$

The perturbation dynamics is the following: the rotating portion of fresh gas is reached by the detonation shock, squeezed by it, and then the portion evolves in the reaction zone with the speed depending on the axial coordinate z and the baseflow velocity u_z^*. The example of solution (6.5) in $t - z$ plane is shown on Fig. 6.1.

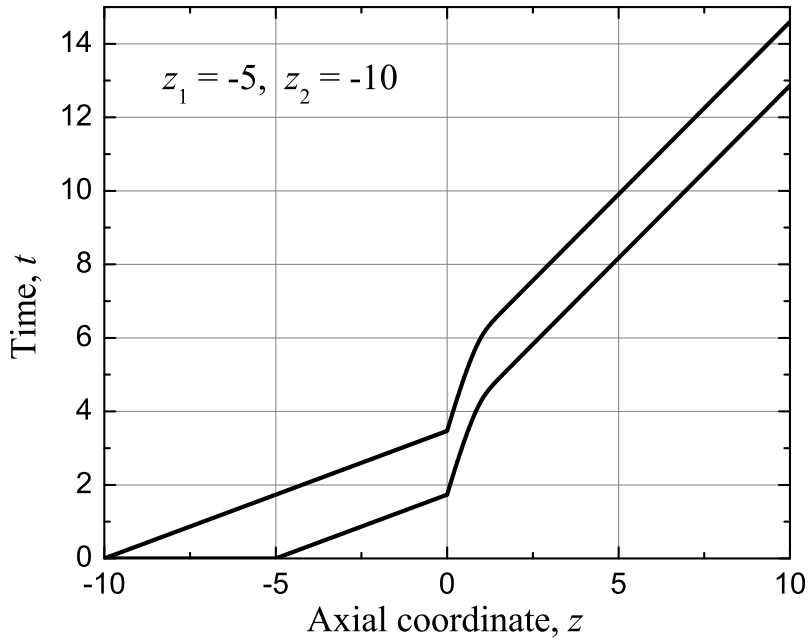

Figure 6.1: The boundaries of perturbation (6.5) depending on time t and axial coordinate z, baseflow parameters are $E = Q = 50$, $f = \gamma = 1.2$.

The considered example illustrates that a perturbation associated with the axial

vorticity only does not generate modes from discrete spectrum. The example serves to point out that the continuous spectrum is required in order to accommodate such perturbations. In the past, the issue was overlooked and the continuous spectrum has not been mentioned until the recent work of Tumin [49].

6.1.2 Periodic Perturbations

Another example of a quiescent gas perturbation to be considered is an axisymmetric isobaric density disturbance proportional to $\sin \tilde{w} z^l$. After performing the Fourier and Bessel expansions with Laplace transform, one can write the perturbation in the leading order (i.e., neglecting the input of shock displacement) as:

$$\rho_{0m}\left(z = 0_-, \tau\right) = -B_{0m} \frac{w}{w^2 + \tau^2} \tag{6.6}$$

where $B_{0m} = \frac{1}{d_{0m}} \int_0^a J_0\left(k_{0m} r\right) r dr$ and subscript '0' indicates that the disturbance is axisymmetric. The frequency is written as $w = \tilde{w}|D_s|$, where $D_s < 0$ is the detonation velocity scaled with the speed of sound behind the shock, c_s.

If the eigenvalue τ_s is close to $\pm iw$, then the amplitude of $\rho_{0m}\left(z = 0_-, \tau\right)$ may become large and lead to resonance. Such eigenvalue can be expected to influence the long-term dynamics due to its large initial amplitude, even if its growth rate is small compared to the other unstable modes. However, the resonance contribution is compensated by the continuous spectrum for large time scales, as it was derived by C. Chiquete in [56].

The general solution is represented by Eq. (3.24). Any initial perturbations in the reaction zone and perturbations of transversal velocity components are absent, so the term in the receptivity coefficient (3.25) that includes $\mathbf{D}_0$ is equal to zero. Therefore,

the coefficients for the considered perturbation can be written as $R_{ms} = B_{0m} r_{ms}$, where

$$r_{ms} = - \left. \frac{\left(\mathbf{y}_1(0), \mathbf{Y}\mathbf{q}_{0m}(0_-, \tau)\right)}{(\partial V/\partial \tau)} \right|_{\tau=\tau_s} \tag{6.7}$$

with $\mathbf{q}_{0m}(0_-, \tau) = \left(\rho_{0m}(z = 0_-, \tau), 0, 0, 0, 0, 0\right)^T / B_{0m}$.

The example of flow receptivity to the isobaric density perturbation for the first discrete mode is shown on Fig. 6.2. The parameter set is the following: $E = Q = 50$, $\gamma = f = 1.2$, the radial parameter $k = 2$ and the eigenvalue $\tau_1 = 0.13128 + 1.20838i$, and w varies from 0 to 5.

The behavior of the first mode on radial parameter k is shown on Fig. 6.3: the mode approaches the imaginary axis $\mathrm{Re}(\tau) = 0$ with the increase of k thus leading the mode to a resonance. In the vicinity of the resonance ($w \approx 1.3$), the input from the continuous spectrum has to be taken into account as well (see [56]).

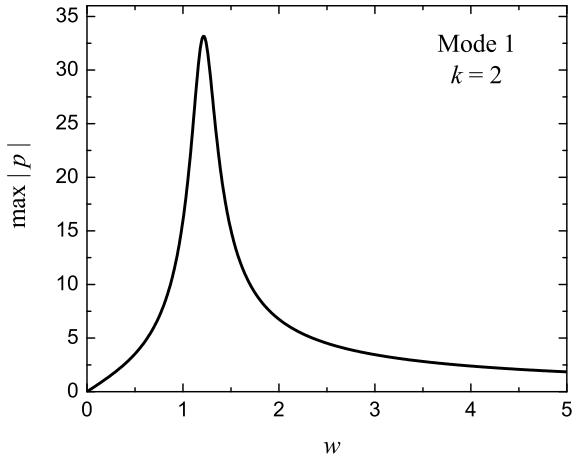

Figure 6.2: Maximum of pressure perturbation in the first discrete mode for the isobaric density initial perturbation placed in the quiescent gas, with $k = 2$, $f = \gamma = 1.2$, $E = Q = 50$.

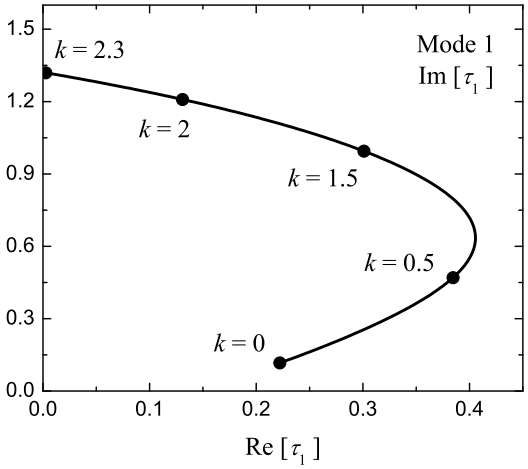

Figure 6.3: Trajectory of the first mode in the complex plane τ, the radial number k varies from 0 to 2.3, $f = \gamma = 1.2$, $E = Q = 50$.

6.2 Initial Perturbations Placed Inside the Reaction Zone

6.2.1 Axial Vorticity Perturbations

The vorticity perturbation of the same type as in Section 6.1.1 is under consideration, but now the rotating portion of gas is placed inside the reaction zone:

$$\mathbf{q}'(r,\phi,z,0) = \left(0,\ 0,\ u'_\phi(r,\phi,z,0),\ 0,\ 0,\ 0\right)^T, \tag{6.8}$$

where the azimuthal velocity component $u'_\phi(r,\phi,z,0) = (H(z-z_1) - H(z-z_2))\,wr$, z_1 is the left boundary and z_2 is the right boundary of perturbation, $z_1 < z_2$; w is the angular velocity of rotation. For now, the perturbation has no azimuthal dependence.

The Fourier and Bessel expansions with Laplace transformation lead to the following form of the initial perturbation:

$$u_{\phi,0m}(z,0) = a_{0m} w\,(H(z-z_1) - H(z-z_2)) \tag{6.9}$$

where 0 in subscripts means that $n = 0$ for the considered perturbation, and the coefficients a_{0m} are defined by Eq. (6.3). Using the properties of matrix $\mathbf{Y}$ and of the adjoint fundamental solution $\mathbf{y}_1$, one can find that the axial vorticity term (E.27) and the receptivity coefficient (3.25) are zeros for the considered perturbation (6.8).

The solution of the transformed system, Eq. (3.18), includes only the azimuthal

velocity component:

$$u_{\phi,0m}(z,\tau) = \exp\left(-\int_0^z \frac{\tau}{u_z^*}dz\right)\int_0^z \exp\left(\int_0^{z'} \frac{\tau}{u_z^*}dz''\right)\frac{u_{\phi,0m}(z,0)}{u_z^*}dz' \tag{6.10}$$

The inverse transformations lead to the general solution of the following form:

$$\begin{aligned} u_\phi(r,z,t) =& \frac{wr}{2\pi i}\int_{-i\infty}^{i\infty} \exp\left(\tau t - \tau\int_0^z \frac{dz}{u_z^*}\right)\times \\ &\times\left[\int_0^z \exp\left(\int_0^{z'} \frac{\tau}{u_z^*}dz''\right)\frac{H(z'-z_1)-H(z'-z_2)}{u_z^*}dz'\right]d\tau \end{aligned} \tag{6.11}$$

This is the solution for the initial perturbation (6.8) that has no dependence on ϕ. The perturbation boundaries evolve along the characteristics

$$t - \int_0^z \frac{dz}{u_z^*} = \text{constant} \tag{6.12}$$

which are shown on Fig. 6.4 for $z_1 = 0.2$ and $z_2 = 0.3$.

Although the considered solution stems from the results of Section 6.1.1, the analysis is repeated for the purpose of clarity of the next example where the perturbation has an azimuthal dependence.

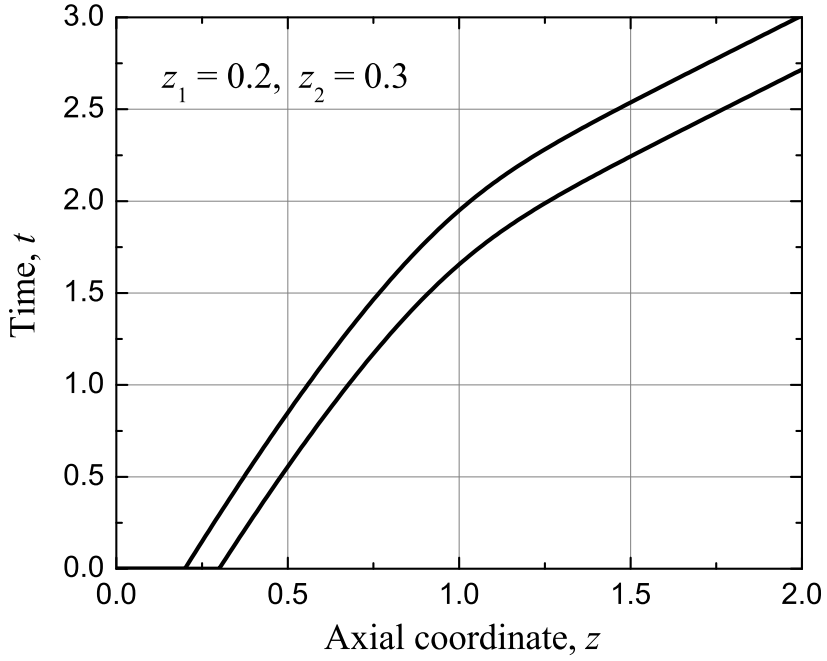

Figure 6.4: The boundaries of perturbation (6.11) depending on time t and axial coordinate z, the baseflow parameters are $E = Q = 50$, $f = \gamma = 1.2$.

The initial perturbation (6.8) with inclusion of periodic azimuthal dependence has the following form:

$$u'_{\phi}\left(r,\phi,z,0\right)=wr\left(H\left(z-z_1\right)-H\left(z-z_2\right)\right)e^{il\phi}, \tag{6.13}$$

the transformed perturbation is

$$u_{\phi,0nm}\left(z\right)=a_{nm}w\left(H\left(z-z_1\right)-H\left(z-z_2\right)\right), \tag{6.14}$$

where the coefficients are the same as the ones defined in Section 6.1.1 for the perturbation in quiescent gas. The axial vorticity term can be written as $G_m = g_m B_{nm}$ where

$$g_m\left(z\right)=\exp\left(-\tau\int_0^z\frac{dz'}{u_z^*}\right)\int_0^z\exp\left(\tau\int_0^{z'}\frac{dz''}{u_z^*}\right)\frac{H\left(z'-z_1\right)-H\left(z'-z_2\right)}{u_z^*}dz' \tag{6.15}$$

and the transversal coefficient is

$$B_{nm}=\frac{inw}{d_{nm}}\left[\int_0^a rJ_n\left(k_{nm}r\right)dr\right] \tag{6.16}$$

The receptivity coefficient can be represented as $R_{ms} = r_{ms} B_{nm}$, where

$$r_{ms} = \left. \frac{\int_0^\infty (\mathbf{y}_1, \mathbf{A}_z^{-1} \mathbf{D}_0)\, g_m dz}{\partial V / \partial \tau} \right|_{\tau=\tau_s} \tag{6.17}$$

with $\mathbf{D}_0 = (\rho^*,\ 0,\ d_3,\ 0,\ \gamma p^*,\ 0)^T$. The component d_3 has no influence on the coefficient due to the form of vector $\mathbf{y}_1$, so it is not shown in the explicit form.

The behavior of the maximum values of pressure perturbation, $\max|p|$, with the weights r_{ms}, for different values of z_1, z_2, k and τ_s are presented on the following figures.

As in Section 6.1.1, the first example describes the perturbations with the same value of z_1 but with different values of z_2. Fig. 6.5 demonstrates the behavior of $\max|p|$ for the first three discrete modes and $z_1 = 0.5$. The parameter $k = 1$ and the flow parameters are the same as in Fig. 6.4.

The behavior of $\max|p|$ is similar to the example of vorticity perturbation outside of the reaction zone, Fig. **??**: the values of $\max|p|$ become constants for large z_2. For perturbations inside the reaction zone the adjoint solution $\mathbf{y}_1$ has the major influence on $\max|p|$: the maxima of pressure distributions become constants due to the vanishing of $\mathbf{y}_1$ for large values of z (see Fig. 5.5).

Again, the flow is more receptive to the discrete modes of lower frequency and to the one-dimensional perturbations rather than for three-dimensional ones, as shown on Fig. 6.6.

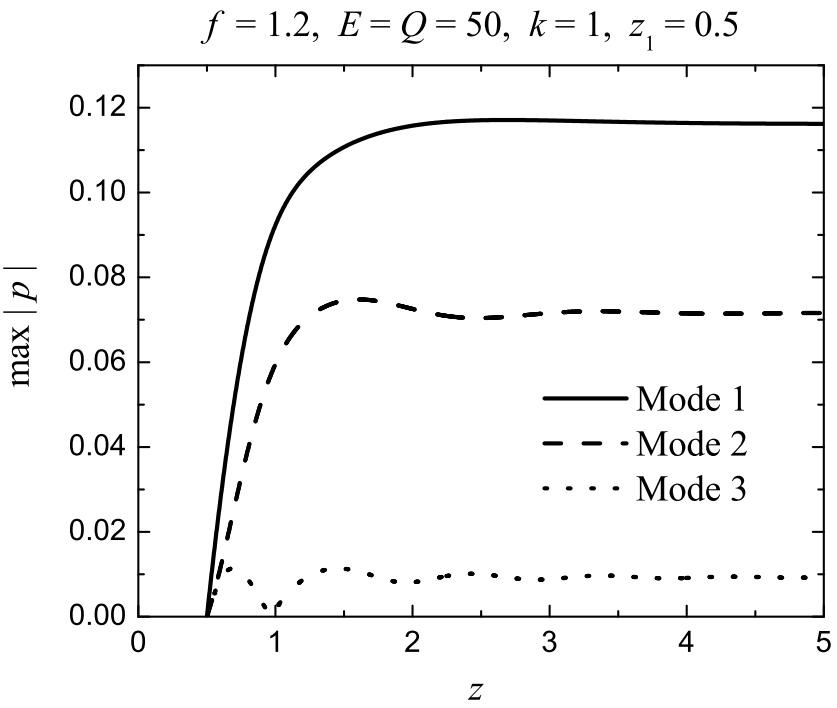

Figure 6.5: Maximum of pressure perturbation in the discrete modes 1, 2 and 3 for vorticity perturbation placed inside the reaction zone, with fixed $z_1 = 0.5$ and z_2 varying from 0.5 to 5.

Figure 6.7 shows the values of $\max|p|$ for perturbations of fixed width, $\Delta z = z_2 - z_1 = 0.2$ with the same parameters as in Fig. 6.5. The values of $\max|p|$ for the first mode and for different values of k are presented on Fig. 6.8. The flow is more receptive to disturbances that possess lower frequency and that are closer to the shock wave. The one-dimensional perturbations possess more influence on the flow than the perturbations with $k \approx 1$.

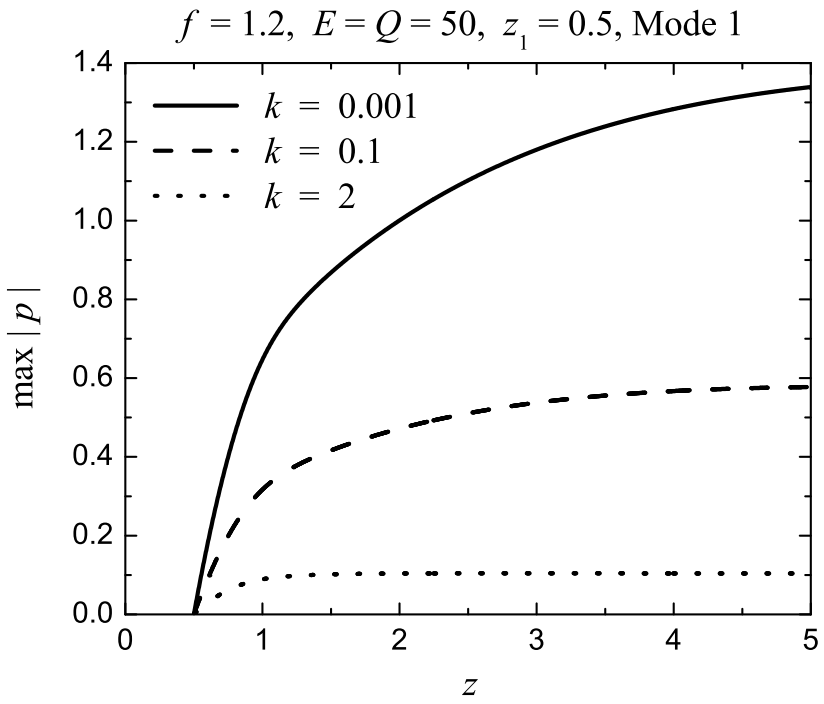

Figure 6.6: Maximum of pressure perturbation in the first discrete mode for vorticity perturbation placed inside the reaction zone, with fixed $z_1 = 0.5$ and z_2 varying from 0.5 to 5.

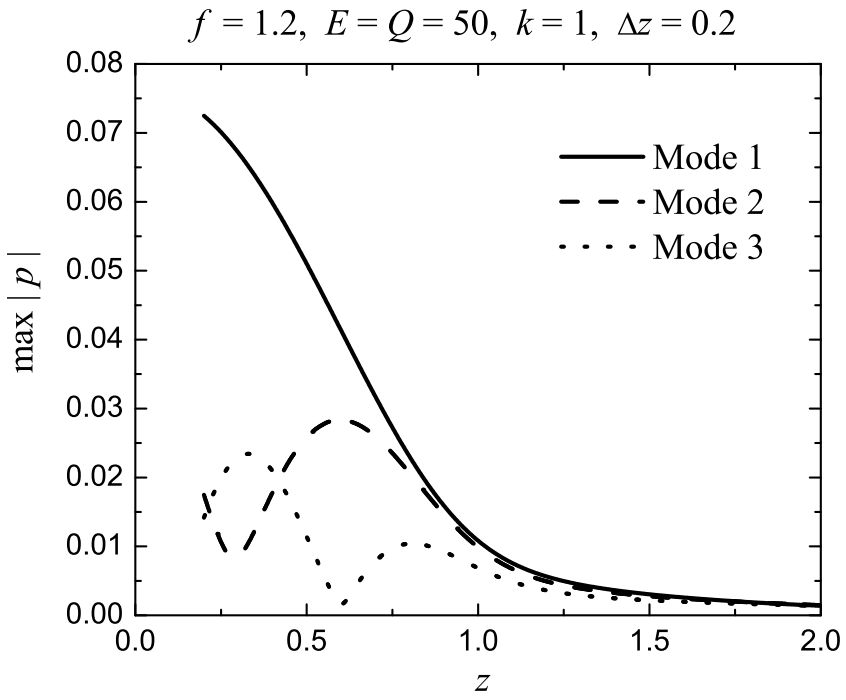

Figure 6.7: Maximum of pressure perturbation in the discrete modes 1, 2 and 3 for vorticity perturbation placed inside the reaction zone, with fixed $\Delta z = z_2 - z_1 = 0.2$ and z_1 varying from 0.2 to 2.

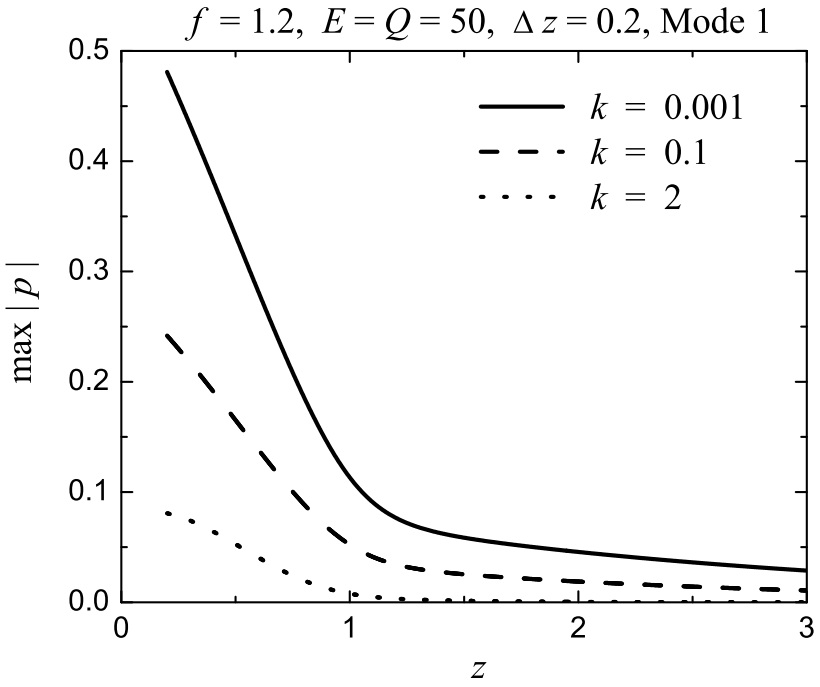

Figure 6.8: Maximum of pressure perturbation in the first discrete mode for vorticity perturbation placed inside the reaction zone, with fixed $\Delta z = z_2 - z_1 = 0.2$ and z_1 varying from 0.2 to 4.

6.2.2 Adiabatic Perturbations

Consider the following initial perturbation placed in the reaction zone:

$$\mathbf{q}_0\left(r,\ \phi,\ z\right)=\mathbf{q}_{rc}\frac{\delta\left(r-r_0\right)\delta\left(\phi\right)\delta\left(z-z_0\right)}{r} \tag{6.18}$$

where $\mathbf{q}_{rc}=\left(-\rho^{*2},0,0,0,-\gamma p^{*}\rho^{*},0\right)^{T}$ represents the adiabatic perturbation. This initial perturbation has the following Fourier transform

$$\mathbf{q}_{0,n}\left(r,z\right)=\mathbf{q}_{rc}\frac{\delta\left(r-r_0\right)\delta\left(z-z_0\right)}{r} \tag{6.19}$$

Expansion into the Bessel functions gives

$$\begin{aligned} q^{(1)}_{0,nm}\left(z\right)=&\frac{1}{d_m}\int_0^a q^{(1)}_{0,n}\left(r,z\right)rJ_n\left(k_{nm}r\right)dr=-\rho^{*2}\frac{J_n\left(k_{nm}r_0\right)}{d_m}\delta\left(z-z_0\right),\\ q^{(5)}_{0,nm}\left(z\right)=&\frac{1}{d_m}\int_0^a q^{(5)}_{0,n}\left(r,z\right)rJ_n\left(k_{nm}r\right)dr=-\gamma p^{*}\rho^{*}\frac{J_n\left(k_{nm}r_0\right)}{d_m}\delta\left(z-z_0\right) \end{aligned} \tag{6.20}$$

Consider perturbations located on the axis ($r_0\to 0$). In this case, the perturbation is axisymmetric and only terms with $n=0$ are to be considered. Then, the receptivity coefficient can be recast as follows:

$$R_{ms}=\frac{2r_{ms}}{a^2J_0^2\left(k_{0m}a\right)} \tag{6.21}$$

where the coefficient

$$r_{ms} = - \left. \frac{(\mathbf{y_1},\ \mathbf{A}_z^{-1}\mathbf{q}_{rc})}{(\partial V/\partial \tau)} \right|_{\tau=\tau_s,\, z=z_0} . \tag{6.22}$$

The values of $\max|p|$ of adiabatic perturbation for the first three modes are shown on Fig. 6.9, the value of radial parameter is fixed and equal to unity, the position of perturbation, z_0 varies from 0 to 2, the flow parameters are the following: $E = Q = 50$, $f = \gamma = 1.2$. The magnitude of pressure maxima for all modes is almost the same, the values of $\max|p|$ decay as the perturbation is moved away from the shock.

Figures 6.10-6.12 demonstrate the behavior of $\max|p|$ for Mode 1, Mode 3 and Mode 5 for different values of k. The one-dimensional perturbations, with $k << 1$, are still surpassing the perturbations with $k \approx 1$ for Mode 1, but for higher-frequency modes the flow is more receptive to the three-dimensional perturbations.

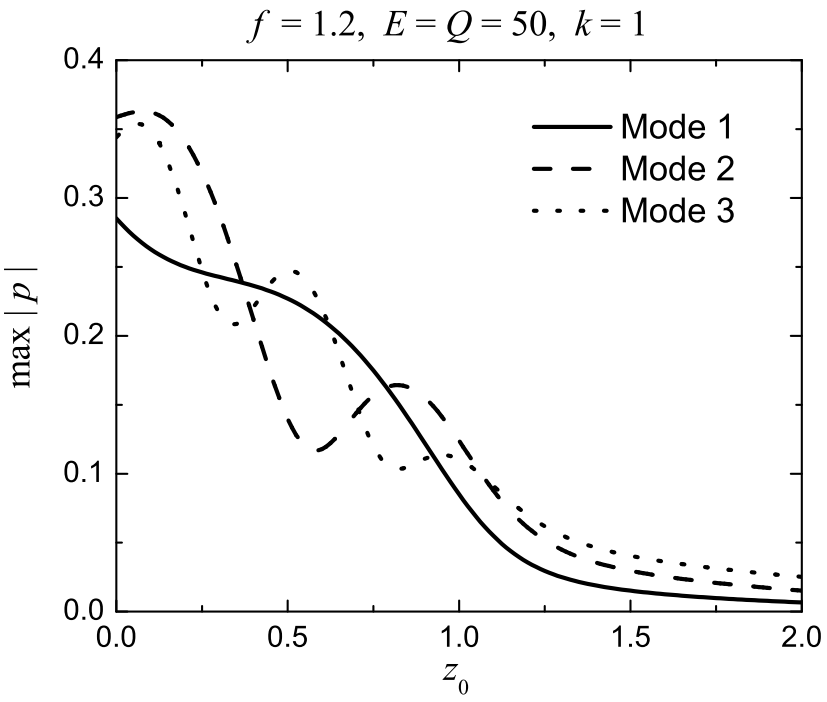

Figure 6.9: Maximum of pressure perturbation in the discrete modes 1, 2 and 3 for adiabatic perturbation placed inside the reaction zone, with z_0 varying from 0 to 2.

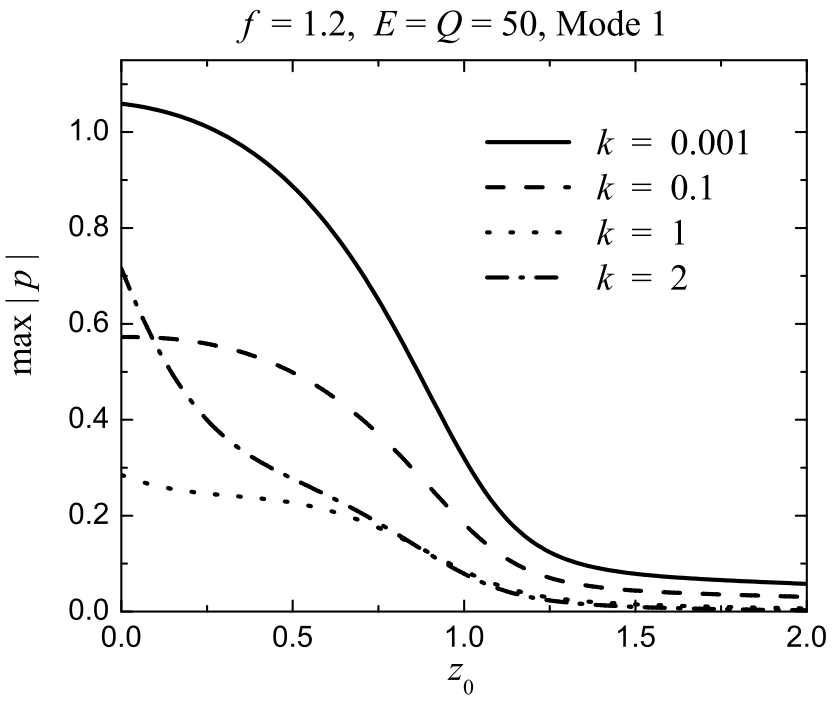

Figure 6.10: Maximum of pressure perturbation in the first discrete mode for adiabatic perturbation placed inside the reaction zone, with z_0 varying from 0 to 2.

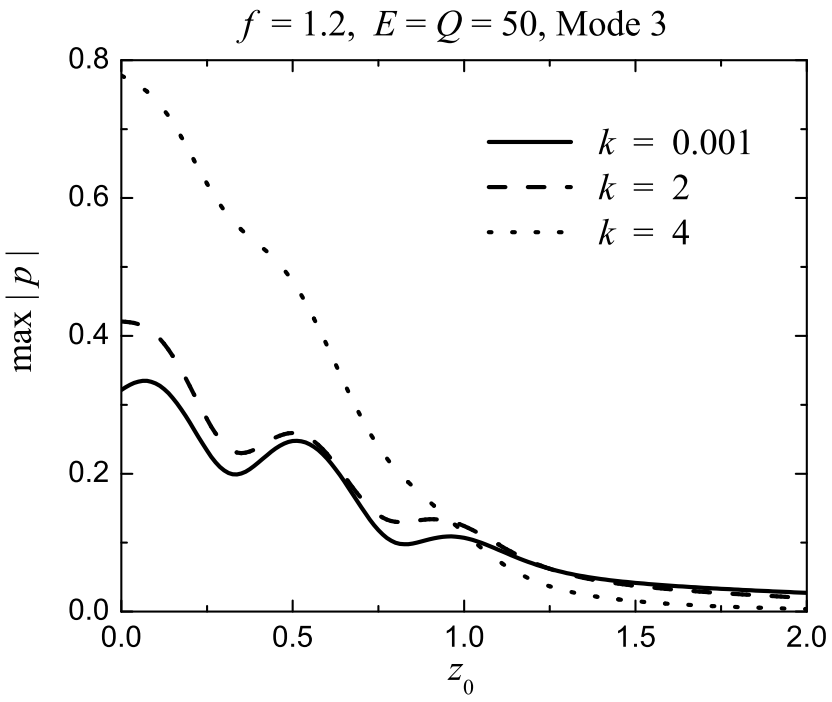

Figure 6.11: Maximum of pressure perturbation in the third discrete mode for adiabatic perturbation placed inside the reaction zone, with z_0 varying from 0 to 2.

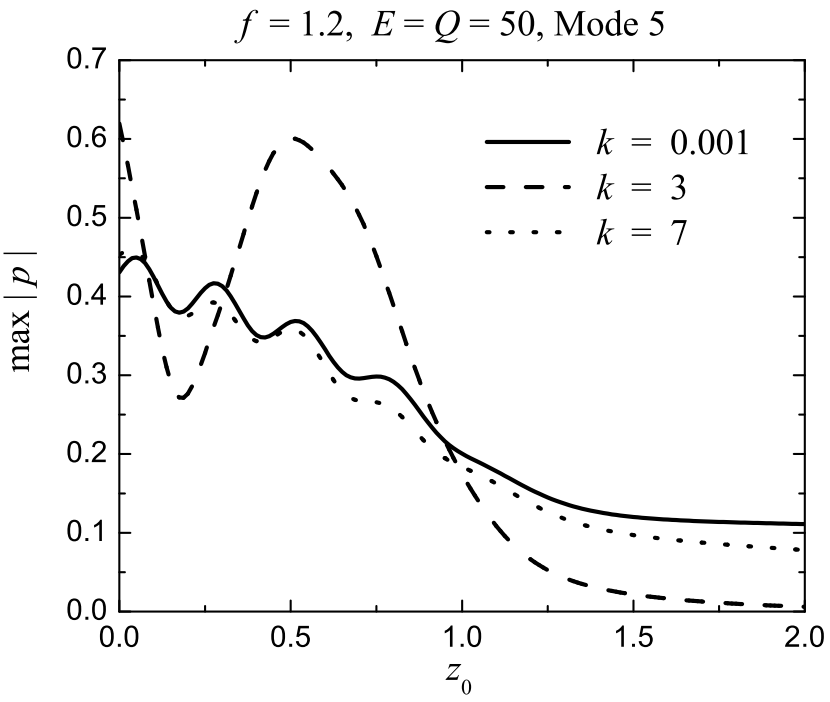

Figure 6.12: Maximum of pressure perturbation in the fifth discrete mode for adiabatic perturbation placed inside the reaction zone, with z_0 varying from 0 to 2.

7. Conclusions

The initial-value problem for perturbations in a circular pipe was solved using the Laplace transform in time.

The inverse Laplace transform leads to the expansion of the solution into the modes of discrete and continuous spectra. The discrete modes represent the waves propagating upstream and downstream the flow. The advantage of the initial-value problem is associated with evaluation of the normal-mode amplitudes depending on the initial perturbations.

As it was noted in Chapter 4, the discrete modes have zero axial vorticity. It means that initial perturbations having nonzero axial vorticity are to be accommodated by the modes of the continuous spectra.

The solution allows evaluation of amplitudes of the unstable modes. The considered examples illustrate that there is a variety of paths for their excitation.

The periodic perturbations placed in the quiescent gas may lead to a resonance caused by discrete modes, but the continuous spectrum has to be taken into account because it can compensate the contribution of discrete modes.

Examples of initial adiabatic perturbations within the reaction zone demonstrate that the flow is more receptive to three-dimensional perturbations. In addition, three-dimensional unstable modes may have larger growth rates than one-dimensional modes. Both these factors are consistent with experimental observations that real

detonation waves have three-dimensional structure.

Appendix A: Matrices of Governing Equations

Nonzero elements of matrices in the linearized Euler equations (2.11), the superscripts (ij) stand for (i,j)-th matrix element:

$$A_r^{(12)} = \rho^*, \quad A_r^{(25)} = \frac{1}{\gamma\rho^*}, \quad A_r^{(52)} = \gamma p^*;$$

$$A_\phi^{(13)} = \rho^*, \quad A_\phi^{(35)} = \frac{1}{\gamma\rho^*}, \quad A_\phi^{(53)} = \gamma p^*;$$

$$A_z^{(ii)} = u_z^*, \ i = 1, ..., 6,$$

$$A_z^{(14)} = \rho^*, \quad A_z^{(45)} = \frac{1}{\gamma\rho^*}, \quad A_z^{(54)} = \gamma p^*;$$

$$C^{(11)} = C^{(44)} = \frac{du_z^*}{dz}, \quad C^{(12)} = \frac{\rho^*}{r},$$

$$C^{(14)} = \frac{d\rho^*}{dz}, \quad C^{(41)} = \frac{u_z^*}{\rho^*}\frac{du_z^*}{dz},$$

$$C^{(51)} = -\kappa\left(\frac{\omega^*}{\rho^*} + \frac{\partial\omega^*}{\partial\rho^*}\right), \quad C^{(52)} = \gamma\frac{p^*}{r}, \quad C^{(54)} = \frac{dp^*}{dz},$$

$$C^{(55)} = \gamma\frac{du_z^*}{dz} - \kappa\frac{\partial\omega^*}{\partial p^*}, \quad C^{(56)} = -\kappa\frac{\partial\omega^*}{\partial\lambda^*},$$

$$C^{(61)} = -\frac{\partial\omega^*}{\partial\rho^*}, \quad C^{(64)} = \frac{d\lambda^*}{dz},$$

$$C^{(65)} = -\frac{\partial\omega^*}{\partial p^*}, \quad C^{(66)} = -\frac{\partial\omega^*}{\partial\lambda^*},$$

where $\kappa = \beta\,(\gamma - 1)\,\rho^*$.

Nonzero components of vectors in the linearized Euler equations (2.11), the superscripts (i) stand for i-th vector component:

$$g_t^{(1)} = \frac{d\rho^*}{dz}, \quad g_t^{(4)} = \frac{du_z^*}{dz}, \quad g_t^{(5)} = \frac{dp^*}{dz}, \quad g_t^{(6)} = \frac{d\lambda^*}{dz};$$

$$g_r^{(2)} = g_\phi^{(3)} = \frac{1}{\gamma\rho^*}\frac{dp^*}{dz}.$$

Appendix B: Matrices of Rankine-Hugoniot Conditions

Nonzero elements of vectors and matrices of the linearized condition on the shock, Eq. (2.12):

$$Y^{(11)} = \frac{D_q^2\left(\gamma+1\right)\left(4+D_q^2\left(\gamma-1\right)\right)}{\left(2+D_q^2\left(\gamma-1\right)\right)^2}, \quad Y^{(14)} = \frac{4}{\left(\gamma+1\right)D_q^2 M_s},$$

$$Y^{(15)} = -\frac{2}{\left(\gamma+1\right)M_s^2}, \quad Y^{(22)} = Y^{(33)} = Y^{(66)} = 1,$$

$$Y^{(41)} = -\frac{2M_s\left(\gamma+1\right)D_q^2}{\left(2+\left(\gamma-1\right)D_q^2\right)^2}, \quad Y^{(44)} = \frac{D_q^2\left(\gamma-1\right)-2}{D_q^2\left(\gamma+1\right)}, \quad Y^{(45)} = \frac{2}{\left(\gamma+1\right)M_s},$$

$$Y^{(51)} = \frac{2\gamma M_s^2\left(\gamma+1\right)D_q^4}{\left(2+\left(\gamma-1\right)D_q^2\right)^2}, \quad Y^{(54)} = \frac{4\gamma M_s}{\gamma+1}, \quad Y^{(55)} = \frac{1-\gamma}{\gamma+1};$$

$$h_t^{(1)} = -\frac{4}{\left(\gamma+1\right)D_q^2 M_s}, \quad h_t^{(4)} = \frac{2\left(D_q^2+1\right)}{D_q^2\left(\gamma+1\right)}, \quad h_t^{(5)} = -\frac{4\gamma M_s}{\gamma+1};$$

$$h_r^{(2)} = h_\phi^{(3)} = |D_s| - M_s.$$

Here the value D_q represents the speed of the shock scaled with the speed of sound in the quiescent gas (shock Mach number). The value $|D_s|$ is the speed of the shock scaled with the speed of sound behind the shock, c_s; M_s is the flow Mach number behind the shock, and γ is the specific heat ratio.

Appendix C: Matrix of Bessel Expansion

The diagonal matrix of the eigenfunction expansion (3.11) is represented as

$$\mathbf{J}_l(r) = \begin{pmatrix} J_n & & & & \\ & dJ_n/dr & & 0 & \\ & & J_n/r & & \\ & & & J_n & \\ & 0 & & & J_n \\ & & & & & J_n \end{pmatrix}$$

where $J_n = J_n(k_{nl}r)$ is the Bessel function of the first order.

Appendix D: Matrices of Transformed Equations

The matrices of the transformed system (3.13) are represented in this Appendix. The superscripts (ij) stand for (i,j)-th matrix element; the elements of matrices $\mathbf{A}_r$, $\mathbf{A}_\phi$, $\mathbf{A}_z$ and $\mathbf{C}$ from the general system (2.11) are also shown to depict the equations' transformations:

$$C_m^{(11)} = C_m^{(44)} = C^{(11)} = C^{(44)} = \frac{du_z^*}{dz},$$

$$C_m^{(12)} = -k_{nm}^2 r C^{(12)} = -k_{nm}^2 A_r^{(12)} = -k_{nm}^2 A_\phi^{(13)} = -k_{nm}^2 \rho^*,$$

$$C_m^{(14)} = C^{(14)} = \frac{d\rho^*}{dz},$$

$$C_m^{(25)} = A_r^{(25)} = \frac{1}{\gamma\rho^*},$$

$$C_m^{(35)} = inA_\phi^{(35)} = \frac{in}{\gamma\rho^*},$$

$$C_m^{(41)} = C^{(41)} = \frac{u_z^*}{\rho^*}\frac{du_z^*}{dz},$$

$$C_m^{(51)} = C^{(51)} = -\kappa\left(\frac{\omega^*}{\rho^*} + \frac{\partial\omega^*}{\partial\rho^*}\right),$$

$$C_m^{(52)} = -k_{nm}^2 r C^{(52)} = -k_{nm}^2 A_r^{(52)} = -k_{nm}^2 A_\phi^{(53)} = -k_{nm}^2 \gamma p^*,$$

$$C_m^{(54)} = C^{(54)} = \frac{dp^*}{dz},$$

$$C_m^{(55)} = C^{(55)} = \gamma\frac{du_z^*}{dz} - \kappa\frac{\partial\omega^*}{\partial p^*},$$

$$C_m^{(56)} = C^{(56)} = -\kappa\frac{\partial\omega^*}{\partial\lambda^*},$$

$$C_m^{(61)} = C^{(61)} = -\frac{\partial\omega^*}{\partial\rho^*},$$

$$C_m^{(64)} = C^{(64)} = \frac{d\lambda^*}{dz},$$

$$C_m^{(65)} = C^{(65)} = -\frac{\partial\omega^*}{\partial p^*},$$

$$C_m^{(66)} = C^{(66)} = -\frac{\partial\omega^*}{\partial\lambda^*},$$

where $\kappa = \beta\left(\gamma - 1\right)\rho^*$.

The superscript (i) stands for the i-th vector element:

$$D_0^{(1)} = \frac{1}{d_m}\int_0^a \rho_{0,n}\left(r,\ z\right) J_n\left(k_{nm}r\right) r dr - \frac{d\rho^*}{dz}\psi_{0,nm} - \rho^* G_m\left(z\right),$$

$$D_0^{(2)} = \frac{1}{d_m}\int_0^a \left[\int_0^r u_{r0,n}\left(r',\ z\right) dr'\right] J_n\left(k_{nm}r\right) r dr,$$

$$D_0^{(3)} = \frac{1}{d_m}\int_0^a u_{\phi 0,n}\left(r,\ z\right) J_n\left(k_{nm}r\right) r^2 dr,$$

$$D_0^{(4)} = \frac{1}{d_m}\int_0^a u_{z0,n}\left(r,\ z\right) J_n\left(k_{nm}r\right) r dr - \frac{du_z^*}{dz}\psi_{0,nm},$$

$$D_0^{(5)} = \frac{1}{d_m}\int_0^a p_{0,n}\left(r,\ z\right) J_n\left(k_{nm}r\right) r dr - \frac{dp^*}{dz}\psi_{0,nm} - \gamma p^* G_m\left(z\right),$$

$$D_0^{(6)} = \frac{1}{d_m}\int_0^a \lambda_{0,n}\left(r,\ z\right) J_n\left(k_{nm}r\right) r dr - \frac{d\lambda^*}{dz}\psi_{0,nm},$$

where $\psi_{0,nm}$ is the coefficient of the initial shock perturbation,

$$\psi_{0,nm} = \frac{1}{d_m}\int_0^a \psi_{0,n}\left(r\right) J_n\left(k_{nm}r\right) r dr,$$

and G_m represents the axial vorticity term derived in Appendix E.

Appendix E: Equations for the Amplitude Functions

The derivation of the system of amplitude coefficients is considered in this Appendix.

For the derivation of amplitude equations here will be considered the system (3.5), the Bessel expansion (3.10) and the orthogonality property of Bessel functions (3.12):

$$\begin{aligned}\tau\hat{\mathbf{q}}_n + \mathbf{A}_r\frac{\partial\hat{\mathbf{q}}_n}{\partial r} + \mathbf{A}_\phi\frac{in}{r}\hat{\mathbf{q}}_n + \mathbf{A}_z\frac{\partial\hat{\mathbf{q}}_n}{\partial z} + \mathbf{C}\hat{\mathbf{q}}_n - \tau\mathbf{g}_t\hat{\psi}_n - \mathbf{g}_r\frac{\partial\hat{\psi}_n}{\partial r} - \mathbf{g}_\phi\frac{in}{r}\hat{\psi}_n = \\ = \mathbf{q}_{0,n} - \mathbf{g}_t\psi_{0,n}\end{aligned} \tag{3.5}$$

$$\hat{\mathbf{q}}_n = \sum_{l=1}^{\infty}\begin{pmatrix}\rho_{nl}(z,\,\tau)\,J_n(k_{nl}r)\\ u_{r,nl}(z,\,\tau)\,k_{nl}J_n'(k_{nl}r)\\ u_{\phi,nl}(z,\,\tau)\,J_n(k_{nl}r)/r\\ u_{z,nl}(z,\,\tau)\,J_n(k_{nl}r)\\ p_{nl}(z,\,\tau)\,J_n(k_{nl}r)\\ \lambda_{nl}(z,\,\tau)\,J_n(k_{nl}r)\end{pmatrix},\ \hat{\psi}_n = \sum_{l=1}^{\infty}\psi_{nl}(\tau)\,J_n(k_{nl}r) \tag{3.10}$$

$$\begin{gathered}\int_0^a J_n(k_{nl}r)\,J_n(k_{nm}r)\,rdr = \delta_{lm}d_m \\ d_m = \frac{k_{nm}^2a^2 - n^2}{2k_{nm}^2}J_n^2(k_{nm}a)\end{gathered} \tag{3.12}$$

To derive the system of the ordinary differential equations, we substitute the expansion (3.10) into the system (3.5) and consider each equation of the system separately.

Continuity equation. Substitute the eigenfunction expansion into the continuity equation:

$$\sum_{l=1}^{\infty}\left(\tau\rho_{nl}+u_z^*\frac{d\rho_{nl}}{dz}+\rho^*\frac{du_{z,nl}}{dz}+\frac{du_z^*}{dz}\rho_{nl}+\frac{d\rho^*}{dz}u_{z,nl}-\tau\frac{d\rho^*}{dz}\psi_{nl}\right)J_n\left(k_{nl}r\right)+$$

$$+\sum_{l=1}^{\infty}\rho^*u_{r,nl}\left(k_{nl}^2J_n''\left(k_{nl}r\right)+\frac{1}{r}k_{nl}J_n'\left(k_{nl}r\right)\right)+\frac{in}{r^2}\rho^*\sum_{l=1}^{\infty}u_{\phi,nl}J_n\left(k_{nl}r\right)= \tag{E.1}$$

$$=\rho_{0,n}\left(r,\ z\right)-\frac{d\rho^*}{dz}\psi_{0,n}\left(r\right)$$

Equation (E.1) is multiplied by $rJ_n\left(k_{nm}r\right)$ and integrated with respect to the radius, r, from zero to a. Taking into account the orthogonality condition (3.12) and the Bessel equation for $J_n\left(k_{nl}r\right)$:

$$k_{nl}^2J_n''+\frac{1}{r}k_{nl}J_n'=-k_{nl}^2J_n+\frac{n^2}{r^2}J_n \tag{E.2}$$

one can derive from Eq. (E.1) that

$$\tau\rho_{nm}+u_z^*\frac{d\rho_{nm}}{dz}+\rho^*\frac{du_{z,nm}}{dz}+\frac{du_z^*}{dz}\rho_{nm}-k_{nm}^2\rho^*u_{r,nm}+\frac{d\rho^*}{dz}u_{z,nm}-\tau\frac{d\rho^*}{dz}\psi_{nm}+$$

$$+\frac{n\rho^*}{d_m}\int_0^a\sum_{l=1}^{\infty}(nu_{r,nl}+iu_{\phi,nl})J_n\left(k_{nl}r\right)J_n\left(k_{nm}r\right)\frac{dr}{r}=\rho_{0,nm}\left(z\right)-\frac{d\rho^*}{dz}\psi_{0,nm} \tag{E.3}$$

where the initial amplitude coefficient is written as

$$\begin{aligned}\rho_{0,nm}(z) =& \frac{1}{d_m}\int_0^a \rho_{0,n}(r,z)\, J_n(k_{nm}r)\, r dr,\\ \psi_{0,nm} =& \frac{1}{d_m}\int_0^a \psi_{0,n}(r)\, J_n(k_{nm}r)\, r dr.\end{aligned} \tag{E.4}$$

The last term in the left-hand side of Eq.(E.3) contains an infinite sum that will be considered after the equations' expansion.

Radial momentum equation. Substitute the eigenfunction expansion into the radial momentum equation gives

$$\sum_{l=1}^{\infty}\left(\tau u_{r,nl} + u_z^*\frac{du_{r,nl}}{dz} + \frac{1}{\gamma\rho^*}p_{nl} - \frac{1}{\gamma\rho^*}\frac{dp^*}{dz}\psi_{nl}\right) k_{nl}J_n'(k_{nl}r) = u_{r0,n}(r,\ z) \tag{E.5}$$

Equation (E.5) is integrated with respect to r from zero to r, then the result is multiplied by $rJ_n(k_{nm}r)$ and integrated again with respect to the radius, r, from zero to a:

$$\begin{aligned}&\tau u_{r,nm} + u_z^*\frac{du_{r,nm}}{dz} + \frac{1}{\gamma\rho^*}p_{nm} - \frac{1}{\gamma\rho^*}\frac{dp^*}{dz}\psi_{nm} -\\ &-\frac{1}{d_m}\sum_{l=1}^{\infty}\left(\tau u_{r,nl} + u_z^*\frac{du_{r,nl}}{dz} + \frac{1}{\gamma\rho^*}p_{nl} - \frac{1}{\gamma\rho^*}\frac{dp^*}{dz}\psi_{nl}\right) J_n(k_{nl}0)\int_0^a J_n(k_{nm}r)\, r dr =\\ &= u_{r0,nm}(r,\ z)\end{aligned}$$

where the initial amplitude coefficient is written as

$$u_{r0,nm}(z) = \frac{1}{d_m}\int_0^a \left(\int_0^r u_{r0,n}(r',\ z)\, dr'\right) J_n(k_{nm}r)\, r dr. \tag{E.6}$$

Taking into account that $J_n(0) = 0$ for $n > 0$ and

$$\int_0^a r J_0(k_{0m}r)\, dr = \frac{a}{k_{0m}} J_1(k_{0m}a) = -\frac{a}{k_{0m}} J_0'(k_{0m}a) = 0 \tag{E.7}$$

due to the boundary condition (the same properties are taken into account in derivation of the shock boundary condition for $u_{r,nm}(0_+)$ in (3.14)), one can derive the following amplitude equation:

$$\tau u_{r,nm} + u_z^* \frac{du_{r,nm}}{dz} + \frac{1}{\gamma\rho^*} p_{nm} - \frac{1}{\gamma\rho^*}\frac{dp^*}{dz}\psi_{nm} = u_{r0,nm}(z) \tag{E.8}$$

Azimuthal momentum equation. Substitute the eigenfunction expansion into the azimuthal momentum equation:

$$\sum_{l=1}^{\infty}\left(\tau u_{\phi,nl} + u_z^*\frac{du_{\phi,nl}}{dz} + \frac{in}{\gamma\rho^*}p_{nl} - \frac{in}{\gamma\rho^*}\frac{dp^*}{dz}\psi_{nl}\right)\frac{J_n(k_{nl}r)}{r} = u_{\phi 0,n}(r,\ z) \tag{E.9}$$

Multiply Eq.(E.9) by $r^2 J_n(k_{nm} r)$ and integrate with respect to the radius, r, from zero to a. The result is the following:

$$\tau u_{\phi,nm} + u_z^* \frac{du_{\phi,nm}}{dz} + \frac{in}{\gamma \rho^*} p_{nm} - \frac{in}{\gamma \rho^*} \frac{dp^*}{dz} \psi_{nm} = u_{\phi 0,nm}(z) \tag{E.10}$$

where

$$u_{\phi 0,nm}(z) = \frac{1}{d_m} \int_0^a u_{\phi 0,n}(r,\ z)\, J_n(k_{nm} r)\, r^2 dr. \tag{E.11}$$

Axial momentum equation. Substitute the eigenfunction expansion into the axial momentum equation:

$$\begin{aligned} &\sum_{l=1}^{\infty} \left(\tau u_{z,nl} + u_z^* \frac{du_{z,nl}}{dz} + \frac{1}{\gamma \rho^*} \frac{dp_{nl}}{dz} + \frac{u_z^*}{\rho^*} \frac{du_z^*}{dz} \rho_{nl} + \frac{du_z^*}{dz} u_{z,nl} - \tau \frac{du_z^*}{dz} \psi_{nl} \right) J_n(k_{nl} r) = \\ &= u_{z0,n}(r,\ z) - \frac{du_z^*}{dz} \psi_{0,n}(r) \end{aligned} \tag{E.12}$$

Using orthogonality of the Bessel functions, Eq. (3.12), one can derive from Eq. (E.12) the following result:

$$\begin{aligned} &\tau u_{z,nm} + u_z^* \frac{du_{z,nm}}{dz} + \frac{1}{\gamma \rho^*} \frac{dp_{nm}}{dz} + \frac{u_z^*}{\rho^*} \frac{du_z^*}{dz} \rho_{nm} + \frac{du_z^*}{dz} u_{z,nm} - \tau \frac{du_z^*}{dz} \psi_{nm} = \\ &= u_{z0,nm}(z) - \frac{du_z^*}{dz} \psi_{0,nm} \end{aligned} \tag{E.13}$$

where

$$u_{z0,nm} = \frac{1}{d_m} \int_0^a u_{z0,n}\left(r,\ z\right) J_n\left(k_{nm} r\right) r dr. \tag{E.14}$$

Energy equation. Substitute the eigenfunction expansion into the energy equation:

$$\begin{aligned}
&\sum_{l=1}^{\infty} \left[\tau p_{nl} + \gamma p^* \frac{du_{z,nl}}{dz} + u_z^* \frac{dp_{nl}}{dz} - \beta\left(\gamma - 1\right) \left(\omega^* + \rho^* \frac{\partial \omega^*}{\partial \rho^*} \right) \rho_{nl} + \frac{dp^*}{dz} u_{z,nl} + \right. \\
&+ \left. \left(\gamma \frac{du_z^*}{dz} - \beta\left(\gamma - 1\right) \rho^* \frac{\partial \omega^*}{\partial p^*} \right) p_{nl} - \beta\left(\gamma - 1\right) \rho^* \frac{\partial \omega^*}{\partial \lambda^*} \lambda_{nl} - \tau \frac{dp^*}{dz} \psi_{nl} \right] J_n\left(k_{nl} r\right) + \\
&+ \sum_{l=1}^{\infty} \gamma p^* u_{r,nl} \left(k_{nl}^2 J_n''\left(k_{nl} r\right) + \frac{1}{r} k_{nl} J_n'\left(k_{nl} r\right) \right) + \gamma p^* \frac{in}{r^2} \sum_{l=1}^{\infty} u_{\phi,nl} J_n\left(k_{nl} r\right) = \\
&= p_{0,n}\left(r,\ z\right) - \frac{dp^*}{dz} \psi_{0,n}\left(r\right)
\end{aligned} \tag{E.15}$$

One can multiply Eq. (E.15) by $r J_n\left(k_{nm} r\right)$ and integrate with respect to the radius, r, from zero to a. Taking into account the orthogonality condition (3.12) and the Bessel equation (E.2), the following result can be achieved:

$$\begin{aligned}
&\tau p_{nm} + \gamma p^* \frac{du_{z,nm}}{dz} + u_z^* \frac{dp_{nm}}{dz} - \beta\left(\gamma - 1\right) \left(\omega^* + \rho^* \frac{\partial \omega^*}{\partial \rho^*} \right) \rho_{nm} - k_{nm}^2 \gamma p^* u_{r,nm} + \\
&+ \frac{dp^*}{dz} u_{z,nm} + \left(\gamma \frac{du_z^*}{dz} - \beta\left(\gamma - 1\right) \rho^* \frac{\partial \omega^*}{\partial p^*} \right) p_{nm} - \beta\left(\gamma - 1\right) \rho^* \frac{\partial \omega^*}{\partial \lambda^*} \lambda_{nm} - \tau \frac{dp^*}{dz} \psi_{nm} + \\
&+ \frac{n \gamma p^*}{b_m} \int_0^a \sum_{l=1}^{\infty} \left(n u_{r,nl} + i u_{\phi,nl} \right) J_n\left(k_{nl} r\right) J_n\left(k_{nm} r\right) \frac{dr}{r} = p_{0,nm}\left(z\right) - \frac{dp^*}{dz} \psi_{0,nm}
\end{aligned} \tag{E.16}$$

where

$$p_{0,nm} = \frac{1}{d_m} \int_0^a p_{0,n}\left(r,\ z\right) J_n\left(k_{nm} r\right) r dr. \tag{E.17}$$

The equation (E.16) contains the same infinite sum as the continuity equation (E.3). The term with the sum will be considered after the expansion of the reaction equation.

Reaction rate equation. Substitute the eigenfunction expansion into the equation for the reaction rate:

$$\begin{aligned} &\sum_{l=1}^{\infty} \left[\left(\tau - \frac{\partial \omega^*}{\partial \lambda^*} \right) \lambda_{nl} + u_z^* \frac{d\lambda_{nl}}{dz} - \frac{\partial \omega^*}{\partial \rho^*} \rho_{nl} + \frac{d\lambda^*}{dz} u_{z,nl} - \frac{\partial \omega^*}{\partial p^*} p_{nl} - \right. \\ &\left. - \tau \frac{d\lambda^*}{dz} \psi_{nl} \right] J_n\left(k_{nl} r\right) = \lambda_{0,n}\left(r,\ z\right) - \frac{d\lambda^*}{dz} \psi_{0,n}\left(r\right) \end{aligned} \tag{E.18}$$

The same procedure as for the above equations leads to the following form of the amplitude equation:

$$\begin{aligned} &\left(\tau - \frac{\partial \omega^*}{\partial \lambda^*} \right) \lambda_{nm} + u_z^* \frac{d\lambda_{nm}}{dz} - \frac{\partial \omega^*}{\partial \rho^*} \rho_{nm} + \frac{d\lambda^*}{dz} u_{z,nm} - \frac{\partial \omega^*}{\partial p^*} p_{nm} - \tau \frac{d\lambda^*}{dz} \psi_{nm} = \\ &= \lambda_{0,nm}\left(z\right) - \frac{d\lambda^*}{dz} \psi_{0,nm} \end{aligned} \tag{E.19}$$

where

$$\lambda_{0,nm} = \frac{1}{d_m} \int_0^a \lambda_{0,n}\left(r,\ z\right) J_n\left(k_{nm} r\right) r dr. \tag{E.20}$$

Analysis of the term with an infinite sum. The main obstacle in resolving the amplitude equations is associated with the infinite sum

$$G_m(z) = \frac{n}{d_m} \int_0^a \sum_{l=1}^{\infty} \left(n u_{r,nl} + i u_{\phi,nl}\right) J_n(k_{nl} r)\, J_n(k_{nm} r)\, \frac{dr}{r} \tag{E.21}$$

that appears in Eqs. (E.3) and (E.16). One can show that this sum is associated with the axial vorticity perturbation and that it can be found from the given initial data. In other words, the sum in Eqs. (E.3) and (E.16) can be considered as a known function.

Using the radial and azimuthal momentum equations from the system (2.11), one can find the following first-order linear partial differential equation:

$$\frac{\partial \Omega_z}{\partial t} + u_z^* \frac{\partial \Omega_z}{\partial z} = 0 \tag{E.22}$$

where Ω_z is a perturbation of the axial vorticity:

$$\Omega_z = \frac{1}{r}\left(\frac{\partial r u'_\phi}{\partial r} - \frac{\partial u'_r}{\partial \phi}\right) \tag{E.23}$$

Solution of Eq. (E.22) can be easily found with the help of the method of characteristics. In order to be consistent with the adopted eigenfunction expansion, the Fourier transform in ϕ, the Laplace transform in time, and the eigenfunction expan-

sions for the velocity components (3.10) are implemented here. After all transformations, the following equation can be written:

$$\left[\tau + u_z^* \frac{\partial}{\partial z}\right] \sum_{l=1}^{\infty} \left(u_{\phi,nl} - i n u_{r,nl}\right) k_{nl} J_n' \left(k_{nl} r\right) = r \Omega_{z0,n} \left(r,\ z\right) \tag{E.24}$$

where $\Omega_{z0,n}\left(r,\ z\right)$ is the Fourier transform of the axial vorticity distribution at $t = 0$.

Equation (E.24) is integrated with respect to r from zero to r, the result is multiplied by $inJ_n\left(k_{nm} r\right)/r$ and integrated with respect to the radius, r, from zero to a. Hence one can find the following differential equation for $G_m\left(z\right)$:

$$\tau G_m + u_z^* \frac{dG_m}{dz} = F_{0,m}\left(z\right) \tag{E.25}$$

where the initial data term is

$$F_{0,m}\left(z\right) = \frac{in}{d_m} \int_0^a \left(\int_0^r r' \Omega_{z0,n}\left(r',\ z\right) dr' \right) J_n\left(k_{nm} r\right) \frac{dr}{r}. \tag{E.26}$$

Solution of Eq. (E.25) can be written in the following form:

$$G_m\left(z\right) = K_0 \exp\left(-\tau \int_0^z \frac{dz}{u_z^*} \right) + \exp\left(-\tau \int_0^z \frac{dz}{u_z^*} \right) \int_0^z \frac{F_{0,m}\left(z'\right)}{u_z^*\left(z'\right)} \exp\left(\tau \int_0^{z'} \frac{dz''}{u_z^*} \right) dz' \tag{E.27}$$

where K_0 is the perturbation of the axial vorticity coming from the quiescent gas. If there are no perturbations of the axial vorticity at $t = 0$, i.e. $F_{0,m} = 0$ and $K_0 = 0$, we have $G_m(z) = 0$.

Now, the amplitude equations can be written in the solvable vector-matrix form as follows:

$$\mathbf{A}_z \frac{d\mathbf{q}_{nm}}{dz} + (\tau \mathbf{I} + \mathbf{C}_m)\, \mathbf{q}_{nm} - (\tau \mathbf{g}_t + \mathbf{g}_r + in\mathbf{g}_\phi)\, \psi_{nm} = \mathbf{D}_0(z) \tag{3.13}$$

where $\mathbf{D}_0$ is known function of the coordinate z and the Laplace variable τ depending on initial distribution of perturbations.

Appendix F: Fundamental Solutions of the Direct Problem

Fundamental solutions of the direct system (3.15) can be written in the form $\mathbf{Q}_j(z) = \mathbf{Q}_{j\infty}\exp(\mu_j z)$, $j = 1, ..., 6$ for $z \to \infty$. The amplitude vectors $\mathbf{Q}_{j\infty}$ are shown in this section.

$$\mathbf{Q}_{1\infty} = \begin{pmatrix} \frac{p^*_\infty \tau + u^*_\infty c_\infty \rho^*_\infty \sqrt{\tau^2 + c^2_\infty (1-M^2_\infty) k^2_{nm}}}{c^2_\infty} \\ u^{*2}_\infty - c^2_\infty \\ in\left(u^{*2}_\infty - c^2_\infty\right) \\ -u^*_\infty \tau - c_\infty \sqrt{\tau^2 + c^2_\infty \left(1 - M^2_\infty\right) k^2_{nm}} \\ \gamma\left(p^*_\infty \tau + u^*_\infty c_\infty \rho^*_\infty \sqrt{\tau^2 + c^2_\infty \left(1 - M^2_\infty\right) k^2_{nm}}\right) \\ 0 \end{pmatrix},$$

$$\mathbf{Q}_{2\infty} = \begin{pmatrix} \frac{p^*_\infty \tau - u^*_\infty c_\infty \rho^*_\infty \sqrt{\tau^2 + c^2_\infty (1-M^2_\infty) k^2_{nm}}}{c^2_\infty} \\ u^{*2}_\infty - c^2_\infty \\ in\left(u^{*2}_\infty - c^2_\infty\right) \\ -u^*_\infty \tau + c_\infty \sqrt{\tau^2 + c^2_\infty \left(1 - M^2_\infty\right) k^2_{nm}} \\ \gamma\left(p^*_\infty \tau - u^*_\infty c_\infty \rho^*_\infty \sqrt{\tau^2 + c^2_\infty \left(1 - M^2_\infty\right) k^2_{nm}}\right) \\ 0 \end{pmatrix},$$

$$\mathbf{Q}_{3\infty} = \begin{pmatrix} 1 \\ 0 \\ 0 \\ 0 \\ 0 \\ 0 \end{pmatrix}, \quad \mathbf{Q}_{4\infty} = \begin{pmatrix} 0 \\ 1 \\ 0 \\ -\frac{k^2_{nm} u^*_\infty}{\tau} \\ 0 \\ 0 \end{pmatrix}, \quad \mathbf{Q}_{5\infty} = \begin{pmatrix} 0 \\ 0 \\ 1 \\ 0 \\ 0 \\ 0 \end{pmatrix},$$

$$\mathbf{Q}_{6\infty} = \begin{pmatrix} -\frac{\rho^*_\infty \left(\left(C^{(66)}_\infty + \tau\right)^2 - k^2_{nm} u^{*2}_\infty\right)}{C^{(66)}_\infty} \\ -u^{*2}_\infty \\ -inu^{*2}_\infty \\ u^*_\infty \left(C^{(66)}_\infty + \tau\right) \\ -C^{(66)}_\infty \gamma u^{*2}_\infty \rho^*_\infty \\ \gamma \frac{p^*_\infty \left[\left(C^{(66)}_\infty + \tau\right)^2 - k^2_{nm} u^{*2}_\infty\right] - {C^{(66)}_\infty}^2 u^{*2}_\infty \rho_\infty}{C^{(56)}_\infty} \end{pmatrix},$$

where n is the azimuthal index, k_{nm} is the m-th root of the boundary-condition equation (3.9). Also, ρ^*_∞ is density, u^*_∞ is mean velocity, c_∞ is the speed of sound and p^*_∞ is pressure in the burnt medium. The symbols $C^{(56)}_\infty$ and $C^{(66)}_\infty$ stand for the elements of matrix $\mathbf{C}_m$ at $z \to \infty$.

Appendix G: Fundamental Solutions of the Adjoint Problem

Fundamental solutions of the adjoint system (3.19) can be written in the form $\mathbf{y}_j(z) = \mathbf{y}_{j\infty}\exp(-\bar{\mu}_j z)$, $j = 1, ..., 6$ for $z \to \infty$. The conjugate form of the amplitude vectors $\mathbf{y}_{j\infty}$ up to normalization factors are shown in this section.

$$\bar{\mathbf{y}}_{1\infty} = \begin{pmatrix} 0 \\ k_{nm}^2 u_\infty^* \\ 0 \\ \tau \\ -\frac{c_\infty}{\gamma p_\infty^*}\sqrt{\tau^2 + k_{nm}^2 c_\infty^2 (1 - M_\infty^2)} \\ \frac{C_\infty^{(56)} u_\infty^* \left(\tau^2 - k_{nm}^2 u_\infty^{*2}\right)}{\gamma p_\infty^* \left(-\tau\left(C_\infty^{(66)} + \tau\right) + k_{nm}^2 u_\infty^{*2}\right) + C_\infty^{(66)} \gamma u_\infty^* c_\infty \rho_\infty^* \sqrt{\tau^2 + k_{nm}^2 c_\infty^2 (1 - M_\infty^2)}} \end{pmatrix}, \tag{G.1}$$

$$\bar{\mathbf{y}}_{2\infty} = \begin{pmatrix} 0 \\ -k_{nm}^2 u_\infty^* \\ 0 \\ -\tau \\ -\frac{c_\infty}{\gamma p_\infty^*}\sqrt{\tau^2 + k_{nm}^2 c_\infty^2 (1 - M_\infty^2)} \\ \frac{C_\infty^{(56)} u_\infty^* \left(\tau^2 - k_{nm}^2 u_\infty^{*2}\right)}{\gamma p_\infty^* \left(\tau\left(C_\infty^{(66)} + \tau\right) - k_{nm}^2 u_\infty^{*2}\right) + C_\infty^{(66)} \gamma u_\infty^* c_\infty \rho_\infty^* \sqrt{\tau^2 + k_{nm}^2 c_\infty^2 (1 - M_\infty^2)}} \end{pmatrix},$$

$$\bar{\mathbf{y}}_{3\infty} = \begin{pmatrix} -1 \\ 0 \\ 0 \\ 0 \\ \frac{1}{\gamma c_\infty^2} \\ \frac{-C_\infty^{(56)}}{C_\infty^{(66)} \gamma c_\infty^2} \end{pmatrix}, \ \bar{\mathbf{y}}_{4\infty} = \begin{pmatrix} 0 \\ \tau^2 \\ 0 \\ \tau u_\infty^* \\ \frac{\tau}{\gamma \rho_\infty^*} \\ 0 \end{pmatrix}, \ \bar{\mathbf{y}}_{5\infty} = \begin{pmatrix} 0 \\ in k_{nm}^2 u_\infty^{*2} \\ \tau^2 - k_{nm}^2 u_\infty^{*2} \\ in\tau u_\infty^* \\ \frac{in\tau}{\gamma \rho_\infty^*} \\ 0 \end{pmatrix}, \ \bar{\mathbf{y}}_{6\infty} = \begin{pmatrix} 0 \\ 0 \\ 0 \\ 0 \\ 0 \\ -C_\infty^{(56)} \end{pmatrix},$$

where n is the azimuthal index, k_{nm} is the m-th root of the boundary-condition equation (3.9). Also, ρ_∞^* is density, u_∞^* is mean velocity, c_∞ is the speed of sound

and p^*_∞ is pressure in the burnt medium. The symbols $C^{(56)}_\infty$ and $C^{(66)}_\infty$ stand for the elements of matrix $\mathbf{C}_m$ at $z \to \infty$.

Appendix H: Derivation of Coefficients for Solution of Transformed System

The amplitude coefficients a_j and shock displacement ψ_{nm} are derived here.

For the derivation of coefficients we will need the formal solution of the amplitude system:

$$\begin{aligned}
&\mathbf{q}_{nm} = \sum_{j=2}^{6} \left(a_j + \int_0^z (\mathbf{y}_j,\ \mathbf{F})\, dz' \right) \mathbf{Q}_j + \mathbf{Q}_1 \int_\infty^z (\mathbf{y}_1,\ \mathbf{F})\, dz' \\
&\mathbf{F} = \mathbf{F}_1 + \mathbf{F}_2 \psi_{nm},\ \mathbf{F}_1 = \mathbf{A}_z^{-1} \mathbf{D}_0,\ \mathbf{F}_2 = \mathbf{A}_z^{-1} \left(\tau \mathbf{g}_t + \mathbf{g}_r + in\mathbf{g}_\phi \right),
\end{aligned} \tag{3.18}$$

and the condition on the shock front:

$$\mathbf{q}_{nm}(0_+) = \mathbf{Y}\mathbf{q}_{nm}(0_-) + \mathbf{h}_t \left(\tau \psi_{nm} - \psi_{0,nm} \right) + \left(\mathbf{h}_r + in\mathbf{h}_\phi \right) \psi_{nm}, \tag{3.14}$$

Substitution of Eq. (3.18) into condition (3.14) leads to

$$\begin{aligned}
&-\psi_{nm} \left[\mathbf{Q}_1(0) \int_0^\infty (\mathbf{y}_1, \mathbf{F}_2)\, dz + \left(\tau \mathbf{h}_t + \mathbf{h}_r + in\mathbf{h}_\phi \right) \right] = \\
&= \mathbf{Y}\mathbf{q}_{nm}(0_-) - \mathbf{h}_t \psi_{0,nm} - \sum_{j=2}^{6} a_j \mathbf{Q}_j(0) + \mathbf{Q}_{1\infty} \int_0^\infty (\mathbf{y}_1, \mathbf{F}_1)\, dz
\end{aligned} \tag{H.1}$$

Dot product of (H.1) and $\mathbf{y}_1(0)$ gives the following equation for the displacement of

the shock ψ_{nm}:

$$-\psi_{nm}\left[\int_0^\infty (\mathbf{y}_1, \mathbf{F}_2)\, dz + (\mathbf{y}_1(0), \tau\mathbf{h}_t + \mathbf{h}_r + in\mathbf{h}_\phi)\right] =$$

$$= (\mathbf{y}_1(0), \mathbf{Y}\mathbf{q}_{nm}(0_-) - \mathbf{h}_t\psi_{0,nm}) + \int_0^\infty (\mathbf{y}_1, \mathbf{F}_1)\, dz,$$

we use the orthogonality of direct and adjoint fundamental solutions: $(\mathbf{y}_i, \mathbf{Q}_j) = \delta_{ij}$, where δ_{ij} is Kronecker delta, as $\mathbf{y}_i$ are vectors composed of cofactors of the j-th column of the matrix of the fundamental solutions $\mathbf{Q} = [\mathbf{Q}_1,\ \mathbf{Q}_2, ...,\ \mathbf{Q}_6]$ which is divided by $\det(\mathbf{Q})$ [54].

Then we can extract ψ_{nm} as

$$\psi_{nm} = -\frac{U(\tau, k_{nm})}{V(\tau, k_{nm})} \tag{H.2}$$

where

$$U = (\mathbf{y}_1(0), \mathbf{Y}\mathbf{q}_{nm}(0_-) - \mathbf{h}_t\psi_{0,nm}) + \int_0^\infty (\mathbf{y}_1, \mathbf{F}_1)\, dz, \tag{H.3}$$

$$V = \int_0^\infty (\mathbf{y}_1, \mathbf{F}_2)\, dz + (\mathbf{y}_1(0), \tau\mathbf{h}_t + \mathbf{h}_r + in\mathbf{h}_\phi). \tag{H.4}$$

In the same fashion, dot product of Eq. (H.1) and $\mathbf{y}_j(0)$, $j = 2, ..., 6$ give the equations for the coefficients a_j:

$$a_j = (\mathbf{y}_j(0), \mathbf{Y}\mathbf{q}_{nm}(0_-) - \mathbf{h}_t\psi_{0,nm}) - \frac{U}{V}(\mathbf{y}_j(0), \tau\mathbf{h}_t + \mathbf{h}_r + in\mathbf{h}_\phi) \tag{H.5}$$

The explicit form of Eq. (3.18) is

$$\mathbf{q}_{nm} =$$

$$= \sum_{j=2}^{6} \left[\left(\mathbf{y}_j \left(0 \right), \mathbf{Y}\mathbf{q}_{nm} \left(0_- \right) - \mathbf{h}_t \psi_{0,nm} \right) + \int_0^z \left(\mathbf{y}_j, \mathbf{F}_1 \right) dz' \right] \mathbf{Q}_j + \mathbf{Q}_1 \int_\infty^z \left(\mathbf{y}_1, \mathbf{F}_1 \right) dz' -$$

$$- \frac{U}{V} \left(\sum_{j=2}^{6} \left[\left(\mathbf{y}_j \left(0 \right), \tau \mathbf{h}_t + \mathbf{h}_r + in\mathbf{h}_\phi \right) + \int_0^z \left(\mathbf{y}_j, \mathbf{F}_2 \right) dz' \right] \mathbf{Q}_j + \mathbf{Q}_1 \int_\infty^z \left(\mathbf{y}_1, \mathbf{F}_2 \right) dz' \right) \tag{H.6}$$

Appendix I: Derivation of the General Solution

The integral of the inverse Laplace transform, the receptivity coefficients, and the formula of the general solution are discussed in this Appendix.

When all terms of the amplitude solution (3.18) are known, and we can go backward through the transformations to obtain the formula for perturbations $\mathbf{q}'(r, \phi, z, t)$. The Bessel expansion gives the following series:

$$\hat{\mathbf{q}}_n(r, z, \tau) = \sum_{m=1}^{\infty} \mathbf{J}_m(k_{nm} r)\, \mathbf{q}_{nm}(z, \tau)$$

Then the integral of the inverse Laplace transformation can be written as

$$\begin{aligned} \mathbf{q}_n(r, z, t) &= \frac{1}{2\pi i} \int_{\sigma - i\infty}^{\sigma + i\infty} \hat{\mathbf{q}}_n(r, z, \tau)\, e^{\tau t} d\tau = \\ &= \sum_s \mathbf{R}_s e^{\tau_s t} + \frac{1}{2\pi i} \int_{-i\infty}^{i\infty} \hat{\mathbf{q}}_n(r, z, \tau)\, d\tau, \end{aligned} \tag{I.1}$$

where the first term is the summation over all poles τ_s - zeros of the denominator $V(\tau)$ with $\mathrm{Re}(\tau_s) > 0$ - the part of the integral due to the discrete spectrum of the problem. The second term is the integral over the imaginary axis, the contribution of the continuous spectrum to the solution. The integration contour used in the inverse Laplace transformation is shown on Fig. 3.1.

Each element of the sum in the discrete spectrum term of Eq. (I.1) can be written

as:

$$\mathbf{R}_s = \sum_{m=1}^{\infty} \mathbf{J}_m \left(k_{nm} r\right) R_{ms} \mathbf{q}_{DM,s} \left(z, k_{nm}, \tau_s\right)$$

The weight coefficient R_{ms} is produced from the evaluation of residue at the pole τ_s:

$$R_{ms} = Res\left(\frac{U}{V},\ \tau_s\right) = \left.\frac{U}{\partial V/\partial \tau}\right|_{\tau=\tau_s},$$

where the numerator U is given by Eq. (H.3), denominator V - by Eq. (H.4), and the partial derivative $\partial V/\partial \tau$ can be evaluated with finite differences.

The explicit form of the vector $\mathbf{q}_{DM,s}$ follows from the last line of Eq. (H.6):

$$\mathbf{q}_{DM,s} =$$

$$= \left[\sum_{j=2}^{6} \left[\left(\mathbf{y}_j\left(0\right), \tau\mathbf{h}_t + \mathbf{h}_r + in\mathbf{h}_\phi\right) + \int_0^z \left(\mathbf{y}_j, \mathbf{F}_2\right) dz'\right] \mathbf{Q}_j + \mathbf{Q}_1 \int_\infty^z \left(\mathbf{y}_1, \mathbf{F}_2\right) dz'\right]_{\tau=\tau_s} \tag{I.2}$$

Appendix J: Equivalence of Spectra

The equivalence of the discrete spectrum stemming from normal-mode and present analyses is considered in this Appendix.

Equivalence of the dispersion relationship. Consider the dot product of (4.1) and the first fundamental solution (G.1) of the adjoint problem (3.19)

$$\left(\mathbf{y}_1,\ \frac{d\vartheta}{dz}\right) + \left(\mathbf{y}_1,\ \mathbf{A}_z^{-1}\left(\mathbf{C}_m + \tau\mathbf{I}\right)\vartheta\right) - \left(\mathbf{y}_1,\ \mathbf{A}_z^{-1}\left(\tau\mathbf{g}_t + \mathbf{g}_r + in\mathbf{g}_\phi\right)\right) = 0 \qquad \text{(J.1)}$$

After integration by parts of (J.1) with respect to z from zero to infinity, and using Eq. (3.19), we arrive at the following relationship:

$$\left(\mathbf{y}_1\left(0\right),\ \vartheta\left(0\right)\right) + \int_0^\infty \left(\mathbf{y}_1,\ \mathbf{A}_z^{-1}\left(\tau\mathbf{g}_t + \mathbf{g}_r\right)\right) dz = 0,$$

or, with the help of Eq. (4.2):

$$\left(\mathbf{y}_1\left(0\right),\ \tau\mathbf{h}_t + \mathbf{h}_r + in\mathbf{h}_\phi\right) + \int_0^\infty \left(\mathbf{y}_1,\ \mathbf{A}_z^{-1}\left(\tau\mathbf{g}_t + \mathbf{g}_r + in\mathbf{g}_\phi\right)\right) dz = 0, \qquad \text{(J.2)}$$

which is exactly the same as (3.23).

Equivalence of the solutions. The normal-mode system (4.1) and the system (3.13) for the amplitude functions possess the same solutions of direct and adjoint homogeneous systems, $\mathbf{Q}_i$ and $\mathbf{y}_i$ respectively ($i = 1, ..., 6$).

Therefore, the solution of (4.1) that is bounded at $z \to \infty$ can be written in the form

$$\vartheta = \sum_{j=2}^{6} \left(\alpha_j + \int_0^z (\mathbf{y}_j, \mathbf{F}_2)\, dz' \right) \mathbf{Q}_j + \mathbf{Q}_1 \int_\infty^z (\mathbf{y}_1, \mathbf{F}_2)\, dz' \tag{J.3}$$

where $\mathbf{F}_2 = \mathbf{A}_z^{-1} (\tau \mathbf{g}_t + \mathbf{g}_r + in\mathbf{g}_\phi)$. Coefficients α_j can be found from the initial condition (4.2): substitution of the solution (J.3) into (4.2) gives

$$\sum_{j=2}^{6} \alpha_j \mathbf{Q}_j + \mathbf{Q}_1 (0) \int_\infty^0 (\mathbf{y}_1, \mathbf{F}_2)\, dz' = \tau \mathbf{h}_t + \mathbf{h}_r + in\mathbf{h}_\phi, \tag{J.4}$$

then, by multiplication of Eq. (J.4) on $\mathbf{y}_j (0)$, and with implementation of orthogonality of asymptotic solutions, we get the coefficients:

$$\alpha_j = (\mathbf{y}_j (0), \tau \mathbf{h}_t + \mathbf{h}_r + in\mathbf{h}_\phi)$$

The solution ϑ is equal to

$$\vartheta = \sum_{j=2}^{6} \left((\mathbf{y}_j (0), \tau \mathbf{h}_t + \mathbf{h}_r + in\mathbf{h}_\phi) + \int_0^z (\mathbf{y}_j, \mathbf{F}_2)\, dz' \right) \mathbf{Q}_j + \mathbf{Q}_1 \int_\infty^z (\mathbf{y}_1, \mathbf{F}_2)\, dz' \tag{J.5}$$

and, evaluated at $\tau = \tau_s$, it is exactly the discrete mode vector $\mathbf{q}_{DM,s}$, given by Eq. (I.2).

Thus, we can conclude that the discrete spectra found by both normal-mode and present analyses are identical, and that the normal-mode solution is included into the present solution of the initial-value problem.

Appendix K: Numerical Methods

In the numerical integration of the differential equations several different solvers were used.

In the first solver, the IMSL routine DIVPAG implementing Gear's BDF method [60] was utilized. The second code was based on LAPACK package, and the calculations were performed using DDASSL subroutine developed by L. R. Petzold (downloaded from software repository of the National Institute of Standards and Technology). The third solver was developed by means of Mathematica, the computational system by Wolfram Research. All solvers were found to be efficient for solution of direct and adjoint problems. A shooting procedure together with Newton's algorithm was used in order to find a root of Eqs. (4.6) (direct problem) and (3.23) (adjoint problem).

The shooting method requires an initial guess of the eigenvalue τ_s. Multi-domain spectral collocation method (SCM) with Chebyshev polynomials was utilized to find the eigenvalues that could be used in the shooting iterations. The method is thoroughly explained in [57] for the case of one-dimensional detonations. The LAPACK solver ZGGEV and subroutine DG6CCG of IMSL FORTRAN library were used in SCM investigations of spectrum.

The SCM calculations need large amounts of computing power to investigate cases with many domains and high numbers of collocation nodes. Such massive calculations

were conducted with the help of the CFD laboratory of the University of Arizona.

Appendix L: Supplemental Receptivity Results

The dependence of maximum values of pressure distribution $\max|p|$ on overdrive factor f, activation energy E and heat release Q are described here.

The results are demonstrated for Mode 1 (see Fig. 5.6) with the radial parameter k fixed and equal to unity, $\gamma = 1.2$. The dependence of coordinates of Mode 1 on f is shown on Fig. L.1. The curves start at $f = 1.01$, as the value of $f = 1$ is beyond the scope of the present research, and end at $f = 4.14$, where the discrete mode merges with the continuous spectrum.

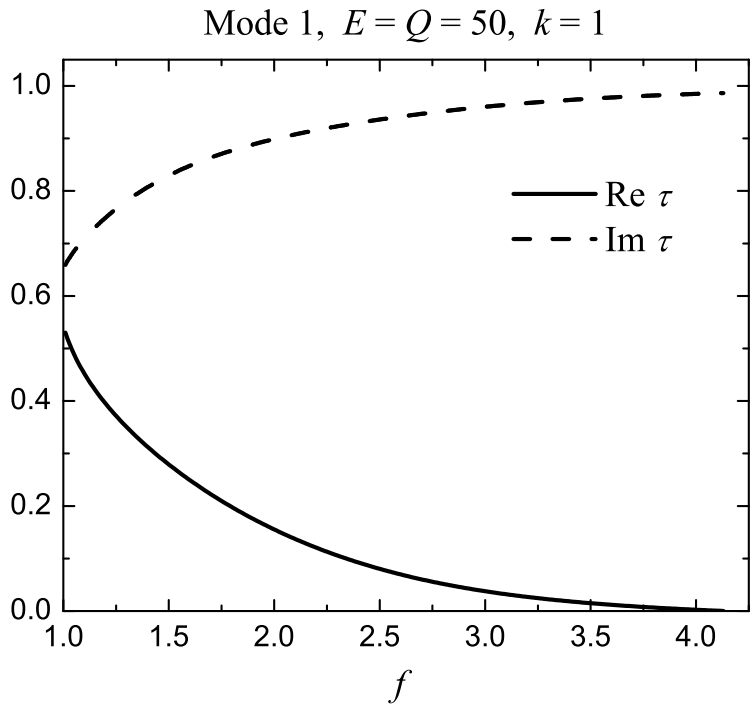

Figure L.1: Dependence of coordinates of the first discrete mode on overdrive factor f, for $k = 1$, $E = Q = 50$.

The behavior of coordinates of Mode 1 with respect to E are shown on Fig. L.2. The range of E from 0 to 50 is covered.

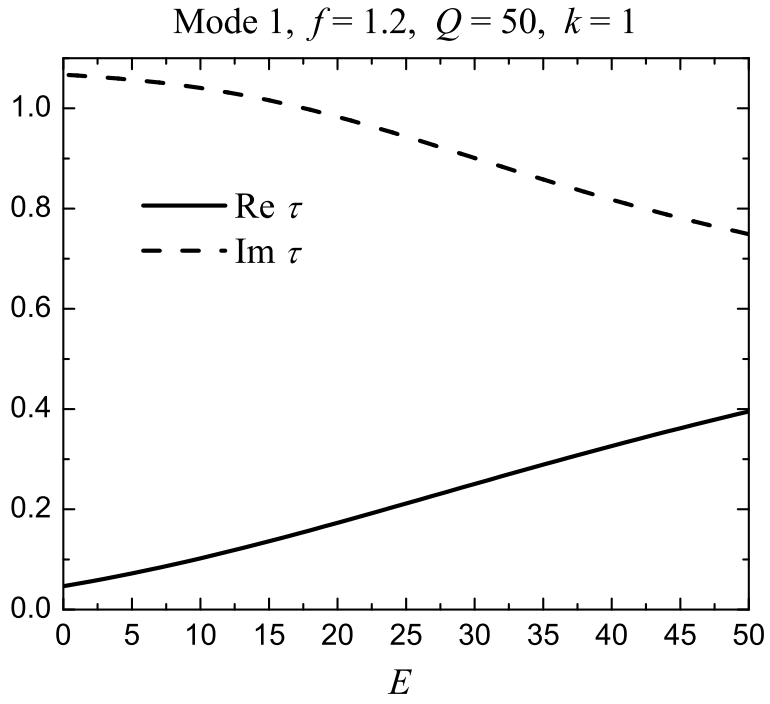

Figure L.2: Dependence of coordinates of the first discrete mode on activation energy E, for $k = 1$, $Q = 50$ and $f = 1.2$.

The dependence of coordinates of Mode 1 on Q is shown on Fig. L.3. The considered range of Q is between 20 and 50, as the values $Q < 20$ for constant activation energy $E = 50$ are difficult to analyze due to the stiffness of the problem.

Three types of perturbations are considered: vorticity perturbation placed outside of the reaction zone (see Section 6.1.1), vorticity perturbation placed inside the reaction zone (Section 6.2.1) and adiabatic perturbation placed inside the reaction zone (Section 6.2.2).

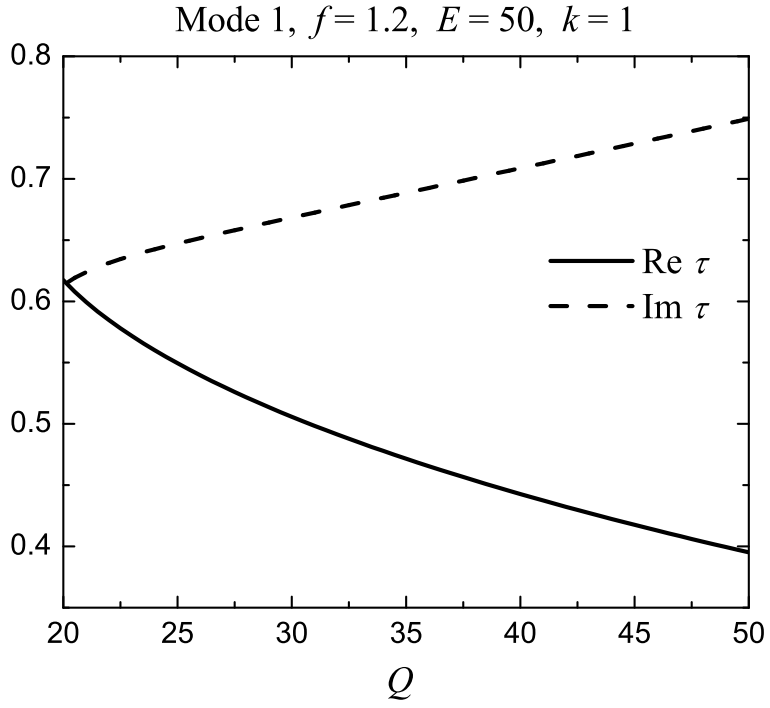

Figure L.3: Dependence of coordinates of the first discrete mode on heat release Q, for $k = 1$, $E = 50$ and $f = 1.2$.

Vorticity perturbations inside the reaction zone. The two considered types of vorticity perturbations are now placed inside the reaction zone. For the disturbance with fixed boundary $z_1 = 0.5$, the receptivity results are shown on Figs. L.4-L.6: flow receptivity increases with increase of f and decrease of Q, the effect of the activation energy change is small.

The fixed-width perturbation is described by Figs. L.7-L.9. The flow receptivity decays with distance from the shock wave, as well as with decrease of E, and increase of f and Q.

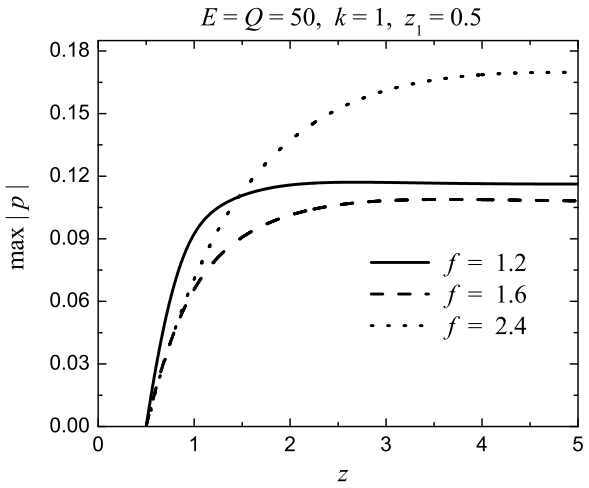

Figure L.4: Maximum of pressure perturbation in the first discrete mode for vorticity perturbation placed inside the reaction zone, with fixed $z_1 = 0.5$ and z_2 varying from 0.5 to 5. The dependence is shown for three values of the overdrive factor f.

Adiabatic perturbations inside the reaction zone. The receptivity of the flow to adiabatic perturbations analyzed in Section 6.2.2 is described on Figs. L.10-L.12 for different values of f, E and Q. The flow becomes more receptive to the considered perturbation with increase of activation energy E, and decrease of heat release Q and overdrive factor f.

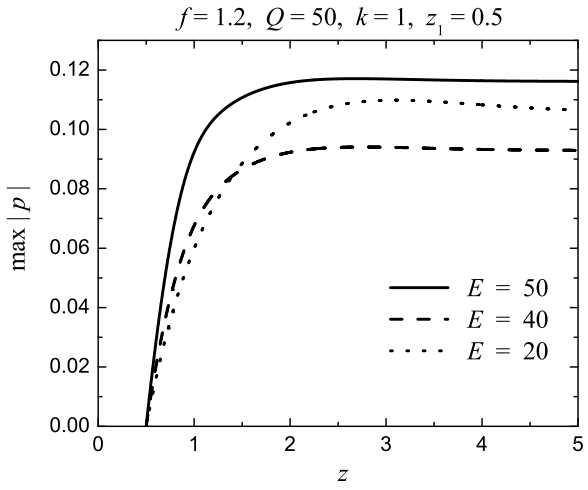

Figure L.5: Maximum of pressure perturbation in the first discrete mode for vorticity perturbation placed inside the reaction zone, with fixed $z_1 = 0.5$ and z_2 varying from 0.5 to 5. The dependence is shown for three values of the activation energy E.

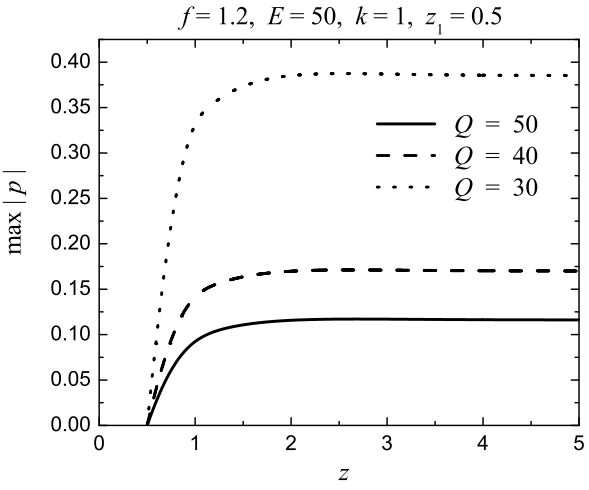

Figure L.6: Maximum of pressure perturbation in the first discrete mode for vorticity perturbation placed inside the reaction zone, with fixed $z_1 = 0.5$ and z_2 varying from 0.5 to 5. The dependence is shown for three values of the heat release Q.

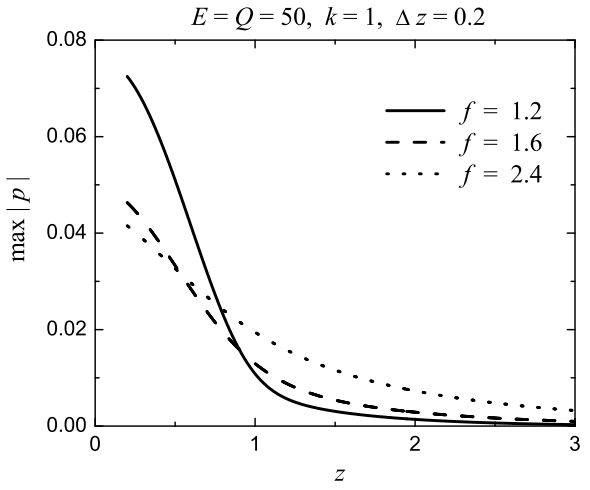

Figure L.7: Maximum of pressure perturbation in the first discrete mode for vorticity perturbation placed inside the reaction zone, with fixed $\Delta z = z_2 - z_1 = 0.2$ and z_1 varying from 0.2 to 3. The dependence is shown for three values of the overdrive factor f.

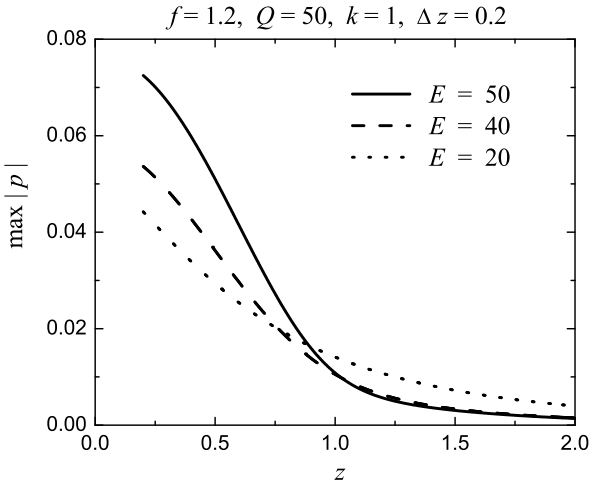

Figure L.8: Maximum of pressure perturbation in the first discrete mode for vorticity perturbation placed inside the reaction zone, with fixed $\Delta z = z_2 - z_1 = 0.2$ and z_1 varying from 0.2 to 2. The dependence is shown for three values of the activation energy E.

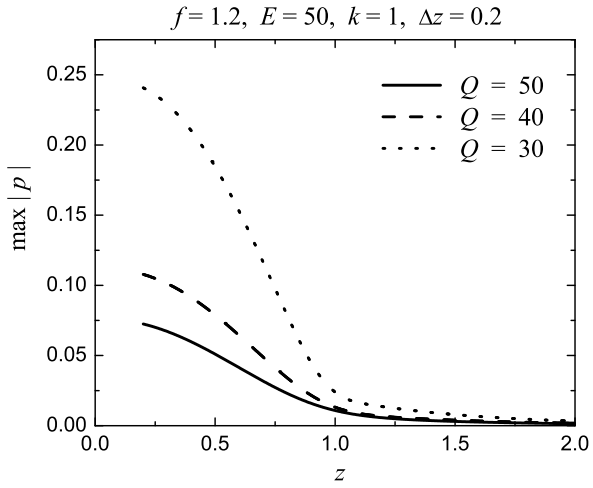

Figure L.9: Maximum of pressure perturbation in the first discrete mode for vorticity perturbation placed inside the reaction zone, with fixed $\Delta z = z_2 - z_1 = 0.2$ and z_1 varying from 0.2 to 2. The dependence is shown for three values of the heat release Q.

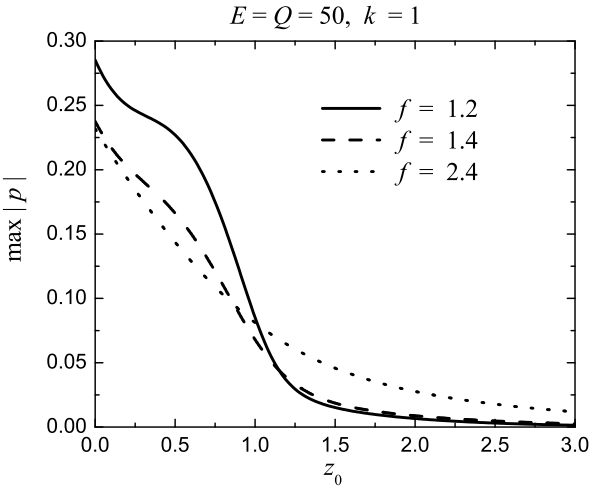

Figure L.10: Maximum of pressure perturbation in the first discrete mode for adiabatic perturbation placed inside the reaction zone at $z = z_0$. The dependence is shown for three values of the overdrive factor f.

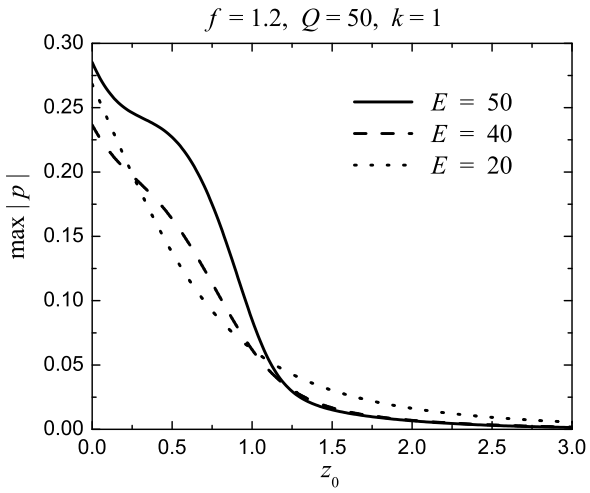

Figure L.11: Maximum of pressure perturbation in the first discrete mode for adiabatic perturbation placed inside the reaction zone at $z = z_0$. The dependence is shown for three values of the activation energy E.

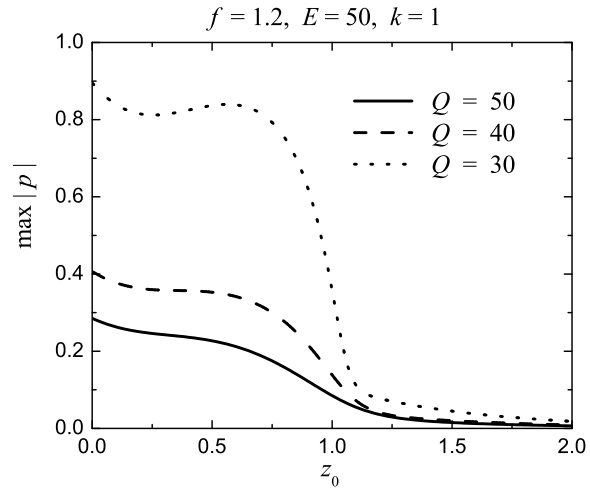

Figure L.12: Maximum of pressure perturbation in the first discrete mode for adiabatic perturbation placed inside the reaction zone at $z = z_0$. The dependence is shown for three values of the heat release Q.

References

[1] M. Short and D. S. Stewart. Cellular detonation stability. Part 1. A normal-mode linear analysis. *J. Fluid Mech.*, 368:229–262, 1998.

[2] R. James. *Pharmacopœia Universalis or, a New Universal English Dispensatory. ... With a copious index*. Eighteenth Century Collections Online. Gale Group, 1747. Based on information from English Short Title Catalogue.

[3] J. B. Van Mons. Addition to New Observations on the Method of producing very loud fulminations with various Bodies, by Means of Phosphorus by Brugnatelly. *Nicholson Journal*, 2:470–473, 1799.

[4] M. Berthelot and P. Vieille. Sur la vitesse de propagation des phénomènes explosives dans les gas. *C. R. Séances Acad. Sci.*, 93:18–22, 1881.

[5] E. Mallard and H. Le Châtelier. Sur les vitesses de propagation de l'inflammation dans les mélanges gazeux explosives. *C. R. Séances Acad. Sci.*, 93:145–148, 1881.

[6] H. B. Dixon. Bakerian lecture: the rate of explosions in gases. *Phil. Trans. Royal Soc. Lond. A*, 184:97–188, 1893.

[7] D. L. Chapman. On the rate of explosions in gases. *Philos. Mag.*, 47:90–104, 1899.

[8] E. Jouguet. Sur la propagation des réactions chimiques dans les gas. *J. de Mathematiques Pures et Appliquees*, 1:347–425, 1905. Continued in volume 2, pages 5–85 (1906).

[9] E. Jouguet. *Mécanique des Explosifs*. Octave Doin et Fils, Paris, 1917.

[10] V. A. Mikhelson. O normalnoy skorosti vosplameneniya gremuchih gazovyh smesey (On normal ignition velocity of explosive gaseous mixtures). *Imperial Moscow University Scientific Bulletin, Phys. & Math. Ser.*, 10:1–92, 1893. In Russian.

[11] J. W. S. Rayleigh. *Theory of sound*. Dover Publications, second edition, 1976.

[12] P.-H. Hugoniot. Sur la propagation du mouvement dans les corps et plus spécialement dans les gaz parfaits. *J. Ecole Polytech.*, 57–58, 1889.

[13] B. J. McBride and S. Gordon. Computer program for calculation of complex chemical equilibrium compositions and applications II. User's manual and program description. NASA Report NASA RP-1311-P2, National Aeronautics and Space Administration, Lewis Research Center, Cleveland, OH, USA, 1996.

[14] W. C. Reynolds. The element potential method for chemical equilibrium analysis: implementation in the interactive program STANJAN. Technical report, Dept. of Mechanical Engr., Stanford University, 1986.

[15] J. H. S. Lee. *The detonation phenomenon*. Cambridge University Press, 2008.

[16] Ya. B. Zel'dovich. K teorii rasprostraneniya detonatsii v gazoobraznykh sistemakh. *Zh. Eksp. Teor. Fiz.*, 10:542–568, 1940. English translation: On the theory of the propagation of detonation in gaseous systems, NACA TM 1261, 1950.

[17] J. von Neumann. Theory of detonation waves. In A. H. Taub, editor, *John von Neumann, collected works*, volume 6, pages 203–218, New York, 1963. Macmillan.

[18] H. B. Döring. Über den detonationsvorgang in gasen. *Ann. Phys.*, 435:421–436, 1943.

[19] Ya. B. Zel'dovich and A. S. Kompaneets. *Teoriya Detonatsii*. Gostekhizdat, Moscow, 1955. English translation: Theory of Detonation. New York, Academic Press, 1960.

[20] C. Campbell and D. W. Woodhead. The ignition of gases by an explosion-wave. Part I. Carbon monoxide and hydrogen mixtures. *J. Chem. Soc.*, pages 3010–3021, 1926.

[21] B. V. Voitsekhovskiy, V. V. Mitrofanov, and M. Ye. Topchiyan. Struktura fronta detonatsii v gazakh. Technical report, Izdatel'stvo Sibirskogo Otdeleniya AN SSSR, Novosibirsk, 1963. English translation: The structure of a detonation front in gases. Wright-Patterson Air Force Base Report FTD-MT-64-527, 1966.

[22] G. L. Schott. Observations of the structure of spinning detonation. *Phys. Fluids*, 8(5):850–865, 1965.

[23] F. A. Williams. *Combustion Theory*. The Benjamin/Cummings Publishing Company, Inc., second edition, 1985.

[24] K. I. Shchelkin. Two cases of unstable combustion. *Zh. Eksp. Teor. Fiz.*, 36:600–606, 1959.

[25] R. M. Zaidel. Ob ustoychivosti detonatsionnyh voln v gazovyh smesyah (The stability of detonation waves in gaseous mixtures). *Dokl. Akad. Nauk SSSR (Phys. Chem. Sect.)*, 136:1142–1145, 1961.

[26] J. J. Erpenbeck. Structure and stability of the square-wave detonation. In *Ninth Symposium (International) on Combustion*, pages 442–453. Academic Press, 1963.

[27] J. D. Buckmaster and G. S. S. Ludford. The effect of structure on the stability of detonations I. Role of the induction zone. In *Twenty-first Symposium (International) on Combustion*, pages 1669–1676. The Combustion Institute, 1986.

[28] J. D. Buckmaster and J. Neves. One-dimensional detonation stability: The spectrum for infinite activation energy. *Phys. Fluids*, 31:3571–3576, 1988.

[29] M. Short. Multidimensional linear stability of a detonation wave at high activation energy. *SIAM Journal on Applied Mathematics*, 57(52):307–326, 1997.

[30] J. J. Erpenbeck. Stability of steady-state equilibrium detonations. *Phys. Fluids*, 5(5):604–614, 1962.

[31] J. J. Erpenbeck. Stability of idealized one-reaction detonations. *Phys. Fluids*, 7(5):684–696, 1964.

[32] J. J. Erpenbeck. Stability of step shocks. *Phys. Fluids*, 5(10):1181–1187, 1962.

[33] J. J. Erpenbeck. Steady detonations in idealized two-reaction systems. *Phys. Fluids*, 7(9):1424–1432, 1964.

[34] J. J. Erpenbeck. Stability of idealized one-reaction detonations: zero activation energy. *Phys. Fluids*, 8:1192–1193, 1965. Research notes.

[35] J. J. Erpenbeck. Detonation stability for disturbances of small transverse wavelength. *Phys. Fluids*, 9(7):1293–1306, 1966.

[36] J. J. Erpenbeck. Nonlinear theory of unstable one-dimensional detonations. *Phys. Fluids*, 10(2):274–289, 1967.

[37] J. J. Erpenbeck. Nonlinear theory of unstable two-dimensional detonation. *Phys. Fluids*, 13(8):2007–2026, 1970.

[38] J. J. Erpenbeck. Theory of detonation stability. In *Twelfth Symposium (International) on Combustion*, pages 711–721. The Combustion Institute, 1969.

[39] V. V. Pukhnachev. Ob ustoichivosti detonatsii Chepmena-Zhuge (The stability of Chapman-Jouguet detonations). *Dokl. Akad. Nauk. SSSR*, 149:798–801, 1963. In Russian.

[40] V. V. Pukhnachev. Ob ustoichivosti detonatsii Chepmena-Zhuge (The stability of Chapman-Jouguet detonations). *Prikl. Mekh. Tekh. Fiz.*, 6:66–73, 1963. In Russian.

[41] G. E. Abouseif and T. Y. Toong. Theory of unstable one-dimensional detonations. *Combust. Flame*, 45:67–94, 1982.

[42] H. I. Lee and D. S. Stewart. Calculation of linear detonation instability: one-dimensional instability of plane detonation. *J. Fluid Mech.*, 216:103–132, 1990.

[43] G. J. Sharpe. Linear stability of idealized detonations. *Proc. R. Soc. Lond. A*, 453:2603–2625, 1997.

[44] A. R. Kasimov and D. S. Stewart. Spinning instability of gaseous detonations. *J. Fluid Mech.*, 466:179–203, 2002.

[45] W. Fickett and W. C. Davis. *Detonation: Theory and Experiment*. Dover Publications, 2000. Republication of the original work published in 1979 by the University of California Press, Berkley.

[46] M. V. Morkovin. Critical evaluation of transition from laminar to turbulent shear layers with emphasis on hypersonic traveling bodies. AFRL Report AFF DL–TR–68–149, Air Force Flight Dynamics Laboratory, Wright-Patterson AFB, OH, USA, 1969.

[47] E. Reshotko. Boundary-layer stability and transition. *Annu. Rev. Fluid Mech.*, 8:311–349, 1976.

[48] E. Forgoston and A. Tumin. Initial-value problem for three-dimensional disturbances in a hypersonic boundary layer. *Phys. Fluids*, 17, 2005. Paper No. 084106.

[49] A. Tumin. Initial-value problem for small disturbances in an idealized one-dimensional detonation. *Phys. Fluids*, 19(106105), 2007.

[50] W. W. Wood and Z. W. Salsburg. Analysis of steady-state supported one-dimensional detonations and shocks. *Phys. Fluids*, 3(4):549–566, 1960.

[51] E. Zauderer. *Partial Differential Equations of Applied Mathematics*. Wiley & Sons, third edition, 2006.

[52] A. R. Kasimov. *Theory of instability and nonlinear evolution of self-sustained detonation waves*. PhD thesis, University of Illinois at Urbana-Champaign, 2004.

[53] G. B. Arfken and H. J. Weber. *Mathematical Methods for Physicists*. Harcourt/Academic press, San Diego, fifth edition, 2001.

[54] E. Kamke. *Differentialgleichungen. Lösungsmethoden und Lösungen*. Akademische Verlagsgesellschaft Geest & Portig, Leipzig, 1959.

[55] A. D. Pierce. *Acoustics: An Introduction to Its Physical Principles and Applications*. Acoustical Society of Amer, 1989.

[56] C. Chiquete, I. Shalaev, and A. Tumin. Receptivity of plane idealized one-reaction detonations to three-dimensional perturbations. AIAA Paper 2008–1038, 2008.

[57] A. Tumin. Multi-domain spectral collocation method for stability of detonations. *AIAA J.*, 45:2356–2359, 2007.

[58] T. J. Bridges and P. J. Morris. Differential eigenvalue problems in which the parameter appears nonlinearly. *J. Comp. Phys.*, 55:437–460, 1984.

[59] L. Hayes and E. Wasserstrom. Solution of non-linear eigenvalue problems by the continuation method. *J. Inst. Maths Applics*, 17:5–14, 1976.

[60] C. W. Gear. Simultaneous numerical solution of differential-algebraic equations. *IEEE Trans. Circuits and Systems*, 18(1):89–95, 1971.